STUDY OF
LUMINESCENT PROPERTIES OF SILICON CARBIDE
AND
APPLICATION TO LIGHT-EMITTING DIODES

BY
MITSUSHI IKEDA

FEBRUARY 1980

DEPARTMENT OF ELECTRONICS
KYOTO UNIVERSITY
KYOTO, JAPAN

STUDY OF
LUMINESCENT PROPERTIES OF SILICON CARBIDE
AND
APPLICATION TO LIGHT-EMITTING DIODES

BY
MITSUSHI IKEDA

FEBRUARY 1980

DEPARTMENT OF ELECTRONICS
KYOTO UNIVERSITY
KYOTO, JAPAN

ABSTRACT

This thesis describes the studies on epitaxial growth and photoluminescence of SiC crystals, diode fabrication processes including gas etching, and characteristics of SiC visible light-emitting diodes. These studies are performed with a purpose to promote the fabrication technology and understanding of luminescent properties of SiC light-emitting diodes.

Chapter I explains the properties of SiC and the present state of the research.

Chapter II describes the liquid phase epitaxial growth of SiC crystals by a dipping technique and the conditions to grow good epitaxial layers. The electrical properties of the layers doped with N donors or Al acceptors are presented.

In chapter III, photoluminescence in undoped 3C, 4H, 6H, and 15R SiC crystals is studied. The phonon energies, exciton band gaps, and free exciton binding energies are determined from the analyses of free exciton luminescence.

Chapter IV describes the photoluminescence study of 3C, 4H, 6H, and 15R SiC crystals doped with Al, Ga, or B acceptors and N donors. The luminescence mechanisms are determined from the results of various measurements and analyses. Based on the configuration coordinate model and curve fittings, the donors and acceptors in 4H, 6H, and 15R SiC are found to take multi-levels due to inequivalent sites in the crystals. The origin of the site effect on the impurity level is studied based on the quantum defect model considering the characteristics of these levels, and the possibility of this effect in other materials is pointed out. The applicability of Haynes rule to N donors in different sites in various SiC polytypes is examined.

In chapter V, blue light-emitting diodes of 6H SiC are

fabricated by the overcompensation method which is proposed in this thesis. By this method high efficiency is attained. The electrical and luminescent properties of the diodes are studied.

Chapter VI presents the observation of broad peaks which shift with current and cover most of the visible range, from red to blue, in diodes heavily doped with donors and acceptors. The mechanism of the peak shift is discussed based on the electrical properties, injection mechanism, and luminescent properties of the diodes.

In chapter VII, various light-emitting diodes, doped in the n layers with Al, Ga, or B acceptors and N donors, are fabricated using the rotation dipping technique which is proposed in this thesis. By this technique high efficiency blue and yellow light-emitting diodes are realized. A detailed study of electroluminescence mechanisms is carried out using various measuring techniques. The origins of the peaks which appear in the electroluminescence and the recombination radiation region in the diodes are determined. The dependence of the electroluminescence efficiency on the N concentration in the n layer is studied, and methods to improve the efficiency are discussed based on the results.

Chapter VIII describes the etching of SiC with Cl_2-O_2-Ar gas system. The dependences of the etch rate on the temperature, gas flow rate, and gas composition are measured. Thermodynamical analysis of this system is carried out, and good agreement is obtained with a simple theory, which enables to predict the etch rate at a given temperature and gas composition. The reason of the large difference of the etch rates between the Si face and C face is discussed. The effect of the mesa etch with this gas system on diode characteristics is examined.

In chapter IX, conclusions of the present study and suggestions for further investigations are presented.

ACKNOWLEDGMENTS

The author wishes to express his deep gratitude to former professor Tetsuro Tanaka for his continuous guidance and encouragement. He wishes to express his grateful appreciation to Associate Professor Hiroyuki Matsunami for his precious guidance and advice. He profoundly acknowledges Professor Akira Kawabata for his genial encouragement and guidance. He acknowledges Professor Akio Sasaki for his useful criticisms and suggestions on the manuscript.

He is grateful to Dr. Akira Suzuki for his guidance in the author's master course. He is also grateful to Dr. Junji Saraie, Mr. Shigehiro Nishino, and Dr. Shigeo Fujita for stimulative discussions.

Much appreciation is due to Messrs. Toshiro Hayakawa, Nobuya Nagao, Minoru Hori, Shinichi Yamagiwa, Michiya Kobayashi, and Toyohiro Nishitani for their valuable participation in crystal growth, diode fabrication, and gas etching. He also thanks other members of Semiconductor Laboratory.

He is grateful to Professor Syoji Yamada and Associate Professor Hiroshi Kuwabara of Shizuoka University for valuable discussion and advice.

Appreciation is due to Dr. W. F. Knippenberg, Dr. W. v. Münch, Dr. I. Swiderski, Dr. R. M. Potter, and Dr. W. Kürzinger for their supply of SiC crystals grown by Lely method. Appreciation is due to Dr. Toshio Inoguchi of Sharp Corporation and Dr. Isamu Akasaki of Matsushita Research Institute Tokyo for their experimental supports. He thanks Nihon Silicon Corporation for the supply of pure silicon and Taiheiyo Kogyo Corporation and Syowa Denko Corporation for the supply of industrial grade SiC crystals.

He is grateful to Dr. Yoshikazu Takeda for his suggestion and

facility in preparing the manuscript.

Part of this work was supported by the Grant-in-Aid for Developmental Scientific Research and Grant-in-Aid for Scientific Research from the Ministry of Education.

CONTENTS

I. INTRODUCTION

The extreme development of silicon technology [1] has brought about great evolution in human life. Sophisticated integrated circuits have enabled a small silicon chip to play a variety of functions. Silicon devices cover almost all the electronic circuits. As a matter of course, there is a limitation in the ability of such a mighty semiconductor, silicon. For the applications where silicon is no more suitable, III-V compound semiconductors perform complementally roles. Laser diodes, light-emitting diodes, and microwave devices have been realized with GaAs, GaP, and other compound semiconductors [2].

Silicon carbide (SiC) studied in this thesis has unique properties which above mentioned materials do not own. The chemical, thermal, and mechanical stabilities of SiC, enable the application to devices operating under extreme conditions [3]. Keyes [4] pointed out the potentiality of SiC to high power devices, field effect transistors, and avalanche transit time devices because of its large saturated drift velocity [5] and breakdown field [6] which are superior or comparable to those of Si and GaAs. The most suitable application of SiC may be visible, especially blue, light-emitting diodes (LED's). Among the candidates for blue LED's, SiC is a unique material in the point that low resistivity p and n type crystals can be easily obtained. Other competitors, ZnS, ZnSe, and GaN have a drawback that low resistivity p type crystals can not be obtained because of the self-compensation effect. This drawback deprives these blue LED's of reproducibility, which is unacceptable for mass production in spite of the high quantum efficiencies of 5×10^{-4} for ZnS [7] and $\geq 1\times10^{-3}$ for GaN [8]. Since LED televisions have been realized with GaP [9], the attainment of blue LED's may enable to realize multi-color LED televisions.

Silicon carbide takes many crystal structures, namely polytypes,

Table I. SiC polytypes with two common notations and exciton band gaps. The sites of atoms are denoted by A, B, and C in the close packed structure.

Ramsdell notation	ABC notation	Exciton band gaps
2H(wurzite)	AB	3.330
3C(zincblende)	ABC	2.390
4H	ABAC	3.265
6H	ABCACB	3.023
15R	ABCACBCABACABCB	2.986

which are determined by the stacking sequence and cycle along the c-axis. Table I shows stacking sequences in the c-axis and the exciton band gaps at 4.2 K of the polytypes studied in this thesis. The polytype is expressed by nM, where n is the stacking cycle in the c-axis and M is the crystal structure; H for hexagonal, R for rhombohedral, C for cubic. The exciton band gaps of various polytypes which are smaller than the band gaps by the free exciton binding energies, have been determined by Choyke, Patrick, and Hamilton [10-14]. The free exciton binding energies of 3C [15,16], 4H [17], and 6H SiC [18] were determined by the absorption and the electroreflectance measurements. However, confirmation of these data by other researchers has not been reported.

A great number of reports have been published on photoluminescence in 3C, 4H, and 6H SiC doped with donors and acceptors with the interest for LED's. The assignment of the luminescence in 3C SiC has been established by extensive researches [19-22]. Whereas, the explanation of the luminescence in 4H and 6H SiC is in confusion in spite of numerous reports [23-28]. Two different explanations are given to the luminescence which is composed of two series of peaks, and the donor levels determined based on the explanations differ as much as 100 meV each other. Gorban et al. [23] and Suzuki et al. [28] explained that these two series were zero phonon lines and their LA phonon replicas. Hagen et al. [27] attributed them to two donor

levels caused by two kinds of sites which exist in 4H and 6H SiC. This confusion, consequently, prevents us from analyzing experimental results related with donor levels.

The first observation of injection electroluminescence (EL) in SiC by Lossev [29] in 1923 has caused interest in SiC as a semiconductor material. However, it was after the invention of sublimation process to grow large and relatively pure crystals by Lely [30], when active investigation was initiated on the properties and devices of SiC. Light-emitting diodes have been mainly fabricated with diffusion [31] using the crystal grown by Lely method. The high temperature processes of diffusion (1900-2200°C) and growth (2300-2600°C) cause the difficulty in controlling doping and polytype. Since the second conference on SiC in 1968, vapour [32-34] and liquid phase [35] epitaxial growths have been studied by many researchers with a purpose to fabricate LED's. A successful result was reported by Brander et al. [35] who carried out liquid phase epitaxial growth at a lower temperature of 1650°C fixing SiC substrate crystals in the Si melt. They realized LED's with the highest quantum efficiency of 1×10^{-5}. However, their growth process has a drawback that the crystals suffer the stress by the solidification of Si melt and that the crucible has to be cut off and the Si melt should be etched away in order to take out the grown crystal.

The indirect band gap of SiC permits only poor efficiency in the interband transition, and therefore proper luminescent centers should be introduced. However, study on the electroluminescence mechanisms is limited [35-37] and the results are primitive because of the lack of reliable knowledge of photoluminescence.

Various device fabrication processes of SiC have been investigated by many researchers [3,38]. Among them, the combination of etching with Cl_2-O_2-Ar gas [3,39] and a good etch mask - SiO_2 [40, 41] is an excellent process which enables photolithography and planar technique. However, detailed study of this system has not been

reported.

In this thesis, study is carried out on the subjects which are pointed out to need research in this chapter. This study includes the crystal growth, photoluminescence mechanisms, fabrication of LED's, electroluminescence mechanisms, and etching with Cl_2-O_2-Ar gas system. The purpose is to prepare epitaxial layers of good quality and high efficiency LED's and to analyze the mechanisms of photoluminescence in order to determine physical constants which are necessary to analyze and design SiC LED's.

References

[1] B. E. Deal and J. M. Early, J. Electrochem. Soc. 126, 20C (1979).

[2] N. Holonyak, Jr., G. E. Stillman, and C. M. Wolfe, J. Electrochem. Soc. 125, 487C (1978).

[3] R. B. Campbell and H. C. Chang, in "Semiconductors and Semimetals",edited by R. K. Willardson and A. C. Beer (Academic Press, New York, 1971), Vol. 7, p. 625.

[4] R. W. Keyes, in "Silicon Carbide - 1973", edited by R. C. Marshall, J. W. Faust, Jr., and C. E. Ryan (University of South Carolina Press, Columbia, 1974), p. 534.

[5] W. v. Münch and E. Pettenpaul, J. Appl. Phys. 48, 4823 (1977).

[6] W. v. Münch and I. Pfaffender, J. Appl. Phys. 48, 4831 (1977).

[7] H. Katayama, S. Oda, and H. Kukimoto, Appl. Phys. Lett. 27, 697 (1975).

[8] G. Jacob, R. Madar, and J. Hallais, Mater. Res. Bull. 11, 445 (1976); G. Jacob, M. Boulou, and D. Bois, J. Lumin. 17, 263 (1978).

[9] T. Niina, S. Kuroda, H. Yonei, and H. Takesada, IEEE Trans. Electron Devices ED-26, 1182 (1979).

[10] L. Patrick, D. R. Hamilton, and W. J. Choyke, Phys. Rev. 143, 526 (1966).

[11] W. J. Choyke, D. R. Hamilton, and L. Patrick, Phys. Rev. 133, A1163 (1964).

[12] L. Patrick, W. J. Choyke, and D. R. Hamilton, Phys. Rev. 137, A1515 (1965).

[13] W. J. Choyke and L. Patrick, Phys. Rev. 127, 1868 (1962).

[14] L. Patrick, D. R. Hamilton, and W. J. Choyke, Phys. Rev. 132, 2023 (1963).

[15] D. S. Nedzvetskii, B. V. Novikov, N. N. Prokofeva, and M. B. Reifman, Sov. Phys. - Semicond. 2, 914 (1969).

[16] V. I. Kiselev, B. V. Novikov, M. M. Pimonenko, and E. B. Shadrim, Sov. Phys. - Solid State 13, 926 (1971).

[17] G. B. Dubrovskii and V. I. Sankin, Sov. Phys. - Solid State 17, 1847 (1976).

[18] V. I. Sankin, Sov. Phys. - Solid State 17, 1191 (1975).

[19] G. Zanmarchi, J. Phys. Chem. Solids 29, 1727 (1968).

[20] N. N. Long, D. S. Nedzvetskii, N. L. Prokofeva, and M. B. Reifman, Opt. Spectrosc. 29, 388 (1970); N. N. Long, D. S. Nedzvetskii, N. K. Prokofeva, and M. B. Reifman, Opt. Spectrosc. 30, 165 (1971); N. N. Long and D. S. Nedzvetskii, Opt. Spectrosc. 35, 645 (1973).

[21] W. J. Choyke and L. Patrick, Phys. Rev. B12, 4959 (1970).

[22] H. Kuwabara, S. Shiokawa, and S. Yamada, Phys. Status Solidi A16, K67 (1973); H. Kuwabara and S. Yamada, Phys. Status. Solidi A30, 739 (1975); H. Kuwabara, K. Yamanaka, and S. Yamada, Phys. Status Solidi A37, K157 (1976).

[23] I. S. Gorban, G. I. Mishinova, and Yu. M. Suleimanov, Sov. Phys. - Solid State 7, 2991 (1966); I. S. Gorban, V. A. Gubanov, and V. M. Efimov, Sov. Phys. - Solid State 14, 2010 (1973).

[24] E. E. Bukke, L. A. Vinokurov, I. S. Gorban, A. F. Gumenyk, Yu. M. Suleimanov, and M. V. Fok, Sov. Phys. - Semicond. 1, 1164 (1967).

[25] M. P. Lisitsa, Yu. S. Krasnov, V. F. Romanenko, M. B. Reifman, and O. T. Sergeev, Opt. Spectrosc. 28, 264 (1970).

[26] V. I. Pavlichenko, I. V. Ryzhikov, Yu. M. Suleimanov, and Y. M. Shvaidak, Sov. Phys. - Solid State, 10, 2205 (1969).

[27] S. H. Hagen, A. W. C. van Kemenade, and J. A. W. van der Does de Bye, J. Lumin. 8, 18 (1973).

[28] A. Suzuki, H. Matsunami, and T. Tanaka, J. Phys. Chem. Solids 38, 693 (1977); A. Suzuki, H. Matsunami, and T. Tanaka, J.

Electrochem. Soc. 124, 241 (1977).

[29] O. V. Lossev, Wireless Telegraphy and Telephony 18, 16 (1923).

[30] J. A. Lely, Ber. Dtsch. Keram. Ges. 32, 229 (1955).

[31] For example, E. E. Violin, and G. F. Kholuyanov, Sov. Phys. - Solid State 6, 1331 (1964); R. M. Potter, Mater. Res. Bull. 4, S223 (1969).

[32] A. Todkill and R. W. Brander, Mater. Res. Bull. 4, S293 (1969).

[33] G. Gramberg and M. Kröniger, Solid-State Electron. 15. 285 (1972).

[34] W. v. Münch and I. Pfaffender, Thin Solid Films 31, 39 (1976).

[35] R. W. Brander and R. P. Sutton, J. Phys. D2, 309 (1969).

[36] R. W. Brander, General Electric Company J. Science Tech. 32, (1965).

[37] Yu. S. Krasnov, T. G. Kmita, I. V. Ryzikov, V. I. Pavlichenko, O. T. Sergeev, and Yu. M. Suleimanov, Sov. Phys. - Solid State 10, 905 (1968).

[38] For a review, see for example, J. W. Faust, Jr., and H. M. Liaw, in "Silicon Carbide - 1973", edited by R. C. Marshall, J. W. Faust, Jr., and C. E. Ryan (University of South Carolina Press, Columbia, 1974), P. 657.

[39] R. W. Bartlet and M. Barlow, J. Electrochem. Soc. 117, 1436 (1970).

[40] E. Fitzev and R. Ebi, in "Silicon Carbide - 1973", edited by R. C. Marshall, J. W. Faust, Jr., and C. E. Ryan (University of South Carolina Press, Couminbia, 1974), p. 320.

[41] R. C. A. Harris and R. C. Call, ibid., p. 329.

II. EPITAXIAL GROWTH OF SiC AND ELECTRICAL PROPERTIES OF GROWN LAYERS

2-1. Introduction

The Lely method [1] has been conventionally employed to prepare SiC single crystals for the study of its properties and device fabrications. However, this method has a demerit of high growth temperatures of 2300-2600°C which cause the difficulty in controlling impurity doping and the polytype. Brander et al. [2,3] reported liquid phase epitaxial growth at a lower temperature of 1650°C fixing substrate crystals in the Si melt. The high quantum efficiency of 1×10^{-5} [3,4] in the LED's prepared by this method seems to indicate the excellent quality of the epitaxial layers. This method however, has drawbacks that the crystal suffers the stress by solidification of the Si melt and that cut-off of the crucible and etch-away of the Si melt are necessary to take out the grown crystal.

In order to avoid these problems, co-workers and the author [5, 6] have proposed a dipping technique using the Si melt. Pellegrini et al. [7] had reported a similar method using a melt of Ti-Si. However, the doping of Ti in the crystal estimated to be about 1×10^{19} cm^{-3} [8] is inevitable by their method.

In this chapter, growth process and the results of the crystal growth are described. Doping of Al acceptors and N donors is carried out, and the electrical properties of the grown layers are measured.

2-2. Growth Procedure

Figure 1 shows the growth system of the dipping technique. The crucible and the holder were made of dense and high purity graphite (apparent density 1.60 gcm^{-3}, ash content of 0.02 %). In order to avoid evaporation of Si, a graphite lid was equipped. The

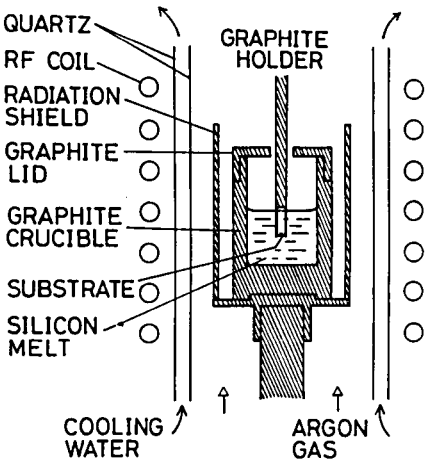

Fig. 1 Growth system for the dipping technique.

crucible and the holder were baked at about 1800°C for 2 h in high purity Ar gas ambient. The crucible was heated inductively, and the temperature of its wall was measured with an optical pyrometer. High purity Si was used for the melt. Silicon lumps were etched with HF and HNO_3 mixture (1:8) and rinsed with deionized water and acetone.

Crystals of 6H SiC grown by Acheson method [9] were used for substrates. The (0001) faces of the crystal were lapped with SiC abrasive powders and polished with diamond paste. The crystal was cut into a dimension of 1×7 mm^2 with thicknesses of 0.2-0.4 mm. The polytype was examined with the x-ray oscillation photography. The surface polarity was identified using the pits by etching in H_2 gas [10] at 1550°C for 20 min. After being cleaned with HF and HNO_3 mixture (1:1), the crystal was rinsed with deionized water and acetone. The substrate was attached to the graphite holder with the (0001) face perpendicular to the holder axis.

After the crucible was heated up to growth temperature and Si lumps were melted, the substrate was dipped. The crystal was hold for 5 h and pulled out before turn off of the input power. The growth was carried out in the flow of pure Ar of 200 cc/min. Silicon melt adhered to the crystal was etched away with HF and HNO_3

mixture (1:1).

2-3. Results of Crystal Growth

In order to obtain flat and smooth epitaxial layers of good quality, crystal growth was carried out under various conditions. In every growth run, two crystals with opposite direction of the surface polarities (Si and C faces) were attached to the holder side by side in order to examine the effect of the direction of the (0001) face. However, no remarkable difference was found between the two grown layers on these two kinds of substrates.

Firstly, the effect of temperature gradient was examined. When temperature difference of 30°C was imposed on the crucible wall with setting the substrate at the low temperature part, the surface of the grown crystal was very rough for both the Si and C faces. The growth rate was 2-3 tmies as much as the case of no temperature difference on the crucible wall. Smooth and flat surfaces were obtained in the case of no intentional temperature difference. Secondly, the position of the substrate in the melt was varied without imposing any intentional temperature gradient. When the substrate was kept near the surface of the Si melt or the bottom of the crucible, the growth rates were about two times as much as the case of setting the substrate at the middle of the melt. The grown surfaces were relatively rough for the former, but were smooth for the latter.

Based on these results, the growth temperature was varied between 1500 and 1650°C imposing no intentional temperature gradient and setting the substrate at the middle of the melt. Figure 2 shows that the growth rate increases with increasing the growth temperature. The growth rate on the C face is 2-3 times as much as that on the Si face at every temperature. The growth rate is expressed as $\exp(-E_a/RT)$ and E_a is about 150 kcal/mol for both the

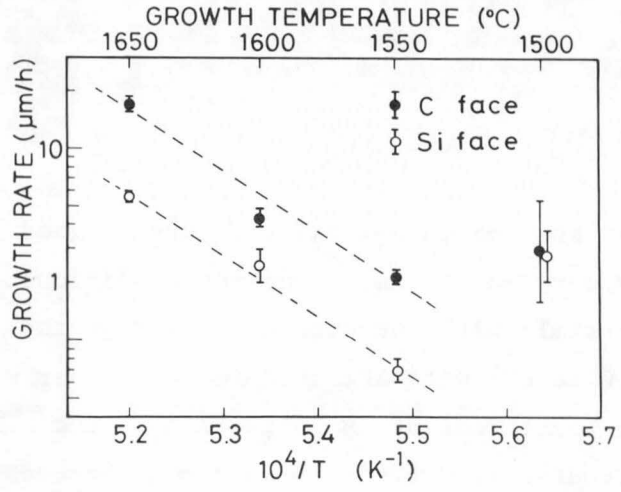

Fig. 2 Growth rate as a function of the growth temperature.

Si and C faces except for the case of 1500°C. In the case of the vapour phase epitaxial growth by sublimation, the activation energies of the Si and C faces were both about 150-170 kcal/mol [11], and the activation energy of the C solubility in the Si melt was about 59 kcal/mol [12]. Therefore, the growth rate may be limited by the surface reaction velocity rather than C solubility in the Si melt. With increasing the growth temperature, the flatness and the smoothness of the grown layers were improved, and the best result was obtained at 1600°C. Figure 3 shows the surfaces of the Si and C faces of the crystal grown at 1600°C. The surface of the Si face was fairly smooth and composed of wavy patterns, while the surface of the C face

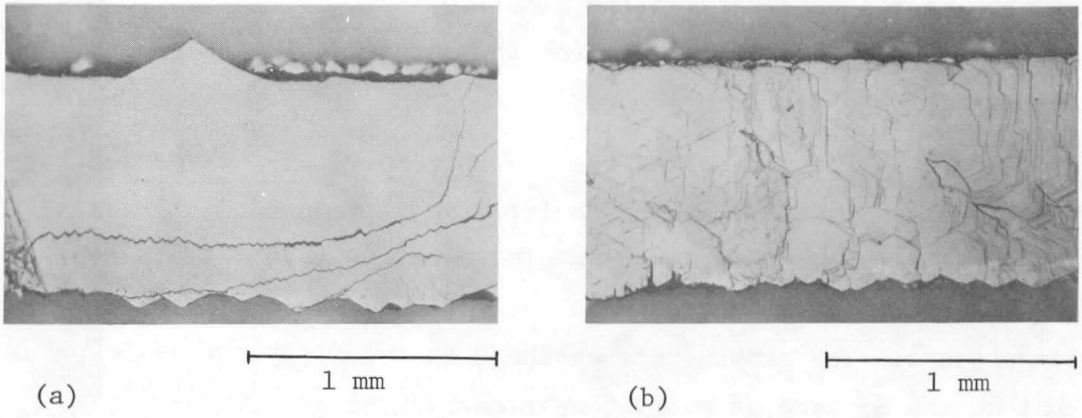

Fig. 3 Surfaces of grown layers at 1600°C; (a) Si face, (b) C face.

was composed of straight lines and hexagonal patterns, and indicated high growth steps.

The polytype of the grown layer was identified with the x-ray oscillation photography around the c-axis and photoluminescence spectra at 77 K (Chapt. IV) [13]. A slight amount of Al metal ($\sim 10^{-2}$ at. %) was added to the Si melt. By these analyses, the layers grown in the range of 1550-1650°C were found to be 6H SiC single crystals. Good quality of the layers were certified from the clear spot patterns of x-ray oscillation photographs. However, some parts of the grown layers at 1500°C was found to be 3C SiC, which may have caused the deviation of the growth rate at 1500°C from the straight line in Fig. 2.

2-4. Electrical Properties of Epitaxial Layers

Epitaxial layers doped with impurities were grown by the dipping technique under the condition determined in Sec. 2-3. Nitrogen was doped as donors and Al as acceptors. Doping of N was carried out by mixing N_2 gas (99.99 %) into Ar gas ($\sim$99.9999 %), and Al was doped by adding Al metal (99.99 %) to the Si melt. Electrical properties of the epitaxial layers were measured by van der Pauw method [14]. The ohmic contact to the n layer was made by alloying Au-Ta (99:1) at 1200°C for a few minutes in Ar gas ambient. For the p layer, Al-Si (89:11) was evaporated and alloyed at 930°C for 5 min in a vacuum lower than 10^{-5} Torr. For the electrical separation, the substrate with conduction type different from the epitaxial layer was used.

Crystals grown by the process described in Sec. 2-2 were n type with very high electron concentration of 5×10^{19} cm^{-3} at room temperature. The donor may be N due to the contamination of the ambient by leaked air. In order to decrease the carrier concentration, the following improvements were made:- (i) Before the growth, the

Table I Electrical properties of epitaxial layers at 300 K.

Sample	Conduction type	Dopant Al (at.%)	N_2 (vol.%)	Carrier concentration (cm^{-3})	Mobility (cm^2/Vsec)	Resistivity (Ωcm)
U1	n	0	0	6.3×10^{17}	130	7.6×10^{-2}
U2[a)]	n	0	0	1.4×10^{18}	48	9.5×10^{-2}
N1	n	0	0.1	5.1×10^{19}	12	1.0×10^{-2}
N2	n	0	0.2	9.0×10^{19}	22	3.2×10^{-3}
A11	n	0.01	0	3.9×10^{17}	94	1.7×10^{-1}
A12	p	0.6	0	———	——	———
A13	p	2.5	0	1.6×10^{18}	13	3.1×10^{-1}
A14	p	5.0	0	4.5×10^{18}	10	1.4×10^{-1}
A15	p	10.0	0	5.2×10^{18}	7	1.7×10^{-1}

[a)]The vacuum before the growth was rather poor (3.4×10^{-4} Torr).

crucible and the holder were baked at 1800°C for 2 h in a vacuum of 1×10^{-5} Torr or less. (ii) After being filled with Si and Al, the crucible was baked at about 600°C for 1 h in the same vacuum before the introduction of Ar gas. By this improvemet, the carrier concentration of the nominally undoped layer decreased to 6.3×10^{17} cm^{-3}. Table I shows the electrical properties of typical layers.

By doping 0.1-0.2 vol % N_2 gas to the Ar gas, strong n type crystals of $n = (5.1\text{-}9.0)\times10^{19}$ cm^{-3} are obtained. These crystals were found to be degenrated from the result of the temperature dependence of Hall measurement. By adding 0.6-10 at. % of Al to the Si melt, p layers with hole concentration up to 5.2×10^{18} cm^{-3} were obtained. Low resistivity p ($\sim10^{-1}$ Ωcm) and n ($\sim10^{-3}$ Ωcm) layers are obtained, which enables to decrease the series resistance of SiC diodes. Mobilites up to 130 cm^2/Vsec are obtained for the n layer, and those of the p layers are about 10 cm^2/Vsec at room temperature.

Figures 4(a)-4(c) show the temperature dependences of carrier concentrations (p,n), resistivities (ρ), and mobilities (μ) of typical

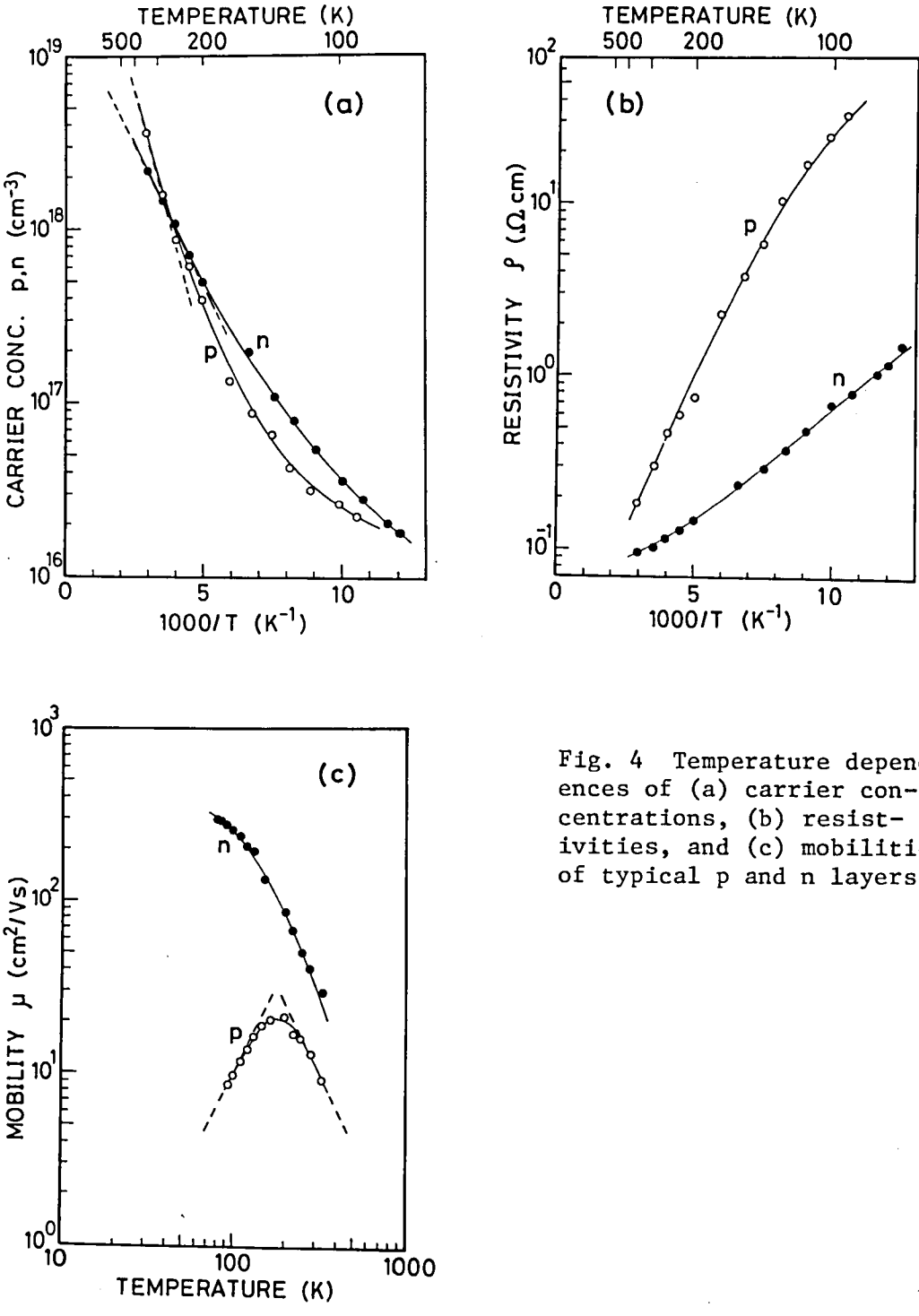

Fig. 4 Temperature dependences of (a) carrier concentrations, (b) resistivities, and (c) mobilities of typical p and n layers.

p type and n type crystals. The carrier concentrations of both samples increase nearly exponentially with decreasing reciprocal temperature. The activation energies of the donor and acceptor are determined to be E_D = 66 meV and E_A = 86 meV from the slopes of the high temperature region in Fig. 4(a), respectively. These values are considerably smaller than those determined by photoluminescence measurements (E_D = 100, E_A = 245 meV) (Chapt. IV) [13] and Hall measurements (E_D = 95, $E_A \simeq$ 240 meV) [15,16]. These small values may be attributed to screenig by the ionized impurities because of the large impurity concentrations of the present crystals. The mobility of the p type crystal varies as $\mu \propto T^{\frac{1}{2}}$ in the low temperature region and $\mu \propto T^{-\frac{1}{2}}$ in the high temperature region in Fig. 4(c). These results indicate that ionized impurity scattering is dominant for the former, and acoustic phonon scattering is dominant for the latter. For the n type crystal, temperature dependence of the mobility is compared with caluculated mobilities due to various scattering mechanisms. The dominant mechanism is acoustic phonon scattering and polar optical phonon scattering in the high temperature region ($T \gtrsim 200$ K), and in the low temperature region mechanism can not be determined, probably piezoelectric scattering or neutral impurity scattering.

2-5. Summary

Epitaxial growth of 6H SiC is carried out with the dipping technique using the Si melt. The condition to obtain good quality epitaxial layers is determined to grow on the Si face at 1600°C imposing no intentional temperature gradient on the crucible wall and setting the substrate at the middle of the Si melt. Hall measurements are carried out on the layers doped with Al acceptors or N donors. The electron concentrations of 6×10^{17}- 9×10^{19} cm^{-3} and hole concentrations of $(2\text{-}5)\times10^{18}$ cm^{-3}, and the electron mobility up to 130 $cm^2/Vsec$ and the hole mobility of about 10

$cm^2/Vsec$ are obtained at room temperature. The temperature dependences of the electrical properties of typical p and n layers are also measured.

References

[1] J. A. Lely, Ber. Dtsch. Keram. Ges. 32, 229 (1955).

[2] R. W. Brander and R. P. Sutton, J. Phys. D2, 309 (1969).

[3] R. W. Brander, Mater. Res. Bull. 4, S187 (1969).

[4] R. W. Brander, Proc. IRE 116, 329 (1969).

[5] A. Suzuki, M. Ikeda, H. Matsunami, and T. Tanaka, J. Electrochem. Soc. 112, 1741 (1975).

[6] A. Suzuki, M. Ikeda, H. Matsunami, and T. Tanaka, J. Appl. Phys. 47, 4550 (1976).

[7] P. W. Pellegrini and J. M. Feldman, in "Silicon Carbide - 1973", edited by R. C. Marshall, J. W. Faust, Jr., and C. E. Ryan (University of South Carolina Press, Columbia, 1974), p. 161.

[8] M. Hori, Bachelor Thesis, Kyoto University, 1977.

[9] See, for example, W. F. Knippenberg, Philips Res. Rep. 18, 161 (1963).

[10] E. Modrak, I. Swiderski, and T. Niemski, J. Cryst. Growth 22, 181 (1974).

[11] I. Swiderdki, J. Cryst. Growth 32, 350 (1976).

[12] R. I. Scace and G. A. Slack, J. Chem. Phys. 30, 1551 (1959).

[13] M. Ikeda, H. Matsunami, and T. Tanaka, J. Lumin. 20, 111 (1979).

[14] L. J. van der Pauw, Philips Res. Rep. 13, 1 (1955).

[15] S. H. Hagen and C. J. Kapteyns, Philips Res. Rep. 25, 1 (1970).

[16] G. A. Lomakina, Yu. A. Vodakov, E. N. Mokhov, V. G. Oding, and G. F. Kholuyanov, Sov. Phys. - Solid State 12, 2356 (1971).

III. EXCITON LUMINESCENCE IN UNDOPED 3C, 4H, 6H, AND 15R SiC

3-1. Introduction

Silicon carbide takes various crystal structures, namely polytypes, according to the stacking in the c-axis direction. The author reported that one impurity atom took many levels in 4H, 6H, and 15R SiC depending on the site which the impurity replaced (Chapt. IV) [1]. The study on the effect of the site on intrinsic property, free exciton, is worthy of research in comparison with the strong effect of the site on extrinsic property, impurity levels. Strong free exciton luminescence was observed in the room temperature electroluminescence in 6H SiC LED's in the author's report (Chapt. VII) [2]. The efficiency of electroluminescence may be affected by free exciton luminescence. In spite of these physical and practical interests, there have been no reports on free exciton recombinations except for 3C SiC [3] and a part of spectrum of 6H SiC [4] at 4.2 K.

Since SiC polytypes have many atoms per unit cell, many phonon branches exist. The phonons determined from the luminescence of bound excitons were explained in terms of the standard large zone (Sec. 4-3-1) [4-11]. There exists only one report for each of the exciton band gaps of 4H [8], 6H [4], and 15R SiC [9]. Therefore, confirmation of these data by other measurements is desirable. The free exciton binding energies of 3C [3,12], 4H [13], and 6H SiC [14] were already reported. However, the free exciton binding energy of 15R SiC, which is a rather abundant polytype, has not yet been reported.

In this chapter, photoluminescence due to free excitons and excitons bound to N donors in 3C, 4H, 6H, and 15R SiC crystals are studied. The energies of phonons associated with free excitons, exciton band gaps, and free exciton binding energies of these

polytypes are determined.

3-2. Sample Preparation

Crystals grown as described in Chapt. II were used for the measurement. The following modifications in the crystal growth were made: - (i) Graphite of high purity (ash content less than 20 ppm, boron content less than 0.1 ppm) was used as a crucible material. (ii) The graphite crucible was baked at about 1950°C for about 8 h until a vacuum of better than 3×10^{-6} Torr was obtained in order to reduce impurities. (iii) After being filled with Si lumps, the crucible was baked at about 1200°C until a vacuum of better than 1×10^{-6} Torr was obtained to remove N from the reaction tube. (iv) The growth temperature and time were 1600-1850°C and 5-8 h, respectively. When growth was carried out at 1850°C, small single crystals grew on the surfaces of the crucible and holder.

Epitaxial layers of 30-200 μm and small single crystals ($\sim$0.7×0.7×0.5 mm^3) of 4H, 6H, and 15R SiC crystals were used for the measurements. For 3C SiC, only small single crystals were used. The polytype was identified by x-ray oscillation photography and photoluminescence. The electron concentration of the epitaxial layers and small single crystal of 6H SiC was 1.0×10^{17} cm^{-3} at room temperature. According to the reports of the temperature dependence of the carrier concentration [15,16], a donor concentration of 3×10^{17} cm^{-3} was estimated. Similar donor concentration may be applied for other polytypes. The donor may be N due to contamination of the ambient from air.

3-3. Optical Measurements

3C SiC crystals were excited with 365 nm light from a suitably filtered 250 W high pressure Hg lamp. Other polytype crystals were excited with 325 nm light from a suitably filtered He-Cd laser of about 10 mW. Spectra were detected using a Ritsu MC-30N monochromator and an H.T.V. R636 photomultiplier. Samples were immersed in liquid helium at 4.2 K, and above 4.2 K natural rise of temperature was utilized. Temperature was monitored by a Chromel vs. Gold-0.7 at. % Iron thermocouple.

3-4. Results and Discussion

3-4-1. Spectra and phonon energies

Figures 1(a)-1(d) show that spectrum of each polytype consists of a series of sharp peaks and broad peaks. Since high resolution was necessary, the obtained signals were rather weak, and signal to noise ratios were small, 4-30. Therefore, spectra were determined by taking the average of the spectra with noise.

At 4.2 K, only sharp lines were observed for each polytype, and these lines coincided with the reports by Choyke, Patrick, and Hamilton (C.P.H.) [4,7-10] who explained these lines to be due to excitons bound to neutral nitrogen donors. With increasing temperature, bound exciton lines on the higher energy side due to nitrogens in hexagonallike sites [17] (P_0 for 3C, 4H, and 6H; P_0 and Q_0 for 15R in Fig. 1) disappeared, and new lines (e.g., R_{02} and S_{02} for 6H) appeared on the higher energy position by about 5 meV than the exciton lines due to nitrogens in cubiclike sites (e.g., R_0 and S_0 for 6H). These new lines were explained to be due to bound excitons associated with spin-orbit splitting of the valence band [4,9]. Simultaneously, a series of broad peaks appeared and became dominant with increasing temperature. These peaks are due

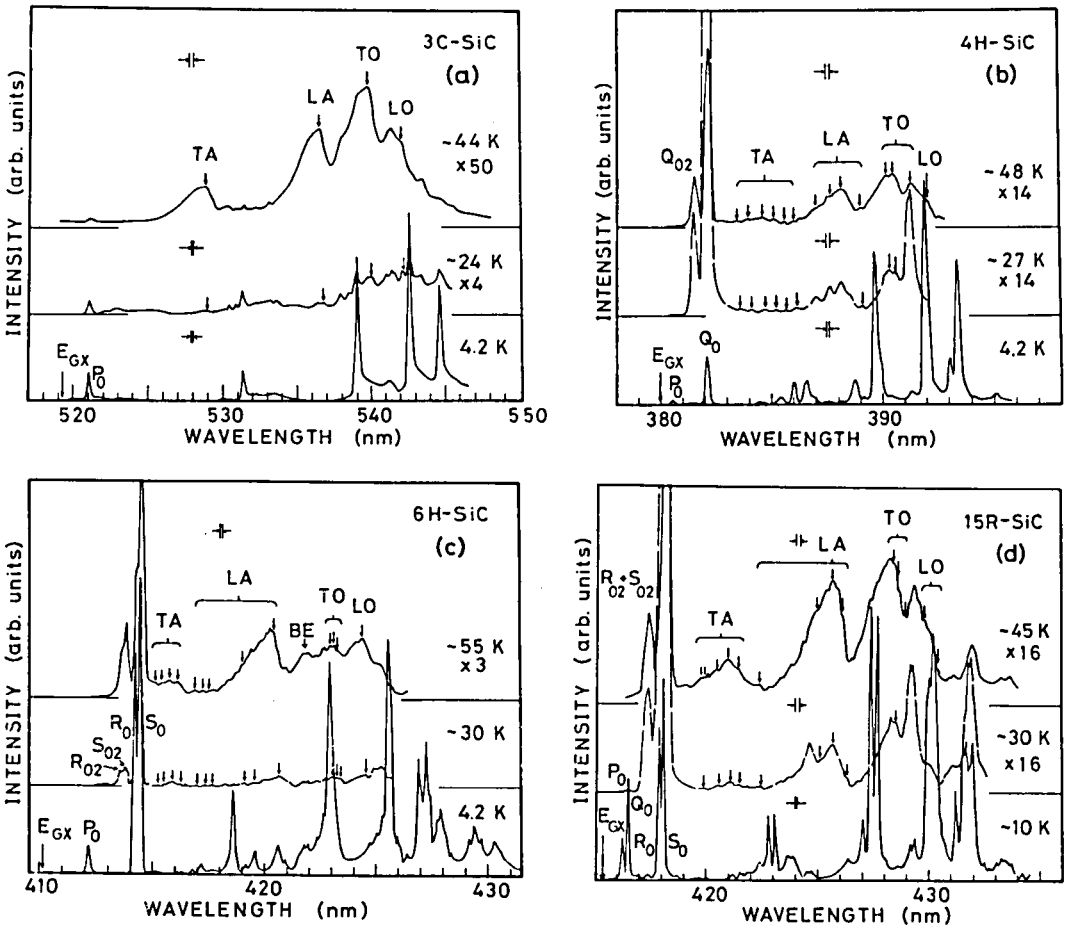

Fig. 1 Excitonic luminescence in (a) 3C, (b) 4H, (c) 6H, and (d) 15R SiC.

to free excitons, because the differences between the exciton band gaps [3,4,7-9] and peak energies nearly coincide with the phonon energies [3,4,7-9].

Many small peaks were observed on the broad free exciton peaks, especially for 4H, 6H, and 15R SiC. These peaks can be phonon replicas of bound exciton and free exciton peaks. When a difference of the energy of the peak and the exciton band gap is taken, some peaks indicate k/2 dependence and the other no dependence as shown in Fig. 2. Free exciton lines indicates k/2

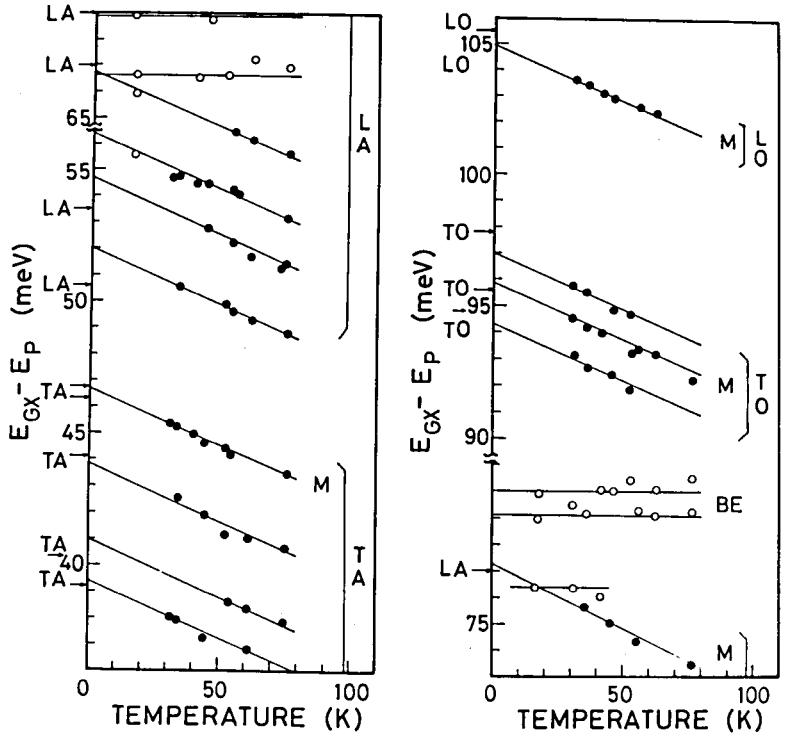

Fig. 2 Temperature dependence of the difference between peak energy (E_p) and the free exciton band gap (E_{GX}) for 6H SiC. The slope of the lines for free exciton peaks (closed circles) is -k/2. The phonon energies reported by C.P.H. are indicated by arrows. The phonon with a letter M is associated with a strong peak (main phonon), and the peak with letters BE correspond to the BE peak in Fig. 1(c).

dependence because of the thermal energy of excitons. By this way we can distinguish free exciton lines and bound exciton lines. Similar analyses were carried out for other polytypes. By extrapolating these lines to T=0, one can obtain phonon energies. The main phonon which is associated with the largest peak in each kind of phonon branch (e.g., TA and so on) is indicated by a letter M. In Fig. 2, the phonon energies associated with bound exciton luminescence reported by C.P.H. [4] are indicated by arrows. Some free exciton lines are hidden by bound exciton lines such as 69.0 meV

Table I Energies of phonons associated with free excitons (F_x) are compared with those associated with bound excitons (N_x) reported by C.P.H. for 4H, 6H, 15R, and 3C SiC in units of meV. The values with underlines are energies of phonons associated with strong peaks (main phonons).

	4H		6H		15R		3C	
	F_x	N_x	F_x	N_x	F_x	N_x	F_x	N_x
	33.9	33.5		33.5	33.9	34.4		
	38.0	37.2		36.3	35.0	35.0		
	40.8	41.4	39.4	39.2	39.2	39.3		
TA	43.5	42.4	41.0	40.3		39.7		
	47.7	46.7	43.8	44.0	42.7	43.2		
	51.0	51.4	46.7	46.3	46.0	46.3	46.3	45.8
	55.3	53.4						
	63.2		52.0	50.6		51.3		
	68.6	68.7	54.7	53.5	52.4	51.9		
LA	72.6	69.7	66.8	67.0		69.2		
		76.9		69.0	70.3	70.2		
	79.4	78.8	77.3	77.0	75.2			
					78.2	78.2	79.5	79.4
	89.7		94.3	94.7	94.2	94.6		
	91.8		95.8	95.6		95.3		
TO		95.0	97.0	97.8	95.5	95.7	94.4	93.7
		96.1			96.7	97.1		
	99.0	96.7						
		104.0		104.2	103.2	103.7	102.8	103.3
LO	104.6	104.3	105.0	105.5		106.3		
		107.0		107.0	107.2	106.9		
		107.4						

phonons of 6H SiC. The large peaks indicated as BE in Fig. 1(c) are bound exciton lines because they indicate no temperature dependences as shown in Fig. 2.

In Table I the energies of phonons associated with the free exciton lines determined by this way and the energies of phonons associated with bound exciton lines reported in the literature [4,7-9] are compared for 3C, 4H, 6H, and 15R SiC. Most of the phonons associated with free excitons have corresponding phonons associated

with bound excitons. However, some phonons associated with free excitons do not have corresponding phonons associated with bound excitons. One example of such phonons is 75.2 meV phonon of 15R SiC, which is associated with one of the main peaks. Although the peak which associates this phonon can be a bound exciton line, no phonon replicas of the bound exciton lines correspond to this peak, and this peak indicates k/2 dependence. Therefore, this phonon is really associated with free excitons. Also is the same case for 63.2, 72.6, 89.7, and 91.8 meV phonons of 4H SiC which have no corresponding phonon associated with bound excitons as in Table I.

From these results the position of the Brillouin zone of the phonons associated with free excitons seem to be different from that associated with bound excitons. This result differs from the reports by C.P.H. [4,5,7-9] that main phonons associated with free excitons and bound excitons in different polytypes have almost the same energy. The selection rules for free exciton and bound exciton transitions seem to be the same, because electrons in the conduction band and holes in the valence band which form excitons recombine in both cases. However, in bound exciton transitions, excitons are more strongly bound to impurities and localized. By this localization the wave functions of electrons and holes of bound excitons may be slightly changed from those in the conduction and the valece bands, and therefore the selection rule may be slightly modified from that of free exciton transitions and different phonon in the Brillouin zone may be associated.

The k/2 dependence of the peak energy of free exciton lines is explained by the spectral shape of the free exciton recombination, $E^{\frac{1}{2}} \exp(-E/kT)$ [18]. For example, the shape of the TA phonon peak of 3C SiC at 77 K was really well explained by this formula.

3-4-2. Exciton band gaps

Table II The exciton band gaps (E_{GX}) of 4H, 6H, and 15R SiC determined from luminescence bands and absorption bands of free exciton transitions associated with various phonons at 77 K with energies in meV. The values of absorption bands and E_{GX} are taken from the reports by C.P.H.

		TA	LA	TO	LO	C.P.H.
4H	Lumi.	3220.7	3191.4	3172.1	3159.4	
	Abs.		3337.3	3357.5	3365.7	
	E_{GX}		3264.4	3264.8	3262.6	
	E_{GX}:av		E_{av} = 3263.9			3263.9
6H	Lumi.	2979.5	2946.0	2927.5	2918.4	
	Abs.		3097.8	3117.5	3126.7	
	E_{GX}		3021.9	3022.5	3022.5	
	E_{GX}:av		E_{av} = 3022.3			3023.3
15R	Lumi.	2942.4	2909.9	2891.0	2881.9	
	Abs.		3061.8	3080.3	3084.9	
	E_{GX}		2985.8	2985.6	2983.4	
	E_{GX}:av		E_{av} = 2984.9			2985.1

The exciton band gaps (E_{GX}) of 4H [8], 6H [4], and 15R SiC [9] were determined by taking the average of phonon emitting and phonon absorbing free exciton absorption by C.P.H. However, the free exciton absorption spectra were broad and only phonon emitting processes were significant at 77 K. Therefore, a confirmation by other method seems to be desirable. The exciton band gaps at 77 K were estimated using free exciton luminescence of our data and phonon emitting free exciton absorption by C.P.H. The threshold of luminescence was estimated from the peak energy as $E_{GX} - \hbar\omega = h\nu_p - \frac{1}{2}kT$, because the temperature dependence indicated such a characteristics. Here, $\hbar\omega$ and $h\nu_p$ are the energies of the phonon and the peak of the luminescence, respectively. The results are shown in Table II. LA, TO, and LO phonon peaks were used to determine the exciton band gaps, since TA phonon peaks were not reported by C.P.H. The scattering of the values might be caused by

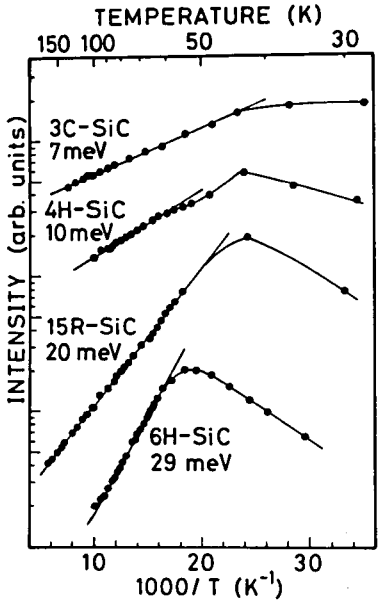

Fig. 3 Temperature dependences of free exciton luminescence intensities of 3C, 4H, 6H, and 15R SiC.

the discrepancy in assigning the main phonons among same kind of phonons (e.g., LA phonons) which is dominant in absorption measurement by C.P.H. and this luminescence measurement. However, the average values agree fairly well with the reported data within experimental uncertainty (± 1 meV) and the error in reading C.P.H.'s data. Therefore, the exciton band gaps of these polytypes might be considered to be established.

3-4-3. Free exciton binding energies

Figure 3 shows the dependences of free exciton luminescence intensities on temperature for 3C, 4H, 6H, and 15R SiC. The intensities take maxima at 30-50 K and maximum temperature tends to increase with the increase of the exciton binding energy. The activation energies obtained are 7 meV for 3C, 10 meV for 4H, 20 meV for 15R, and 29 meV for 6H SiC. These values are about half of the reported values of 14 meV [3,12] for 3C, 20 meV [13] for 4H, and 78

meV [14] for 6H SiC. This half value may be caused by the interference by the defect luminescence [19] (for 6H SiC, see Fig. 15 in Chapt. VII). Therefore, the free exciton binding energy of 15R SiC is expected to be about 40 meV. The intensities of the defect spectra, which have been explained to be due to divacancies [19-22] are more than 100 times as strong as those of free exciton luminescence for the present crystals at 77 K.

3-5. Summary

Photoluminescence due to free excitons and excitons bound to neutral nitrogen donors in 3C, 4H, 6H, and 15R SiC are studied in the temperature range of 4.2 and about 100 K. The energies of phonons associated with free excitons are compared with those associated with bound excitons for these polytypes. Slight difference is found between these energies, which is attributed to the difference of the position in the Brillouin zone where these two kinds of phonons associate. The exciton band gaps at 77 K of these polytypes are determined, and the free exciton binding energies are estimated from the activation energies of thermal quenchings of the free exciton luminescence.

References

[1] M. Ikeda, H. Matsunami, and T. Tanaka, J. Lumin. 20, 111 (1979).

[2] M. Ikeda, T. Hayakawa, S. Yamagiwa, H. Matsunami, and T. Tanaka, J. Appl. Phys. 50, 8215 (1979).

[3] D. S. Nedzvetskii, B. V. Novikov, N. K. Prokofeva, and M. B. Reifman, Sov. Phys. - Semicond. 2, 914 (1969).

[4] W. J. Choyke and L. Patrick, Phys. Rev. 127, 1868 (1962).

[5] W. J. Choyke, Mater. Res. Bull. 4, S141 (1969).

[6] L. Patrick, D. R. Hamilton, and W. J. Choyke, Phys. Rev. 143, 526 (1966).

[7] W. J. Choyke, D. R. Hamilton, and L. Patrick, Phys. Rev. 133, A1163 (1964).

[8] L. Patrick, W. J. Choyke, and D. R. Hamilton, Phys. Rev. 137, A1515 (1965).

[9] L. Patrick, D. R. Hamilton, and W. J. Choyke, Phys. Rev. 132, 2023 (1963).

[10] D. R. Hamilton, L. Patrick, and W. J. Choyke, Phys. Rev. 138, A1472 (1965).

[11] W. J. Choyke, D. R. Hamilton, and L. Patrick, Phys. Rev. 139, A1262 (1965).

[12] V. A. Kiselev, B. V. Novikov, M. M. Pimonenko, amd E. B. Shadrin, Sov. Phys. - Solid State 13, 926 (1971).

[13] G. B. Dubrovskii and V. I. Sankin, Sov. Phys. - Solid State 17, 1876 (1976)

[14] V. I. Sankin, Sov. Phys. - Solid State 17, 1191 (1975).

[15] S. H. Hagen and C. J. Kapteyns, Philips Res. Rep. 25, 1 (1970).

[16] G. A. Lomakina, Yu. A. Vodakov, E. N. Mokhov, V. G. Oding, and G. F. Kholuyanov, Sov. Phys. - Solid State 12, 2356 (1971).

[17] L. Patrick, Phys. Rev. 127, 1878 (1962).

[18] C. D. Mobsby, E. C. Lightowlers, and G. Davies, J. Lumin. 4, 29 (1971).

[19] V. V. Makarov, Sov. Phys. - Solid Stake 9, 457 (1967).

[20] W. J. Choyke and L. Patrick, Phys. Rev. B4, 1843 (1971).

[21] L. Patrick and W. J. Choyke, Phys. Rev. B5, 3253 (1972).

[22] P. J. Dean, D. Bimberg, and W. J. Choyke, in "Defects and Radiation Effects in Semiconductors 1978", edited by J. H. Albany (The Institute of Physics, Bristol and London, 1979), p. 447.

IV. PHOTOLUMINESCENCE IN 3C, 4H, 6H, AND 15R SiC DOPED WITH DONORS AND ACCEPTORS: SITE EFFECT ON IMPURITY LEVELS

4-1. Introduction

SiC takes many crystal structures, namely polytypes, which are classified by the stacking sequence and cycle along the c-axis direction. Owing to long unit cells, many inequivalent sites exist for 4H, 6H, and 15R SiC in contrast to one kind for 3C SiC (zinc-blende) [1]. Figure 1 illustrates inequivalent sites, for example, in 6H SiC. The inequivalent sites are divided into two kinds. One is cubiclike arrangement of first and second neighbour atoms (B atom in the sequence of ABC in the close packed structure) and the other is hexagonallike arrangement (B atom in the sequence of ABA). The stacking sequence in the c-axis direction and the number of cubic-like and hexagonallike sites are given for 2H, 3C, 4H, 6H, and 15R SiC in Table I.

These inequivalent sites are expected to cause site dependent impurity levels. There have been a few reports which imply the existence of site dependent donor levels of N. Choyke, Patrick, and Hamilton [2-7] reported that the number of zero-phonon lines of bound exciton luminescence of N donors agreed with the number of inequivalent sites in various SiC polytypes (Chapt. III). Lomakina et al. [8] reported that in order to explain the results of Hall measurements of annealed 6H and 15R SiC second N donor levels were necessary. Colwell et al. [9] and Dean et al. [10] proposed that three extra Raman scattering lines in heavily N-doped 6H SiC were due to three donor levels of N in inequivalent sites. Although the existence of site dependent donor levels seems to be sure, the values of site dependent donor levels still remain uncertain, and systematic study on various polytypes has not been carried out yet.

Table I SiC polytypes with two common notations and numbers of inequivalent sites.

Ramsdell notation	ABC notation	No. of inequivalent sites hexagonallike	cubiclike
2H(wurzite)	AB	1	0
3C(zincblende)	ABC	0	1
4H	ABAC	1	1
6H	ABCACB	1	2
15R	ABCACBCABACABCB	2	3

In contrast to a number of reports on N donors, there had been no reports on site dependent acceptor levels. Recently Gorban et al. [11] proposed that excitons bound to B acceptors in 6H and 15R SiC took many different levels depending on the inequivalent site from a study of absorption. However, there have been no reports on levels of acceptors in inequivalent sites.

In this chapter, photoluminescence of 3C, 4H, 6H, and 15R SiC doped with Al, Ga, or B acceptors and N donors are studied. From the comparative study of these polytypes and impurities, general existence of the site dependent donor and acceptor levels is verified. The donor and acceptor ionization energies in 4H, 6H, and 15R SiC are determined from the analyses of the luminescence. Explanation of the origin of the site effect on the impurity levels is tried based on the quantum defect model. The site effect is well

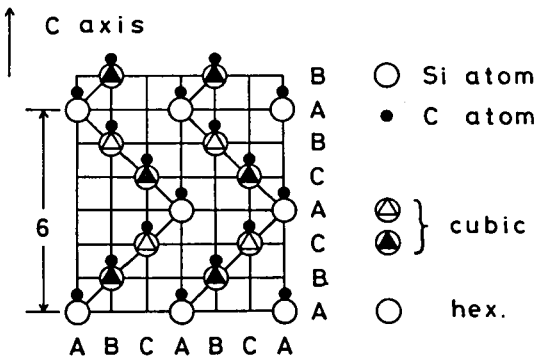

Fig. 1 The arrangement of Si and C atoms in the $(11\bar{2}0)$ plane in 6H SiC. The sites of atoms are denoted by A, B, and C in the close packed structure.

explained by assuming local physical constants around hexagonallike or cubiclike sites. The result of this analysis predicts the existence of the site dependent impurity levels extensively in other polytype SiC crystals and furthermore in other materials. Though many materials such as ZnS and AgI indicate polytypism, there have been no reports on site dependent impurity levels except for SiC, and no reports on the origin of this effect.

SiC crystals doped with Al acceptors and N donors emit bright visible luminescence due to donor-acceptor (D-A) pair transitions. The spectra of these luminescence in 4H and 6H SiC were reported to be composed of two kinds of series peaks [12-14]. Two different explanations have been given for these two series, and the donor levels determined in their reports differ as much as 100 meV each other. Gorban et al. [12] and Suzuki et al. [13] explained that these two series in 4H and 6H SiC were zero phonon lines and their LA phonon replicas. Hagen et al. [14] explained them to be due to two kinds of donor levels associated with cubiclike and hexagonallike sites. In this chapter, confirmation that these two series are due to site dependent donor levels is tried by studying the configuration coordinate phonons of 3C, 4H, 6H, and 15R SiC.

4-2. Experimental Procedure

4-2-1. Sample preparation

Crystals studied were epitaxial layers of 6H and 15R SiC ($\simeq$ 100 -300 μm) and small single crystals of 3C, 4H, 6H, and 15R SiC ($\simeq$ 0.7 $\times$0.7$\times$0.5 mm^3). The growth procedure was the same as described in Chapt. III except that evacuation of the growth system after being assembled was carried out at room temperature without heating in order to avoid evaporation of dopant. Acceptor materials were Al

metal (99.999 %), Ga metal (99.9999 %), B powders (99.5 %) and B_4C powders (99.9 %). Donors were doped by using high purity Ar gas (99.999 %) mixed with 0.2 vol % N_2 gas.

The carrier concentration was measured by van der Pauw method at room temperature, and donor and acceptor concentrations were estimated using the temperature dependence of the carrier concentration in the literatures [15-18]. This measurement was carried out only for epitaxial layers of 6H SiC and the same value was assumed for 3C, 4H, and 15R SiC grown in the same growth run. The nominally undoped crystals were n type of $n = 1.0\times10^{17}$ cm^{-3} (estimated donor concentration, $N_D \simeq 3\times10^{17}$ cm^{-3}), which may be due to nitrogen contamination of the ambient from air. The crystal doped with 5×10^{-5} vol % N_2 gas had $n = 4.2\times10^{17}$ cm^{-3} ($N_N \simeq 1\times10^{18}$ cm^{-3}). The crystals doped with 0.015-2.1 at. % Al metal had $p = 3.5\times10^{16}$-2.7×10^{18} cm^{-3} ($N_{Al} \simeq 1\times10^{18}$-$1\times10^{20}$ cm^{-3}). The amount of Ga metal was 0.5-10 at. %, and $p = 5.6\times10^{15}$ cm^{-3} ($N_{Ga} \simeq 1\times10^{18}$ cm^{-3}) for a 2 at. % Ga-doped sample and $p = 7.1\times10^{16}$ cm^{-3} ($N_{Ga} \simeq 6\times10^{18}$ cm^{-3}) for a 10 at. % Ga-doped sample. The amount of B was 0.02-0.5 at. %, and $p = 1.2\times10^{15}$ cm^{-3} ($N_B \simeq 5\times10^{18}$ cm^{-3}) for a 0.02 at. % B-doped sample [19]. The polytype was identified with x-ray oscillation photography and photoluminescence.

4-2-2. Optical measurements

Most of the procedures were the same as those described in Chapt. III. For weak excitation, weak light of near the absorption edge from a Xe lamp monochromated by a Ritsu MC-20 monochromator was used. The raw spectra were normalized for the system response using an EOAL-101 standard lamp. Samples were immersed in liquid helium or nitrogen, or a cryostat with a heater was used. The temperature was monitored by a chromel-alumel thermocouple.

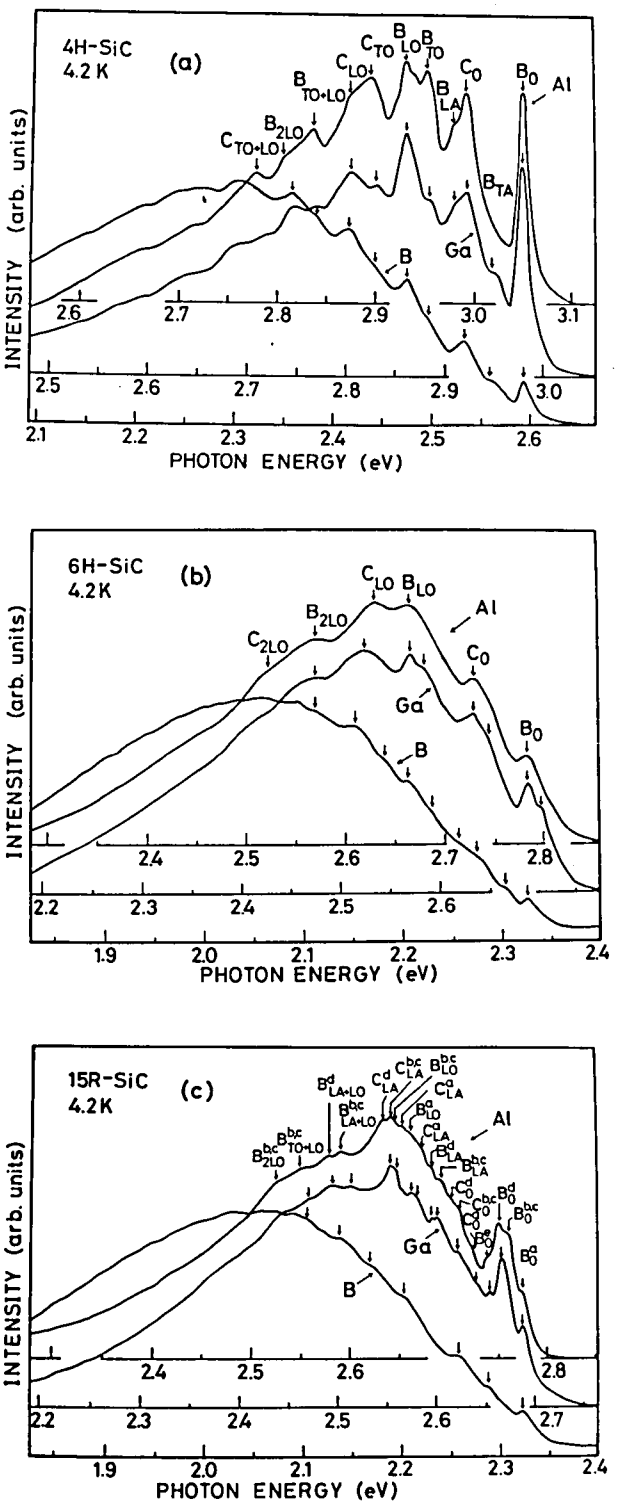

Fig. 2 Photoluminescence spectra of Al-doped, Ga-doped, and B-doped crystals of (a) 4H, (b) 6H, and (c) 15R SiC at 4.2 K. Subscripts indicate the kinds of phonons and superscripts indicate the kinds of sites which acceptors replaced.

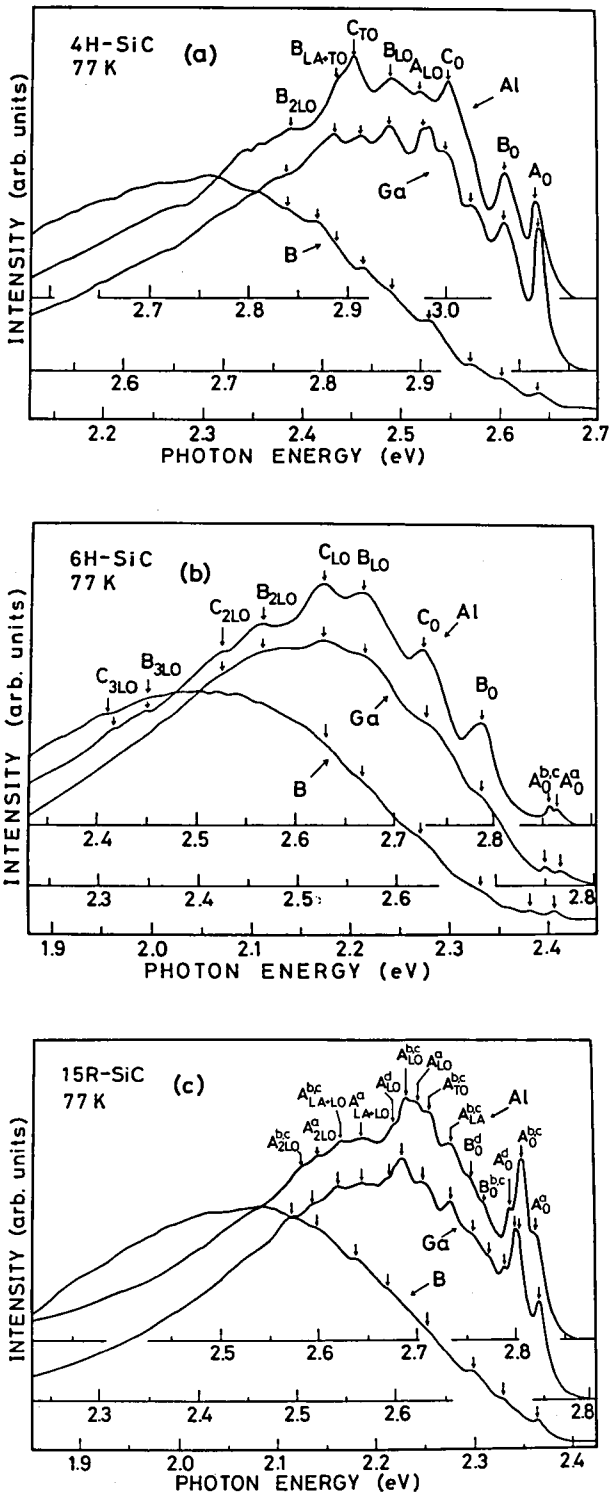

Fig. 3 Photoluminescence spectra of Al-doped, Ga-doped, and B-doped crystals of (a) 4H, (b) 6H, and (c) 15R SiC at 77 K. Subscripts indicate the kinds of phonons and superscripts indicate the kinds of sites which acceptors replaced.

4-3. Results and Discussion

4-3-1. General spectra

Figures 2(a)-2(c) show photoluminescence spectra of 4H, 6H, and 15R SiC doped with moderate amount of Al, Ga, or B acceptors and N donors under low excitation at 4.2 K. Since the assignment of the spectra of 3C SiC has been established by extensive researches [20-25], results on 3C SiC are not shown here. The spectra are adjusted at zero phonon peaks. These spectra are composed of two series of peaks B and C which are due to D-A pair transitions (Sec. 4-3-3). Another peaks A, due to free-to-acceptor transitions (Sec. 4-3-4), appear at 77 K as shown in Figs. 3(a)-3(c) for 4H, 6H, and 15R SiC. The relative intensity of A peaks to B and C peaks varies from polytype to polytype and has a relation 15R>3C$\backsim$4H>6H. For the spectrum of 15R SiC at 77K almost all the peaks are A peaks. The values of the ionization energy of donors have a relation 6H>4H$\gtrsim$15R>3C and those of acceptors are almost equal as in Sec. 4-4. Therefore, this difference of the relative intensity may be due to the difference of the oscillator strength of the transitions between the conduction band and acceptor levels because of the difference of the conduction band structure in various polytypes. Each of D-A pair and free-to-acceptor peaks is composed of many smaller peaks, which seems to be caused by the same origin, because the separation energy is almost same. The numbers of these peaks are one for 3C and 4H, two for 6H, and three or four for 15R SiC. The number of peaks increases with the increase of the number of inequivalent sites (see Table I).

Figures 2 and 3 show that the phonon replicas in the spectra of the samples doped with different acceptors are similar. The tentative phonons are indicated in the figures. Both D-A pair and free-to-acceptor peaks can be explained by assuming phonons common to all polytypes. The phonons are TA$\simeq$28, LA$\simeq$68, TO$\simeq$95, and two kinds of LO

phonons of ≃107 and ≃118 meV. These values are in good agreement with the values determined by lattice absorption of 6H and 15R SiC [26], and by Raman scattering of 3C, 4H, 6H, 15R, and 21R SiC [27]. Phonons of nearly same energy exist for various polytypes [27], because the Brillouin zone of these polytypes can be expressed by one standard large zone, which corresponds to that of wurzite (2H), by extending each normal Brillouin zone until the large zone in the c-axis direction. The values of all the phonons observed here agree with those of phonons at Γ point reported by Feldman et al. [27]. Two values of LO(Γ) phonon energies of ≃120 and ≃104 meV exist at zone center and zone edge of the extended standard large zone, respectively [27]. For 3C SiC phonon energies of LO(X) = 106 and LO(Γ) = 120 meV were assigned for the phonon replicas in the luminescence by Long et al. [20]. However, the location of the conduction band minimum varies from polytype to polytype [5,28-30], and LO≃107 meV is commonly observed for 3C, 4H, 6H, and 15R SiC. Therefore, the 107 meV phonon seems to be more reasonably assigned to be LO phonon at Γ point. For 4H SiC, TA phonon lines are obseved in both Ga-doped and B-doped samples, but it is very weak in Al-doped samples as in Fig. 2(a). Similar results were reported for 3C SiC [20-22].

4-3-2. Free-to-acceptor spectra

A peaks emerged at tempetatures slightly below 77 K on the higher energy side of B_0 peaks. A peaks broadened and became dominant over B_0 peaks with increasing temperature, and indicated no shifts with the change of the excitation intensity. These characteristics are similar to free-to-acceptor transitions reported for 3C SiC [22-25].

Free-to-acceptor transitions are expressed by the function of electron kinetic energy [31] as

$$I(E_K) = N_A^0\, n(E_K)\, \sigma(E_K)\, v_{th}. \qquad (1)$$

Here, N_A^0 is the concentration of neutral acceptors, $n(E_K)$ the concentration of free electrons of kinetic energy E_K, and v_{th} the thermal velocity of the electrons. $\sigma(E_K)$ is the cross section for radiative capture of a free electron by a neutral acceptor, and is given as [32]:

$$\sigma(E_K) = C_1(E_K + E_G - E_A)^2/E_K^{1/2} \simeq C_2 E_K^{-1/2}, \qquad (2)$$

because $E_G - E_A >> E_A$. By expressing $n(E_K)$ and v_{th} as functions of E_K, Eq. (1) is transformed into the following relation,

$$I(E_K) = CE_K^{1/2}\exp(-E_K/kT). \qquad (3)$$

From Eq. (3), peak energy E_p is given by

$$E_p = E_{GX} + E_X - E_A + \tfrac{1}{2}kT, \qquad (4)$$

where E_{GX} is the exciton band gap and E_X is the free exciton binding energy. Because of the existence of inequivalent sites given in Table I, many acceptor levels (E_A^i) are expected. In this case, Eq. (1) is transformed into,

$$I(E_K) = C \sum_i E_{Ki}^{1/2} \exp(-E_{Ki}/kT), \qquad (5)$$

where $E_{Ki} = h\nu - E_{GX} - E_X + E_A^i$ and $h\nu$ is the energy of emitted light.

The temperature dependences of $E_{GX} - E_p$ for A_0 peaks of Ga-doped and B-doped 4H SiC, Ga-doped 15R SiC, and Al-doped and Ga-doped 6H SiC are shown in Figs. 4(a)-4(e). The values of E_{GX} were taken from reports [5-7], and these values were confirmed by free exciton luminescence measurements at 77 K (Chapt. III). $E_{GX} - E_p$ indicates k/2 dependence for all the polytypes, 3C [22], 4H, 6H, and 15R SiC doped with Al or Ga acceptors within experimental uncertainty. As for B acceptors, 4H SiC indicated nearly k/2 dependence [Fig. 4(b)]. In the case of B-doped 6H and 15R SiC crystals, $E_{GX} - E_p$ did not indicate clear linearity with temperature, which might be due to their broad peaks and due to interference by the defect luminescence

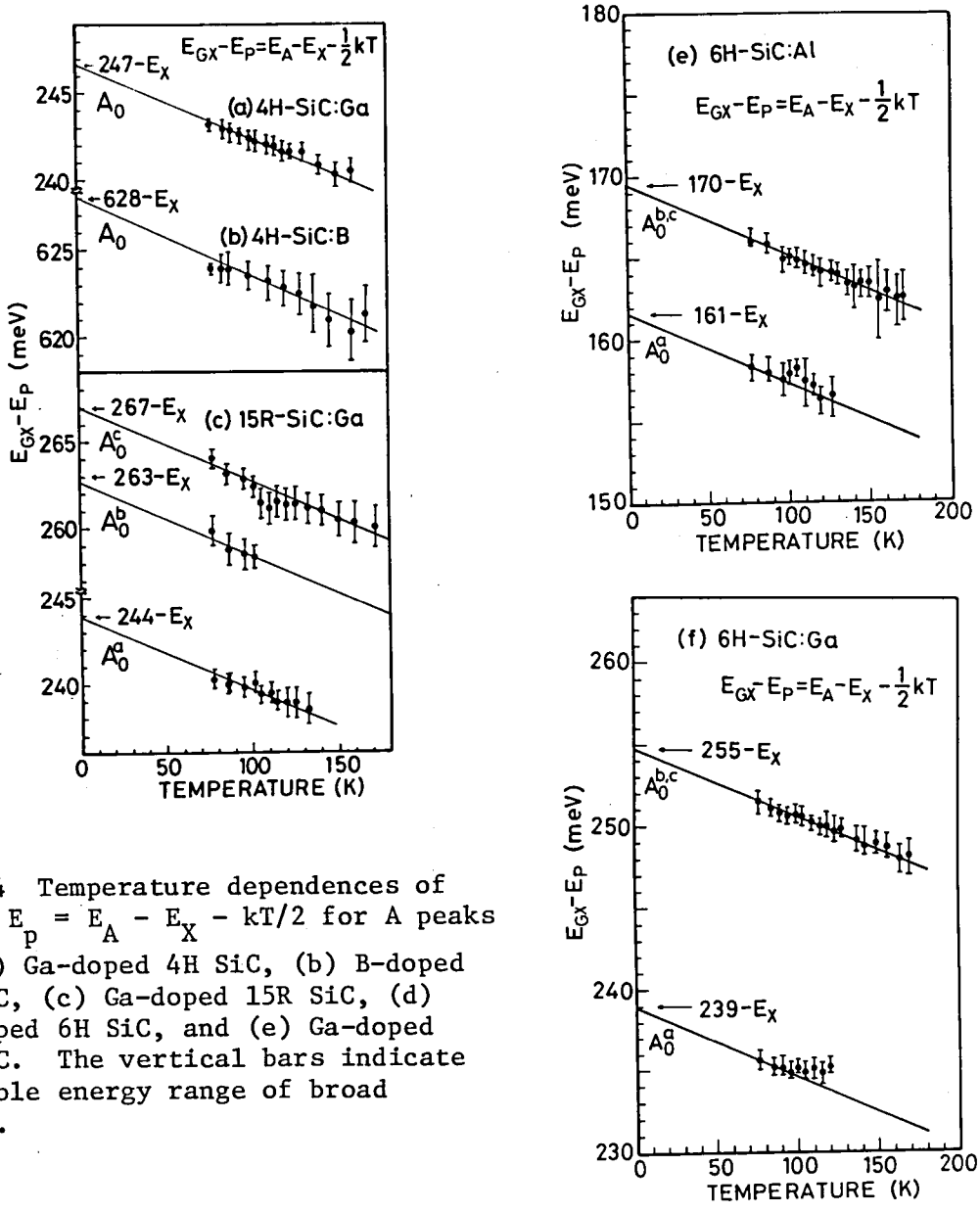

Fig. 4 Temperature dependences of $E_{GX} - E_p = E_A - E_X - kT/2$ for A peaks of (a) Ga-doped 4H SiC, (b) B-doped 4H SiC, (c) Ga-doped 15R SiC, (d) Al-doped 6H SiC, and (e) Ga-doped 6H SiC. The vertical bars indicate possible energy range of broad peaks.

[33] on the higher energy side of A_0 peaks. When we dared to estimate the slope from the linear part of the line, the slopes for B-doped 6H and 15R SiC crystals were about k/2 or less. Kuwabara et al. [25] reported a slope of 0.7k for B-doped 3C SiC. Though the slope can be varied by the kinetic energy dependence of $\sigma(E_K)$, we

take k/2 dependence for B-doped 4H, 6H, and 15R SiC considering the experimental results. We can determine site dependent acceptor levels from extrapolation of the $E_{GX} - E_p$ line to T=0 as indicated in Fig. 4.

Figures 5(a)-5(f) show comparison of observed spectra and theoretical curves given by Eq. (5). Good agreements are obtained for 3C [22,24], 4H, and 6H SiC doped with Al or Ga acceptors. For 4H SiC, two site dependent acceptor levels exist, but only one impurity level is assumed in the calculation. From the good agreements in

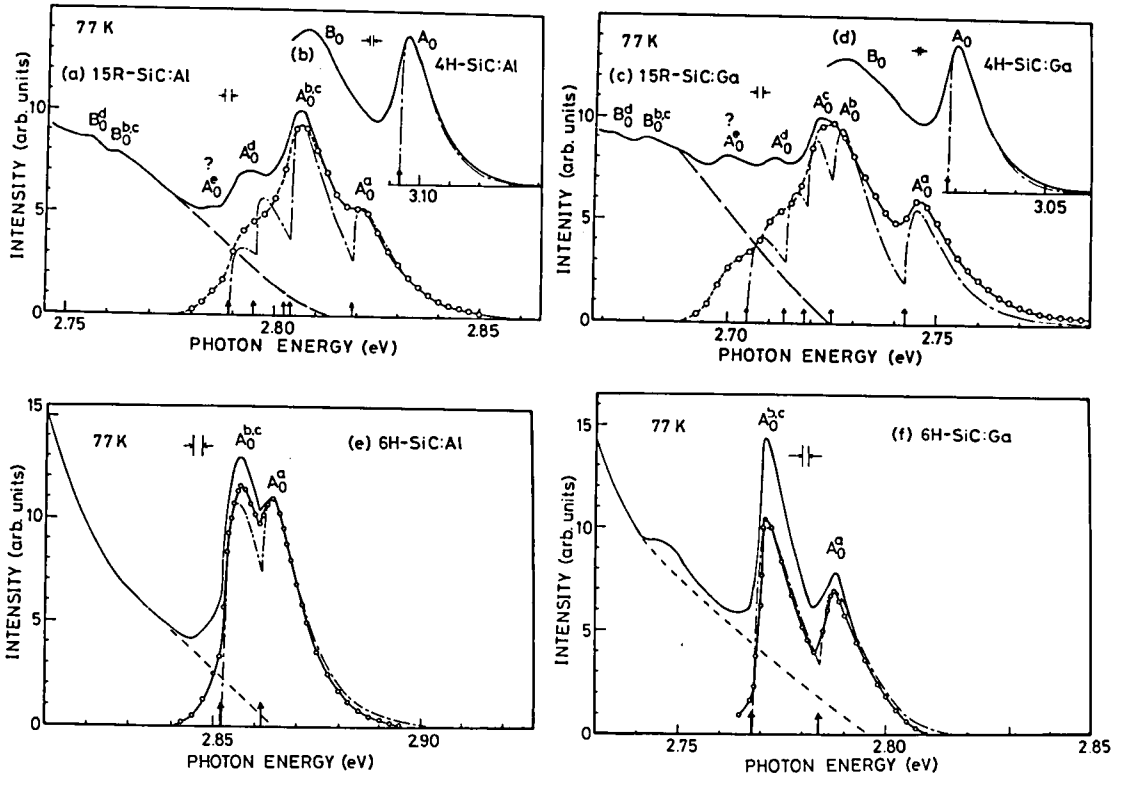

Fig. 5 Comparison of experimental spectra and the calculated spectra at 77 K for (a) Al-doped 15R SiC, (b) Al-doped 4H SiC, (c) Ga-doped 15R SiC, (d) Ga-doped 4H SiC, (e) Al-doped 6H SiC, and (f) Ga-doped 6H SiC. Lines with open circles of 6H and 15R SiC indicate spectra of A_0 peaks after subtracting the background D-A pair spectra assumed as dashed lines. The dot-dash lines indicate calculated spectra using Eq. (5) with $E_A^i - E_X$ indicated by arrows.

Figs. 5(b) and 5(d), two inequivalent acceptor levels in 4H SiC are considered to be close each other, probably within ±1 meV of experimental uncertainty. For 6H SiC, the impurity levels due to two cubiclike sites are assumed to be equal in the calculation. The good agreements between the experimental spectra after subtracting the background D-A pair spectra and calculated ones in Figs. 5(e) and 5(f) imply that two acceptor levels due to cubiclike sites in 6H SiC are close each other, probably within ±1 meV. As to 15R SiC, spectra are complicated. A_0^a, A_0^b, A_0^c, and A_0^d peaks in Fig. 5 seem to be due to free-to-acceptor transitions. Based on the positons of $B_0^{b,c}$ and B_0^d peaks, A_0^e peak seems to be overlapped with B_0^a peak for both Al-doped and Ga-doped 15R SiC. [A_0^e peak can be also considered as TA phonon replica of $A_0^{b,c}$ (or A_0^b and A_0^c) peaks. However, the intensity of TA phonon replica is generally very weak compared with that of the zero phonon line and the separation energy of 21 meV in the spectrum differs from the value determined in Sec. 4-3-1, TA≃28 meV. Therefore, this does not seem to be the case.] Since it is difficult and uncertain to properly estimate the buried B_0^a peaks, the background D-A pair spectra are assumed as simple lines in the figures. For the curves after subtracting the background D-A pair spectra from the observed spectra, best fits are obtained for both Al-doped and Ga-doped 15R SiC crystals. Five inequivalent acceptor levles are assigned so that best fits are obtained for both free-to-acceptor and D-A pair spectra (Sec. 4-3-4). The values of shallower three acceptor levels can be assigned with relatively high accuracy (±2 meV), but the accuracy of the values of deeper two acceptor levels seems to be rather bad, probably ±7 meV. The agreement of the acceptor levels determined from the temperature dependence of $E_{GX} - E_p$ and those by curve fitting, is within ±1 meV for 3C, 4H, and 6H SiC, but those of 15R SiC differ about ±2 meV. For B-doped 4H, 6H, and 15R SiC crystals, curve fitting was not tried, because free-to-acceptor luminescence and defect luminescence were overlapped, and the background defect spectrum could not be properly determined.

For B-doped 15R SiC, only two of five peaks are distinguished [Fig. 3(c)].

The free exciton binding energies were reported to be 13.5 [34] and 14 meV [35] for 3C SiC, 20 meV for 4H SiC [36], and 78 meV for 6H SiC [37]. The free exciton binding energy of 15R SiC is estimated to be 40 meV from thermal quenching of the free exciton luminescence (Chapt. III). The acceptor ionization energies determined using $E_A - E_X$ from the curve fitting and the free exciton binding energies E_X, are given in Table II. Considering the results of acceptors in 6H SiC and donors in 4H, 6H, and 15R SiC (Sec. 4-3-4), deeper three levels are considered to belong to the cubiclike sites for 15R SiC. The ionization energies of B acceptors are determined from the peak energy at 77 K using Eq. (4). The determined ionization energies of Al acceptors are in good agreement with those determind by Hall measurements of lightly doped samples, 230-250 meV for 6H SiC [14], and about 240 meV for 4H, 6H, and 15R SiC [16].

4-3-3. D-A pair spectra

At 4.2 K, A series peaks disappeared and only B and C series peaks were observed. B and C series peaks shifted to the higher energy side and broadened with increasing excitation intensity (for example, Fig. 6) [38], and became broad and shifted to the higher energy side with the increase of the donor and acceptor concentrations. Line spectra due to close pairs were observed (not shown) [39] on the higher energy side than the broad spectra due to distant pairs, in all the crystals of 3C, 4H, 6H, and 15R SiC doped with small amount of donors and acceptors. Peak shifts in the time-resolved spectra were reported for Al-doped 4H and 6H SiC [14], Al-doped and Ga-doped 4H SiC [13], and Al-doped [20] and B-doped [22] 3C SiC. All these characteristics indicate that B and C series are

Table II Ionization energies of donors and acceptors in cubiclike sites (E^C) and hexagonallike sites (E^H), their average ratios, and free exciton binding energies (E_X) in 3C, 4H, 6H, and 15R SiC.

	Site	Ionization energy (meV) N	Al	Ga	B	E_X
3C[a]	C	56.5	254	343	735	13.5[b]
6H	C	155	249	333	723	78[c]
	H	100	239	317	698	
	E^C/E^H	1.55	1.040	1.050	1.036	
15R	C	112	236 230 223	320 311 305	700	40
	H	64	221 206	300 282	666	
	E^C/E^H	1.75	1.076	1.072		
4H	C	124	191	267	647	20[d]
	H	66				
	E^C/E^H	1.88	1.0	1.0	1.0	

a) Refs. 21, 22, and 25.
b) Refs. 34 and 35.
c) Ref. 37.
d) Ref. 36.

due to D-A pair transitions.

In addition to these ordinary characteristics of D-A pair transitions, peak intensity ratio of B and C peaks indicated strong dependence on the excitation intensity and the concentration of acceptors. Figure 6 shows that B series peaks of Al-doped slightly p-type 4H SiC decrease more rapidly than C series peaks with decreasing excitation intensity at 4.2 K. Pairs of peaks resolved in this figure (e.g., C_0 and B_1, B_2 and B_3) have been probably considered to be single peaks in the reports by Suzuki et al. [13] and Hagen et al. [14] and therefore their assignment of peaks is different from the present one. At 77 K, A and B series peaks quench more

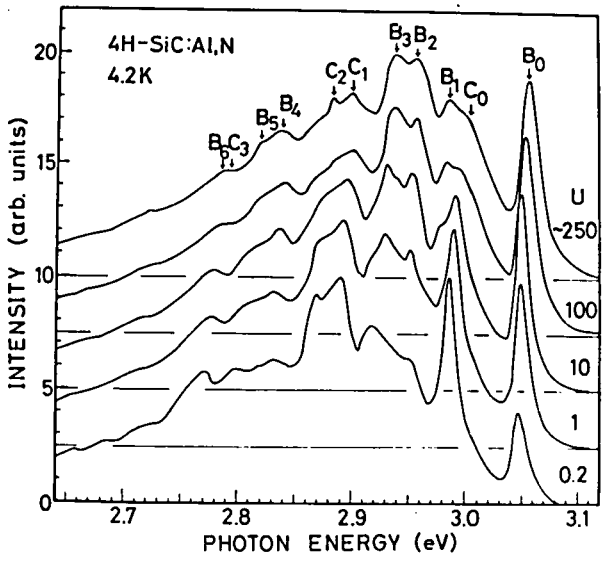

Fig. 6 Photoluminescence spectra of Al-doped slightly p-type 4H SiC at various excitation intensities (U) at 4.2 K.

rapidly than C series peaks and finally disappear with decreasing excitation intensity for 4H, 6H, and 15R SiC in Figs. 7(a)-7(c). With increasing Al concentration, B series peaks become weaker compared with C series and finally disappear. Figures 8(a)-8(c) compare spectra of slightly Al-doped samples under strong excitation and highly Al-doped samples under weak excitation for 4H, 6H, and 15R SiC at 4.2 K. These above mentioned dependences on excitaion intensity and doping, were not observed for 3C SiC crystals grown in the same growth run as 4H, 6H, and 15R SiC crystals. Therefore, these characteristics seem to relate to the inequivalent sites which do not exist in 3C SiC. The peak intensity ratios of C_0 peaks to B_0 peaks under high excitaiton, where both B and C series appear with full intensities, are 0.96 for 4H, 1.9 for 6H, and 1.4 for 15R SiC, respectively. These values are in good agreemant with the ratios of the numbers of cubiclike to hexagonallike sites, i.e., 1 for 4H, 2 for 6H, and 1.5 for 15R SiC. Therefore, B and C series are assumed to be due to D-A pair transitions between acceptors and donors in hexagonallike and cubiclike sites, respectively, as Hagen et al. [14] have suggested.

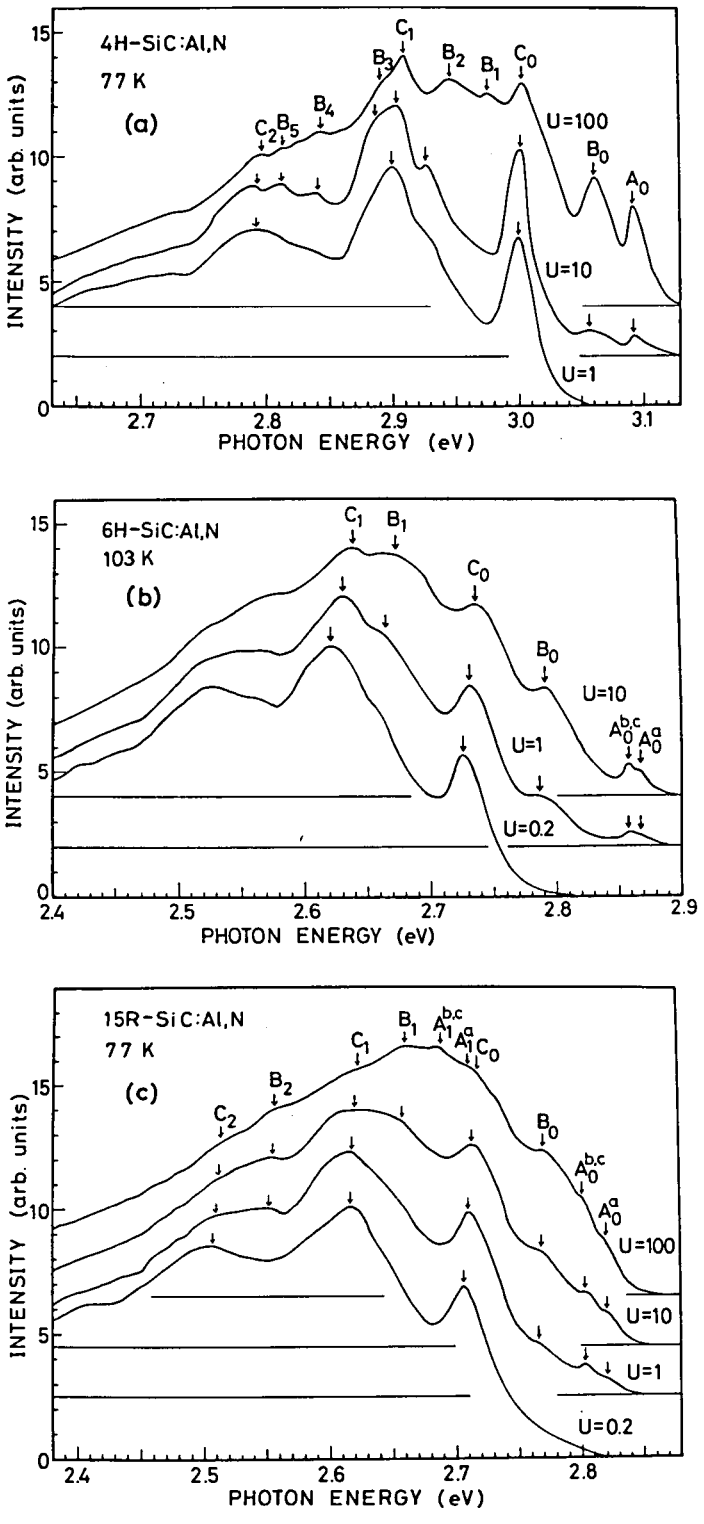

Fig. 7 Photoluminescence spectra of Al-doped (a) 4H, (b) 6H, and (c) 15R SiC at various excitation intensities (U) at 77 K or 103 K.

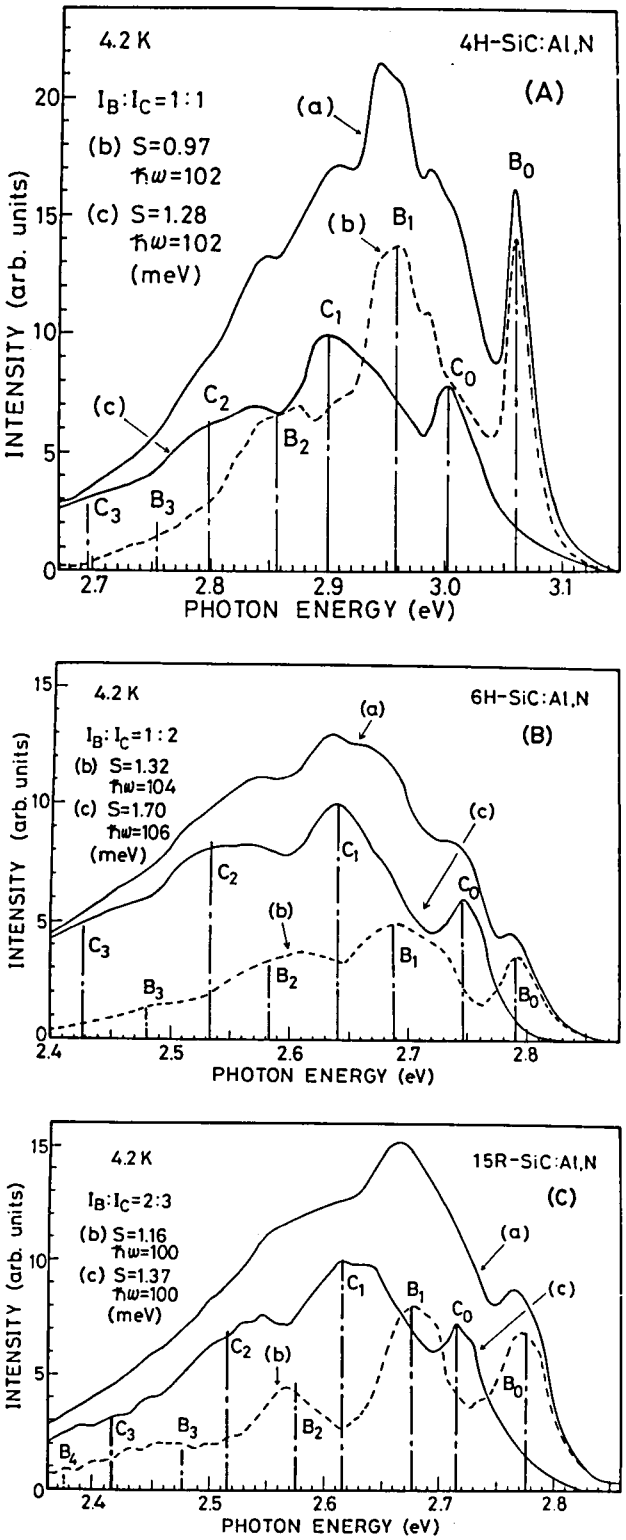

Fig. 8 Comparison of the experimental D-A pair spectra and the theoretical spectra for Al-doped (A) 4H, (B) 6H, and (C) 15R SiC at 4.2 K. The vertical dot-dash lines indicate the intensities of the phonon spectra calculated using Eq. (7) with parameters S and phonon energies $\hbar\omega$ indicated in the figures. (a) Spectra of slightly Al- and N-doped crystals under high excitation with B and C series. (b) Spectra with only B series, which are obtained by subtracting spectra (c) from spectra (a). The ratios of the total luminescence intensities of the spectra (b) to those of the spectra (c) are the same as the ratios of the numbers of hexagonal-like sites to those of cubiclike sites. (c) Spectra of highly Al-doped crystals under weak excitation with only C series.

In order to verify this assumption, configuration coordinate phonon spectra are studied. We consider peaks of site dependent acceptor levels as a single peak for simplicity. In the adiabatic approximation, the normalized line shape function for multi-mode phonons is given by [40],

$$I_{ab}(E) = \sum_{m,n} \left[\sum_{n} \exp(-E_{bn}/kT) \right]^{-1} \exp(-E_{bn}/kT)$$

$$\times \left| \langle bn | M_{ba} | am \rangle \right|^2 \delta(E_{bn} - E_{am} - E). \qquad (6)$$

Here, M_{ba} is the dipole matrix element between the electronic ground and excited states, a and b. The adiabatic potentials E_{am} and E_{bn} are for the vibrational wave functions in the ground state $|am\rangle$ and excited state $|bn\rangle$, respectively. Integers m and n are indices for the ground and excited vibrational states, respectively. Based upon this equation, there are no terms which represent the number of luminescent centers and photon number. Physically the interaction between the lattice vibration and the luminescent center, which determines phonon spectrum, may not be affected by the numbers of photons and luminescent centers. Therefore, if C series are LA phonon replicas of B series as Gorban et al. [12] and Suzuki et al. [13] have suggested, strong dependences on the excitation intensity and the acceptor concentration are not expected. Since the D-A pair spectra exhibit strong dependence on the excitation intensity and acceptor concentration, the C series are not LA phonon replicas of the B_0 peak.

The line shape function for a single mode at T≃0 on the Condon and the linear mode approximations is obtained from Eq. (6) as [41],

$$I_{ab}(E) = \sum_{m=0}^{\infty} \exp(-S) \, (S^m/m!) \, \delta(m\hbar\omega - E_{ab} + S\hbar\omega - E), \qquad (7)$$

where the value S represents the degree of localization of electrons and holes to impurity atoms and $\hbar\omega$ is the energy of the phonon. This leads to an emission spectrum consisting of a series of evenly spaced lines at

$$E_m = (E_{ab} - S\hbar\omega) - m\hbar\omega = E_0 - m\hbar\omega. \quad (8)$$

In Figs. 8(A)-8(C), the spectra of strong p-type crystals under low excitation conditions are taken for C series spectra. The B series spectrum [curve (b)] is taken by subtracting the C series spectrum [curve (c)] from the combined B and C series spectrum [curve (a)] in such a way that the ratio of the total luminescence intensity of the B series spectrum to that of C series spectrum is equal to the ratio of the numbers of the cubiclike sites to hexagonallike sites. Both B and C series spectra are fairly well described by Eq. (7) using appropriate values of S and $\hbar\omega$. Peak intensity ratios of C_0 to B_0 peaks, values of S, sums of donor and acceptor ionization energies averaged among sites, and $\hbar\omega$ are given in Table III. The donor ionization energy E_D will be determined in Sec. 4-3-4. The S parameter increases with increasing $E_D + E_A$, except for 3C SiC. This is consistent with the meaning of S parameter, which represents the strength of the binding energy or degree of localization of electrons and holes to luminescent centers. Increase of S with increase of $E_D + E_A$ was also reported for GaP [42]. The observed phonons with energies of 100-106 meV correspond to the smaller LO phonons shown in Sec. 4-3-1. The small value of the S parameter in the case of 3C SiC may be due to the large phonon energy [43].

The fair agreement of the resultant spectra with Eq. (7) supports the idea that B and C series peaks are due to donors in inequivalent sites with different binding energies. Dependences of the intensity ratio of B and C series on the excitation intensity and the acceptor concentration are also observed in Ga-doped and B-doped samples. But in these cases, quenching of B series peaks is not so remarkable, probably due to the small concentrations of Ga and B acceptors owing to their small solubility limits in SiC [17].

The dependences of the intensity ratio of B and C series peaks on the excitation intensity and the acceptor concentration can be explained by the ratio of the occupied donors in cubiclike sites to

Table III Numbers of cubiclike and hexagonallike sites, ratios of C_0 to B_0 peak intensities, S parameters, sums of the donor and acceptor ionization energies averaged among sites, and phonon energies for 3C, 4H, 6H, and 15R SiC.

	Site	No. of sites	$\frac{I(C_0)}{I(B_0)}$	S	E_D+E_A (meV)	$\hbar\omega$ (meV)
3C	C	1	$\frac{1}{0}$	1.06	311[a]	116
	H	0				
6H	C	2	$\frac{1.9}{1}$	1.70	404	106
	H	1		1.32	339	104
15R	C	3	$\frac{2.8}{2}$	1.37	342	100
	H	2		1.16	278	100
4H	C	1	$\frac{0.96}{1}$	1.28	315	102
	H	1		0.97	257	102

a) Ref. 22.

those in hexagonallike sites. The occupation probability is expressed by the Fermi level and the electron quasi Fermi level. (1) When a sample is strong p-type, the Fermi level is near the acceptor level. In this case, the ratio of the numbers of occupied donors in different sites is

$$N^H/N^C \simeq \frac{1}{2} \exp[-(E^C - E^H)/kT] \ll 1, \qquad (9)$$

using Boltzmann distribution. Here, N^H and N^C are the numbers of donors in hexagonallike sites and in cubiclike sites, respectively. Therefore, transitions due to donors in hexagonallike sites are far fewer than those in cubiclike sites, and only C series are observed. (2) When concentrations of donors and acceptors are small, the electron quasi Fermi levels may be higher than both donor levels, because the number of generated electrons is comparable to that of donors. Therefore, B and C series peaks are comparable at low temperatures. However, when temperature is raised, a larger portion of electrons at shallower donors in hexagonallike sites are

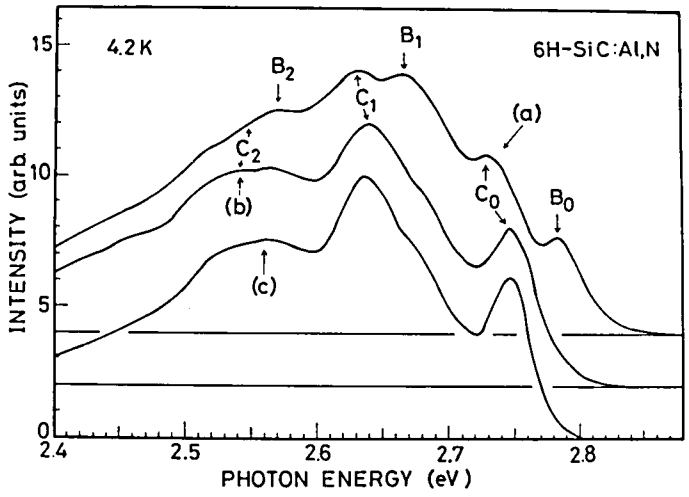

Fig. 9 Photoluminescence spectra of 6H SiC with various concentrations of Al and N impurities. (a) $n = 4\times10^{17}$ cm^{-3} (grown from Si melt with 0.01 at. % Al), (b) $n = 2\times10^{19}$ cm^{-3} (2.5 at. % Al) and degenerated, and (c) $p = 2\times10^{18}$ cm^{-3} (2.5 at. % Al).

thermally excited compared with those at deeper donors in cubiclike sites. Therefore, with increasing excitation intensity, the electron quasi Fermi level descends and the number of occupied donors in hexagonallike sites decreases more rapidly than that in cubiclike sites and B series disappear.

(3) For 6H SiC, when N donor is heavily doped and the conduction band is degenerated, C series disappeared and the spectrum becomes similar to that of a strong p type sample as in Fig. 9. In this case, the tail states of the conduction band may merge with shallower donor level due to hexagonallike sites. Therefore, the pair transitions between shallower donors and acceptors may not occur and B series disappear. Heavy doping of N donor has not been carried out for 4H or 15R SiC. Suzuki et al. [13] reported that B series existed in the photoluminescence of heavily doped 4H SiC with $n \gtrsim 5\times10^{19}$ cm^{-3} where the B series of 6H SiC grown in the same growth run already disappeared. This persistent existence of B series in 4H SiC may be due to the large density of states caused by the large number of the conduction band minima in 4H SiC [44].

4-3-4. Donor levels

Donor levels are estimated from the D-A pair spectra using the acceptor levels determined in Sec. 4-3-2. The energy relation for the D-A pair transitions is written

$$h\nu_{D-A} = E_G - (E_A + E_D) + e^2/4\pi\varepsilon R. \quad (10)$$

In the case of weak excitation and for $N_A >> N_D$, $a_A{}^3 N_A << 1$, and $a_D{}^3 N_d << 1$, the dependence of luminescence intensity on the pair distance (R) can be approximated by [45,46],

$$I(R) \propto R^6 \exp(-4\pi N_A R^3/3), \quad (11)$$

where a_A and a_D are the Bohr radii of a hole and an electron, respectively. The estimated Al concentration of an Al-doped sample is $N_{Al} \simeq 1\times10^{18}$ cm^{-3} ($p = 3.5\times10^{16}$ cm^{-3}) the Ga concentration $N_{Ga} \simeq 1\times10^{18}$ cm^{-3} ($p = 5.6\times10^{15}$ cm^{-3}), and the N concentration of all samples $N_N \simeq 3\times10^{17}$ cm^{-3} ($n = 1.0\times10^{17}$ cm^{-3}) for 3C, 4H, and 15R SiC samples grown in the same growth run. For 6H SiC, the estimated Al and Ga concentrations are $N_{Al} \simeq 1\times10^{19}$ cm^{-3} ($p = 1.4\times10^{17}$ cm^{-3}) and $N_{Ga} \simeq 6\times10^{18}$ cm^{-3} ($p = 7.1\times10^{16}$ cm^{-3}), respectively. The Bohr radius is modified with the observed activation energy in the quantum defect model (Sec. 4-4). The modified Bohr radii [$a^*\nu$ in Eq. (15) in Sec. 4-4] of N in hexagonallike sites are ≃8-15 Å, those of N in cubiclike sites are ≃6-10 Å, those of Al in both kinds of sites are ≃4 Å, and those of Ga in both kinds of sites are ≃3.5 Å in all polytypes (APPENDIX B). These values satisfy the conditions that $N_A >> N_D$, $a_A{}^3 N_A << 1$, and $a_D{}^3 N_D << 1$. The B_0 peak due to transitions between donors in shallower hexagonallike sites and acceptors in inequivalent sites, is used to determine the ionization energy of N donors. On the assumption that the capture cross section, the pair distribution function, and the pair occupation probability do not depend on the inequivalent sites which an impurity atom substitutes, the shape function of the D-A pair spectrum is written as

$$I(E) \propto \sum_i E_i^{-6} \exp[-4\pi N_A (e^2/4\pi\epsilon E_i)^3/3], \qquad (12)$$

where $E_i = E - E_G + E_D + E_A^i$ is the Coulomb energy between the donor in hexagonallike sites and the acceptor in one of inequivalent sites, and E_A^i is the ionization energy of the acceptor at the i-th inequivalent site.

The Coulomb energy is estimated by curve fitting between the calculated spectrum using Eq. (12) and the experimental spectrum under low excitation at 4.2 K. Figures 10(a)-10(f) show best fits between theoretical and experimental spectra. The energies of $E_G - E_D - E_A^i$ are indicated by the arrows in Figs. 10(a)-10(f). The donor ionization energy is determined with the value of $E_G - E_D - E_A^i$ and the acceptor ionization energy determined in Sec. 4-3-2. For Al-doped 3C SiC, $E_G - E_D - E_A = 2.0925$ eV, $N_A = 1.5\times10^{18}$ cm^{-3}, and $E_N = 57$ meV are obtained. For 4H SiC, $E_G - E_D - E_A = 3.0485$ eV, $N_A = 1.5\times10^{18}$ cm^{-3}, and $E_N^H = 66$ meV are obtained for the Al-doped sample, and $E_G - E_D - E_A = 2.9515$ eV, $N_A = 1.5\times10^{18}$ cm^{-3}, and $E_N^H = 66$ meV for the Ga-doped sample. For 6H SiC, $E_G - E_D - E_A^a = 2.7655$ eV, $N_A = 1.0\times10^{18}$ cm^{-3}, and $E_N^H = 96.5$ meV are obtained for the Al-doped sample, and $E_G - E_D - E_A^a = 2.682$ eV, $N_A = 2.25\times10^{18}$ cm^{-3}, and $E_N^H = 102$ meV for the Ga-doped sample. For 15R SiC, $E_G - E_D - E_A^a = 2.7605$ eV, $N_A = 1.5\times10^{18}$ cm^{-3}, and $E_N^H = 63$ meV are obtained for the Al-doped sample, and $E_G - E_D - E_A^a = 2.6785$ eV, $N_A = 1.5\times10^{18}$ cm^{-3}, and $E_N^H = 64$ meV for the Ga-doped sample. The values of E_N^H are determined to be 66 meV for 4H SiC, 100 meV for 6H SiC, and 64 meV for 15R SiC by averaging the values of the Al-doped and Ga-doped samples. The acceptor concentrations determined from curve fitting and those estimated from Hall measurements are in good agreement except for the case of Al-doped 6H SiC. Since defect spectra [33] overlapped D-A pair spectra and the D-A pair spectra were broad, fitting was not tried for B-doped samples. From the separation energy of B_0 and C_0 peaks of 58 meV, $E_N^C = 124$ meV is determined for N donors in cubiclike sites for 4H SiC. Similarly, from the separation energies of

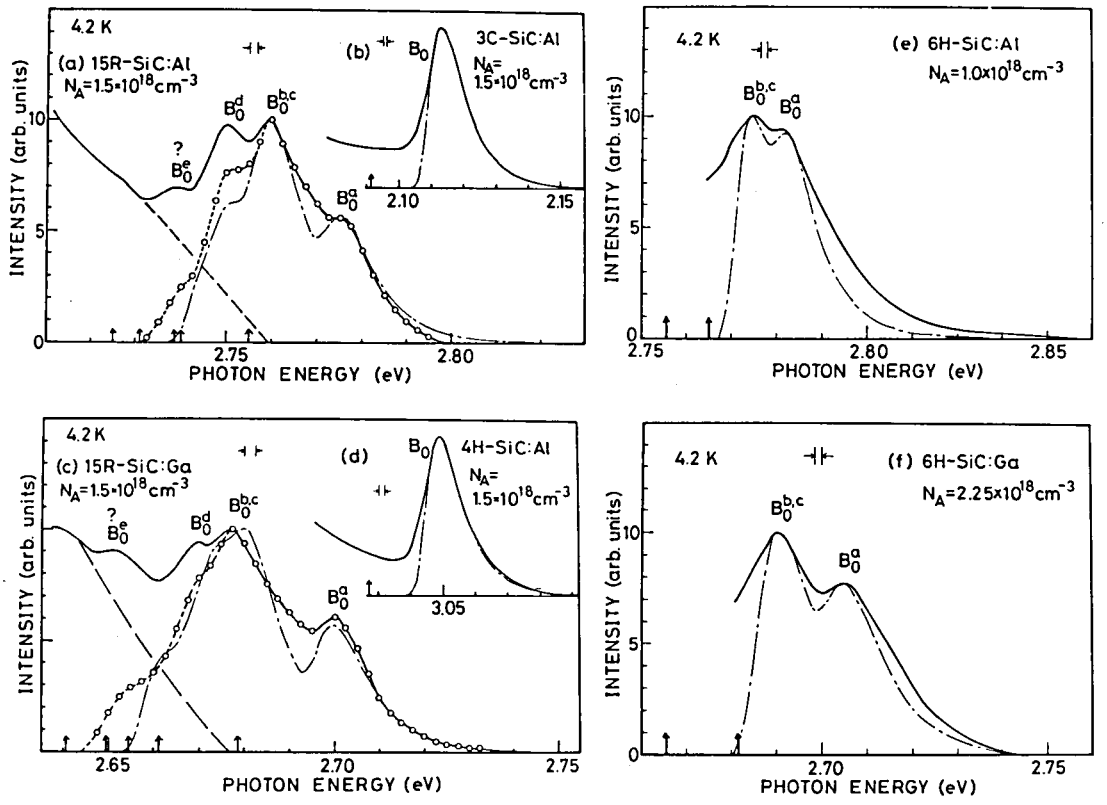

Fig. 10 Comparison of experimental spectra at 4.2 K and calculated spectra for (a) Al-doped 15R SiC, (b) Al-doped 3C SiC, (c) Ga-doped 15R SiC, (d) Al-doped 4H SiC, (e) Al-doped 6H SiC, and (f) Ga-doped 6H SiC. Lines with open circles of 15R SiC indicate spectra after subtracting background B_1 peaks assumed as dashed lines. The dot-dash lines indicate calculated spectra using Eq. (12) with indicated acceptor concentrations and $E_{GX} - E_D - E_A^i$ indicated by the arrows.

55 and 48 meV, 155 and 112 meV are obtained for N donors in cubic-like sites for 6H and 15R SiC, respectively. The ionization energy of 56.5 meV of N in 3C SiC was determined using D-A pair line spectrum by Kuwabara et al. [22]. The present value of 57 meV is in good agreement with their value. Therefore, the accuracy of the determined donor levels seems to be rather high, probably ±3 meV for 4H and 15R, and probably ±5 meV for 6H SiC. The determined donor levels are given in Table II. The ionization energies of N donors determined by Hall measurements, 49 [47] and 50 meV [48] for 3C SiC,

33 meV [16] for 4H SiC, 95 meV [15,16] for 6H SiC, and 52 [15] and 47 meV [16] for 15R SiC, are slightly smaller than the present values of hexagonallike sites, which might be caused by the screening by ionized impurities and the assumption of single donor level in their analyses.

4-4. Origin of the Site Effect

Table II shows the donor ionization energies, the acceptor ionization energies, the average ratios of the ionization energies of donors and acceptors in cubiclike sites to those in hexagonallike sites, and the free exciton binding energies from literatures [34-37]. From these values, the following characters of the donor and acceptor ionization energies are deduced.

1) Donor levels markedly depend on sites and polytypes.

2) Acceptor levels slightly depend on sites and polytypes, and the activation energy decreases with the increase of the hexagonality (percent of the number of hexagonallike sites in all the sites; 0 for 3C, 1/3 for 6H, 2/5 for 15R, 1/2 for 4H).

3) The activation energies of impurities in cubiclike sites (E^C) are larger than those in hexagonallike sites (E^H). For donors E^C/E^H are large and are 1.55-1.88, and for acceptors E^C/E^H are nearly one and are 1.00-1.08.

Commonly used theories on impurity levels, the effective mass theory and the quantum defect model, require a unique impurity level for an impurity atom, since specific effective mass and dielectric constant exist for one material. The existence of the site dependent impurity level seems to imply inapplicability of these theories to this case. However, the nearly constant ratios of E^C/E^H suggest the existence of certain localized physical constants around a cubiclike or a hexagonallike sites, and these theories are still available. This idea is supported by the fact that the nearest neighbour atomic

configurations are the same for cubiclike or hexagonallike sites independent of polytype. By assuming such localized physical constants, explanation of the characteristics of the site dependent impurity levels is tried on the basis of the quantum defect model, because the effective mass theory gives too small ionization energies of 0.2-0.5 times of the observed values.

In the quantum defect model [49], the effective principal quantum number ν is determined from the observed impurity ionization energy, E(obs), by

$$E(obs) = - R^*/\nu^2, \tag{13}$$

$$R^* = m^* e^4/2\hbar^2\varepsilon^2, \tag{14}$$

$$P_\nu(r) = N_\nu r^{\nu-1} \exp(-r/\nu a^*), \tag{15}$$

$$a^* = \hbar^2\varepsilon/m^* e^2. \tag{16}$$

Here, R^* and a^* are referred to as the effective Rydberg and effective Bohr radius, respectively, $P_\nu(r)$ is the radial function, and N_ν is a function of ν. We assume that ν is inherent in the kind of impurity atom, since ν is the correction factor for the effect of core potential of the impurity atom. In this model, factors which depend on the inequivalent sites are the dielectric constant and the effective mass.

The modified Bohr radii $a^*\nu$ of donors are 6.1-13.9 Å and those of acceptors are 2.2-4.2 Å (APPENDIX B). Though the electron modified Bohr radii are a little larger than the distance to the nearest neighbour atoms, 3.08 Å in the a-axis direction and 2.54 Å in the c-axis direction [50], we assume that electron and hole wave functions are localized around cubiclike and hexagonallike sites for simplicity. In this case we may use the dielectric constants and effective masses of 3C and 2H SiC in place of those around cubiclike and hexagonallike sites. The static dielectric constant of 3C SiC was reported as $\varepsilon_S = 9.72$ [51]. The static dielectric constants of

2H SiC were determined to be $\varepsilon_s(\perp) = 9.57$ and $\varepsilon_s(//) = 10.73$ (APPENDIX A) in the same way as Ref. 51. The ratio of square of the dielectric constants is

$$[2\varepsilon_s(\perp,2H)^2 + \varepsilon_s(//,2H)^2]/3\varepsilon_s(3C)^2 = 1.052. \quad (17)$$

For 3C SiC, the density of state electron effective mass has been determined by various methods [47,48,52], but those values largely differ each other. Moreover, there have been no reports on the electron effective mass for 2H SiC. Therefore, the electron effective masses estimated from the curvature of the conduction band minima are used [53]. For 3C SiC, $m_{\perp}^* = 0.24\ m_0$ and $m_{//}^* = 1.12\ m_0$ are obtained, and for 2H SiC $m_{\perp}^* = 0.26\ m_0$ and $m_{//}^* = 0.70\ m_0$. The ratio of the effective masses is obtained as

$$[2m_e^*(\perp,3C)^2 + m_e^*(//,3C)^2]^{1/2}/[2m_e^*(\perp,2H)^2 + m_e^*(//,2H)^2]^{1/2} \quad (18)$$
$$= 1.48$$

Since the valence band maxima of SiC locate at the Γ valley and are nearly spherical independent of polytypes [16,28,29], the hole effective masses of different polytypes may be nearly the same. Whereas, the conduction band minima of different polytypes locate at different valleys [5,16,28-30]; X valleys for 3C SiC and K valleys for 2H SiC. Therefore, the electron effective masses vary from polytype to polytype. Since the physical constant affecting the acceptor level is only the dielectric constant, the ratio of the acceptor activation energies is expected to be 1.052. This value is in good agreement with the observed values of 1.0-1.076. Since both the electron effective mass and the dielectric constant affect the donor activation energy as in Eq. (13), the ratio becomes $1.052 \times 1.48 = 1.56$. This value is in good agreement with the observed values of 1.55-1.88. This fairly good agreements support the existence of the localized effective mass and the dielectric constant. However, the variation of the ratio in different polytypes and sites needs more advanced treatment taking into account of the atomic configuration

farther than the nearest neighbour atoms and needs more accurate values of the effective masses. Site dependent impurity levels are expected to exist extensively in other polytype SiC and furthermore in other materials such as ZnS and AgI, provided that the localized dielectric constants or effective masses differ considerably.

4-5. Haynes Rule

The exciton binding energies (E_{BX}) [54] vs. the ionization energies (E_D) of N donors of 3C, 4H, 6H, and 15R SiC are shown in Fig. 11. This figure shows that Haynes rule [55] relatively well applies to SiC. Choyke et al. [56] suggested inapplicability of this rule to SiC, which might be caused by uncertain ionization energies they had estimated. The average ratio of exciton binding energies to ionization energies of N donors (E_{BX}/E_D) is about 0.17. From theoretical calculations [57], the energy ratio (E_{BX}/E_D) is expected to be nearly constant of about 0.1 in the range of mass ratio (m_e^*/m_h^*) more than 0.2 which various polytype SiC may have. Therefore, Haynes rule can be applied even if the mass ratio varies

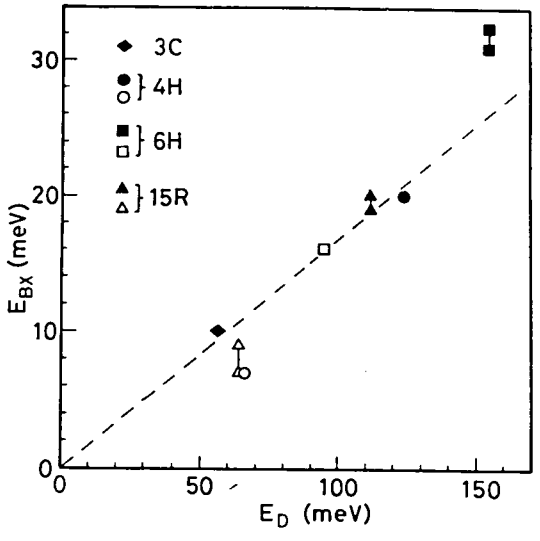

Fig. 11 Exciton binding energies (E_{BX}) vs. ionization energies (E_D) for N donors in 3C, 4H, 6H, and 15R SiC. Open symbols indicate the data for donors in hexagonallike sites and closed symbols for donors in cubiclike sites.

among SiC polytypes and different sites. The data points of donors in hexagonallike sites (open symbols in Fig. 11) tend to deviate from the line of 0.17 in the direction of smaller values of energy ratio, and those in cubiclike sites (closed symbols) in the direction of larger values of energy ratio. Since the mass ratio of cubiclike sites are larger than that of hexagonallike sites (Sec. 4-4), the energy ratio should increase with the increase of the mass ratio. This relation is explained by the calculation by Sharma [58], whereas the other researchers [57] have reported that the energy ratio decreases or does not change with increasing mass ratio.

4-6. Summary

Photoluminescence in 3C, 4H, 6H, and 15R SiC crystals doped with Al, Ga, or B acceptors and N donors has been studied. The peculiar characteristics of D-A pair and free-to-acceptor luminescence are explained assuming site dependent donor and acceptor levels. Site dependent donor and acceptor levels are determined from the analyses of free-to-acceptor and D-A pair luminescence. Good agreement is obtained between the number of sites and the photoluminescence intensity associated with a given site, which indicates that every impurity atom enters each kind of site in equal probability. The characteristics of the site dependent donor and acceptor levels are studied on the basis of the quantum defect model. The origin of the site effect on the impurity levels is explained by assuming the local dielectric constants and effective masses. The applicability of Haynes rule to SiC is shown, and therefore the donor ionization energies can be roughly estimated from the exciton binding energies with a slight modification by the site dependent effective masses. From these results, the site effect on the impurity levels are expected extensively for other polytype SiC crystals and other materials, provided that the local

effective masses or the local dielectric constants differ considerably.

References

[1] L. Patrick, Phys. Rev. 127, 1878 (1962).

[2] W. J. Choyke, Mater. Res. Bull. 4, S141 (1969).

[3] L. Patrick, D. R. Hamilton, and W. J. Choyke, Phys. Rev. 143, 526 (1966).

[4] W. J. Choyke, D. R. Hamilton, and L. Patrick, Phys. Rev. 133, A1163 (1964).

[5] L. Patrick, W. J. Choyke, and D. R. Hamilton, Phys. Rev. 137, A1515 (1965).

[6] W. J. Choyke and L. Patrick, Phys. Rev. 127, 1868 (1962).

[7] L. Patrick, D. R. Hamilton, and W. J. Choyke, Phys. Rev. 132, 2023 (1063).

[8] G. A. Lomakina, G. F. Kholuyanov, R. G. Verenchikova, E. N. Mokhov, and Yu. A. Vodakov, Sov. Phys. - Solid State 6, 988 (1972).

[9] P. J. Colwell and M. V. Klein, Phys. Rev. B6, 498 (1972).

[10] P. J. Dean and R. L. Hartman, Phys. Rev. B5, 4911 (1972).

[11] I. S. Gorban and A. P. Krokhamal, Sov. Phys. - Solid State 19, 733 (1977).

[12] I. S. Gorban, V. A. Gubanov, and B. M. Efimov, Sov. Phys. - Solid State 14, 2010 (1973).

[13] A. Suzuki, H. Matsunami, and T. Tanaka, J. Phys. Chem. Solids 38, 693 (1977); A. Suzuki, H. Matsunami, and T. Tanaka, J. Electrochem. Soc. 124, 241 (1977).

[14] S. H. Hagen, A. W. C. van Kemenade, and J. A. W. van der Does de Bye, J. Lumin. 8, 18 (1973).

[15] S. H. Hagen and C. J. Kapteyns, Philips Res. Rep. 25, 1 (1970).

[16] G. A. Lomakina, Yu. A. Vodakov, E. N. Mokhov, V. G. Oding, and G. F. Kholuyanov, Sov. Phys. - Solid State 12, 2356 (1971); G. A. Lomakina, in "Silicon Carbide - 1973", edited by R. C. Marshall, J. W. Faust, Jr., and C. E. Ryan (University of South Calorina Press, Columbia, 1974), p. 520.

[17] Yu. A. Vodakov, G. A. Lomakina, E. N. Mokhov, E. I. Radovanova, V. I. Sokolov, M. M. Usmanova, G. F. Yuldashev, and B. S. Machmudov, Phys. Status Solidi A35, 37 (1976).

[18] G. A. Lomakina, Sov. Phys. - Solid State 7, 475 (1965).

[19] This value of B concentration seems to be a little too large, which may be caused by the experimental uncertainty due to high resistivity of this sample. This value is about one order higher than the reported one in W. E. Nelson, F. A. Halden, and A. R. Rosengreen, J. Appl. Phys. 37, 333 (1966).

[20] N. N. Long, D. S. Nedzvetskii, N. K. Prokofeva, and M. B. Reifman, Opt. Spectrosc. 30, 165 (1971).

[21] H. Kuwabara, K. Yamanaka, and S. Yamada, Phys. Status Solidi A37, K157 (1976).

[22] H. Kuwabara, Doctoral Thesis, University of Osaka, 1978.

[23] G. Zanmarchi, J. Phys. Chem. Solids 29, 1727 (1968).

[24] N. N. Long and D. S. Nedzvetskii, Opt. Spectrosc. 35, 645 (1973).

[25] H. Kuwabara and S. Yamada, Phys. Status Solidi A30, 739 (1975).

[26] L. Patrick and W. J. Choyke, Phys. Rev. 123, 813 (1961).

[27] D. W. Feldman, J. H. Parker, Jr., W. J. Choyke, and L. Patrick, Phys. Rev. 173, 787 (1968).

[28] H. G. Junginger and W. van Haeringen, Phys. Status Solidi 37, 709 (1970).

[29] L. A. Hemstreet and C. Y. Fong, in "Silicon Carbide - 1973", edited by R. C. Marshall, J. W. Faust, Jr., and C. E. Ryan (University of South Carolina Press, Columbia, 1974), p. 284.

[30] L. Patrick, Phys. Rev. B5, 2198 (1972).

[31] K. Colbow, Phys. Rev. 141, 742 (1966).

[32] J. S. Blakemore, Phys. Rev. 163, 809 (1967).

[33] V. V. Makarov, Sov. Phys. - Solid State 9, 457 (1967).

[34] D. S. Nedzvetskii, B. V. Novikov, N. N. Prokofeva, and M. B. Reifman, Sov. Phys. - Semicond. 2, 914 (1969).

[35] V. A. Kiselev, B. V. Novikov, M. M. Pimonenko, and E. B. Shadrin, Sov. Phys. - Solid State 13, 926 (1971).

[36] G. B. Dubrovskii and V. I. Sankin, Sov. Phys. - Solid State 17, 1847 (1976).

[37] V. I. Sankin, Sov. Phys. - Solid State 17, 1191 (1975).

[38] M. Ikeda, H. Matsunami, and T. Tanaka, J. Lumin. 20, 111 (1979).

[39] Analysis of the line spectra could not be carried out, since separation of the different series due to donors and acceptors in inequivalent sites was impossible at the present state.

[40] R. C. O'Rourke, Phys. Rev. 91, 265 (1953).

[41] T. H. Keil, Phys. Rev. 140, A161 (1965).

[42] M. Tajima and M. Aoki, Jap. J. Appl. Phys. 13, 812 (1974).

[43] Although the condition is slightly different, in the case of an electron bound to an impurity, S parameter is given as $S = E_i(\varepsilon_S/n_0^2 - 1)/\hbar\omega$, where E_i is the binding energy of the impurity, ε_S the static dielectric constant, and n_0 the refractive index (Ref. 23), or $S \propto (\varepsilon_\infty^{-1} - \varepsilon_S^{-1})/\hbar\omega v_0^{1/3}$, where ε_∞ is the high frequency dielectric constant and v_0 the volume of the unit cell; T. Toyozawa, in "Dynamic Processes in Solid State Optics", edited by R. Kubo and H. Kamimura (Syokabo and W. A. Benjamin, Inc., Tokyo and New York, 1967), p. 110. These relations indicate that S parameter decrease in inverse proportion to the increase of $\hbar\omega$.

[44] Y. M. Tairov and Y. A. Vodakov, in "Electroluminescence", edited by J. I. Pankov (Spinger-Verlag, New York, 1977), p. 31.

[45] R. Bindermann and K. Unger, Phys. Status Solidi B66, 133 (1974).

[46] L. V. Takunov, Sov. Phys. - Semicond. 10, 1302 (1976).

[47] L. S. Aivazova, S. N. Gorin, V. G. Sidyakin, and I. M. Shavarts, Sov. Phys. - Semicond. 11, 1069 (1977).

[48] L. S. Aivazova and Yu. M. Altaiskii, Sov. Phys. - Semicond. 12, 861 (1978).

[49] H. B. Bebb and R. A. Chapman, J. Phys. Chem. Solids 28, 2087 (1967); H. B. Bebb, Phys. Rev. 185, 1116 (1969).

[50] R. C. Marshall, J. W. Faust, Jr., and C. E. Ryan, "Silicon Carbide - 1973" (University of South Carolina Press, Columbia, 1974), p.669.

[51] L. Patrick and W. J. Choyke, Phys. Rev. B2, 2255 (1970).

[52] P. J. Dean, W. J. Choyke, and L. Patrick, J. Lumin. 15, 299 (1977).

[53] L. A. Hemstreet (private communication) kindly estimated the

effective masses of 2H and 3C SiC by calculating the curvatures of the conduction band minima of 2H and 3C SiC based on the data in Ref. 29.

[54] The values of E_{BX} were determined from the free exciton luminescence and the bound exciton luminescence of 3C, 4H, 6H, and 15R SiC (Chapt. III). These values are in good agreement with the data in Refs. 4-7.

[55] J. R. Haynes, Phys. Rev. Lett. 4, 361 (1960).

[56] W. J. Choyke, D. R. Hamilton, and L. Patrick, Phys. Rev. 139, A1262 (1965).

[57] Yia-Chung and T. C. McGill, Solid State Commu. 30, 187 (1979).

[58] R. R. Sharma and S. Rodringuez, Phys. Rev. 159, 649 (1067).

V. 6H SiC BLUE LED'S BY OVERCOMPENSATION METHOD

5-1. Introduction

Commercial production of light-emitting diodes (LED's) with luminescence colors from infrared to green has been realized with GaAs, GaP, and other III-V compound semiconductors. By extensive researches, the efficiencies of these diodes have been remarkably improved [1], which resulted in appearance of LED televisions [2]. However, fabrication of blue LED's has not gone farther than the laboratory research. Continuous investigations have been devoted to the candidates for blue LED's, and high quantum efficiencies of 5×10^{-4} [3] and $\gtrsim 1\times10^{-3}$ [4] are realized with ZnS and GaN, respectively. However, these semiconductors have a disadvantage that low resistivity p type crystals can not be obtained because of the self-compensation effect, which spoils reproducibility and life time of these blue LED's. In contrast to these semiconductors, SiC crystals of low resistivity p and n type can be easily obtained, which provides good reproducibility and long life [5] for SiC LED's.

The overcompensation method proposed by the author [6,7] has an advantage that relatively high efficiencies can be reproducibly obtained by a simple process with one growth run. Furthermore, Münch et al. [8] have reported the highest efficiency of SiC blue LED's of 4×10^{-5} by employing this method.

In this chapter, fabrication processes of LED's by the overcompensation method and the electrical and luminescent characteristics of the diodes are described.

5-2. Diode Fabrication

The epitaxial growth was carried out by the dipping technique under the condition determined in Chapt. II [6]. Junctions were prepared by the overcompensation method [6,7]. Substrate crystals were epitaxial layers grown from Si melts doped with 5 at. % Al, and crystals grown by Acheson method [9] with $p \sim 1\times10^{18}$ cm^{-3}, $\mu \sim 10$ $cm^2/Vsec$, and $\rho \sim 0.5$ Ωcm were also used. The graphite crucible and the holder were baked at 1800°C for 2 h in a vacuum of 1×10^{-5} Torr in order to reduce impurities. After being filled with Si and Al, the crucible was baked at about 600°C for 1 h in the same vacuum before introduction of Ar gas.

The p layers were grown for 5 h in the Si melt doped with 2.5 at. % Al. Subsequently, N_2 gas of 0.05-0.5 vol % was supplied into the Ar gas in order to overcompensate Al acceptors, and the n layer was grown for 5 h. Thus, the p and n layers were grown in one crystal growth. The thicknesses of the p and n layers were about 20 μm. After lapping the n layer on the back side, the crystal was cut into small dies of about 1×1 mm^2. Al-Si alloy was used for an ohmic contact for the p layer, and for the n layer Au-Ta alloy (Sec. 2-3) or Ni-Au alloy was used. The Ni-Au contact was formed by evaporating Ni and Au in this order, and alloyed in Ar gas for 5 min at about 1050°C. The p layer was attached to a copper block and Au wire was taken from the ohmic contact on the n layer with silver paste.

5-3. Diode Characteristics

Figure 1 shows the current-voltage characteristics of a typical diode at room temperature. The diffusion potential is found to be about 2.5 V from the forward bias characteristics. In the reverse bias characteristics, some leakage currents flow and the breakdown voltage is more than 10 V. Figure 2 shows the capacitance-voltage

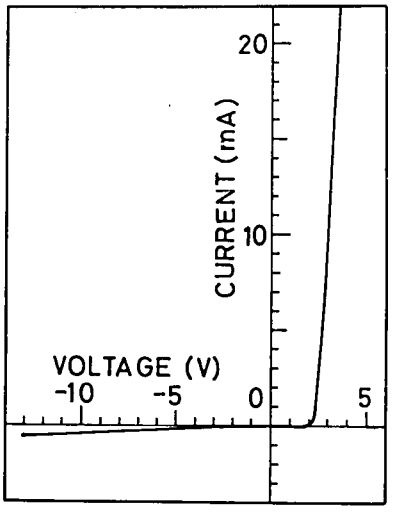

Fig. 1 Current-voltage characteristics of the diode.

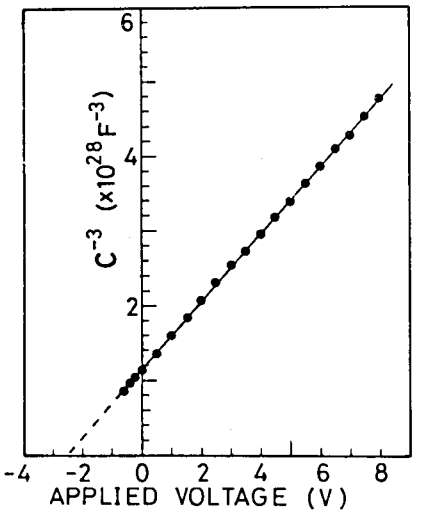

Fig. 2 Capacitance-voltage characteristics of the diode.

characteristics of the diode. The linear relation between C^{-3} and V indicates that this diode has a linear graded junction. From this figure, the diffusion voltage of about 2.5 V is obtained, and this value is in good agreement with the value of 2.5 V in the I - V characteristics. A few diodes indicated different C - V characteristics which deviated from the C^{-3} - V line in the direction of larger capacitance from some reverse bias. This variation may be caused by the impurity profile which was determined from the rate of supply of N_2 gas and the growth rate.

Electroluminescence (EL) was measured by driving diodes with pulse currents of 1 kHz and duty cycles of 0.2-0.005. Figure 3 shows the EL spectrum of the diode with the best quantum efficiency of 1.0×10^{-5} ($n \simeq 5.1\times10^{18}$ cm^{-3}, $p \simeq 2.5\times10^{18}$ cm^{-3}). The spectral width decreases and the peak slightly shifts to the higher energy side with increasing the current. The EL spectrum at 150 K indicated more distinct peak shift and the spectral shape was much similar to that of the N-Al pair luminescence (Chapt. IV) [10].

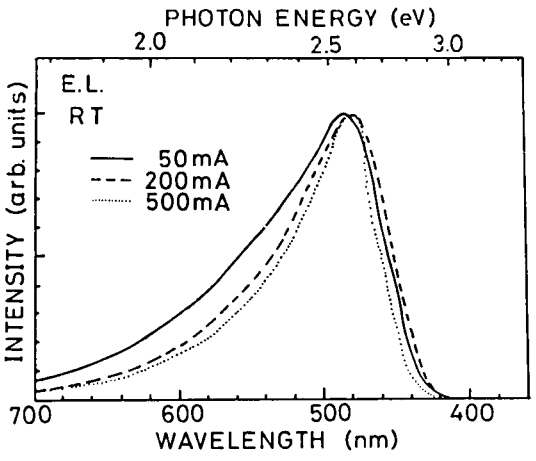

Fig. 3 Electroluminescence spectra at room temperature under various driving currents.

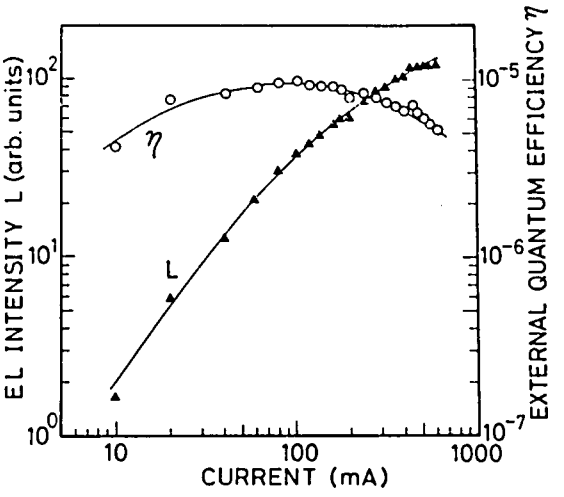

Fig. 4 Electroluminescence intensity (L) and external quantum efficiency (η) at room temperature as functions of current.

Figure 4 shows the EL intensity (L) and the external quantum efficiency (η) of the diodes as functions of the current. The results were obtained using the integrating sphere method. The L - I characteristics relatively well follow the relation of $L \propto I$, and in the low current region the slope is larger than unity, and in the high current region smaller than unity. The quantum efficiency is nearly constant except for the lower current region, and in the high current region it gradually decreases. The maximum efficiency is 1.0×10^{-5} at 100 mA. At 77 K, the efficiency increased to 1.5×10^{-4}.

5-4. Discussion

The blue luminescence at room temperature may be mainly due to N-Al pair luminescence from the peak shift and the similarity of the EL spectrum with the N-Al pair luminescence at 77 K (Chapt. IV) [10]. Slight contribution by free-to-acceptor luminescence may also exist

because of the dominance of this mechanism at higher temperatures (Chapt. IV and VII) [11]. The detailed study of the EL mechanism in Chapt. VII [11] will prove that this assignment is reasonable. The deviation from the relation of $L \propto I$ in the low current region may be caused by the larger nonradiative component by leakage current compared with diffusion current. The deviation in the high current region may be due to saturation of the luminescence caused by the exhaustion of available luminescent centers against the injected minority carriers.

Several diodes were prepared by the conventional two step process. These diodes indicated poor quantum efficiencies less than 4×10^{-7}. These poor efficiencies may be caused by contamination of the junction plane by the processes in the interval between two growths of the p and n layers, and also by the stress near the junction plane through the solidification of the melt at the end of the first growth. Since the crystal remains in the Si melt through the junction formation by the overcompensation method, the contamination and the stress around the junction can be avoided. Fairly good reproducibility of the overcompensation method may be resulted from this reason. The overcompensation method has an advantage that large numbers of donors and acceptors locate near the junction plane, which is desirable for D-A pair transitions. The quantum efficiency may be improved by controlling the impurity concentrations and the impurity profiles more precisely.

5-5. Summary

Silicon carbide blue LED's have been fabricated by the overcompensation method with the dipping technique which is proposed in this thesis. Electrical and luminescent properties of the diodes are presented. The quantum efficiency of 1.0×10^{-5} had been one of

the highest values [5,12]. The advantageous points of the over-compensation method are simpleness of the process and relatively good reproducibility.

References

[1] M. Iwamoto, M. Tashiro, T. Beppu, and A. Kasami, IEEE Trans. Electron Devices ED-26, 1258 (1979); T. Niina and T. Yamaguchi, ibid. ED-24, 946 (1977).

[2] T. Niina, S. Kuroda, H. Yonei, and H. Takesada, IEEE Trans. Electron Devices ED-26, 1182 (1979).

[3] H. Katayama, S. Oda, and H. Kukimoto, Appl. Phys. Lett. 27, 697 (1975).

[4] G. Jacob, R. Mader, and J. Hallais, Mater. Res. Bull. 11, 445 (1976); G. Jacob, M. Boulou, and D. Bois, J. Lumin. 17, 263 (1978).

[5] R. W. Brander, Proc. IRE 116, 329 (1969); R. W. Brander, Mater. Res. Bull. 4, S187 (1969).

[6] A. Suzuki, M. Ikeda, N. Nagao, H. Matsunami, and T. Tanaka, J. Appl. Phys. 47, 4546 (1976).

[7] H. Matsunami, M. Ikeda, A. Suzuki, and T. Tanaka, IEEE Trans. Electron Devices ED-24, 958 (1977).

[8] W. v. Münch and W. Kürzinger, Solid-State Electron. 21, 1129 (1978).

[9] See, for example, W. F. Knippenberg, Philips Res. Rep. 18, 161 (1963).

[10] M. Ikeda, H. Matsunami, and T. Tanaka, J. Lumin. 20, 111 (1979).

[11] M. Ikeda, T. Hayakawa, S. Yamagiwa, H. Matsunami, and T. Tanaka, J. Appl. Phys. 50, 8215 (1979).

[12] R. F. Rutz and J. J. Cuomo, in "Silicon Carbide - 1973", edited by R. C. Marshall, J. W. Faust, Jr., and C. E. Ryan (University of South Carolina Press, Columbia, 1974), p.72.

VI. PHOTON ASSISTED TUNNELING IN SiC LED'S PREPARED BY OVERCOMPENSATION METHOD

6-1. Introduction

The overcompensation method, which is described in Chapt. V and proposed by the author [1,2], has a merit that relatively high efficiency can be reproducibly obtained with a simple process. Later, Münch et al. [3] reported the highest quantum efficiency of SiC blue LED's, 4×10^{-5}, by employing this method. However, when donors and acceptors were heavily doped in order to get high efficiency, the electroluminescence (EL) spectrum greatly changed compared with those of slightly doped diodes and a broad shifting peak which covered most of the visible range, red to blue, was observed. Münch et al. [3] also reported such a change and shift of spectrum. Barns [4] also reported shifting peaks from red to yellow in SiC LED's with abrupt junctions doped with B acceptors.

Such shifting peaks in GaAs and GaP have been extensively studied [5], and photon assisted tunneling and band filling models were proposed to explain this phenomenon. In the photon assisted tunneling, electrons in the conduction band of the n layer tunnel into the depletion layer and the p layer, where they recombine with holes in the valence band or acceptor levels with emission of photons. The energy of the emitted photon is approximately proportional to the applied voltage. In the band filling, electrons tunnel through the depletion layer into the empty band tail states of the conduction band of the p layer, where they recombine with holes with emission of photons. The maximum emission rate is expected to occur near the quasi Fermi level separation which increases with the filling of the tail states by electrons with increasing bias. Most of those studies were carried out on abrupt junctions, and some were on

linearly graded junctions [6-9]. In this chapter, explanation of the shifting peaks in SiC LED's with a linear and a quadratic impurity profiles are tried.

6-2. Diode Fabrication

The procedures of the overcompensation method and diode fabrication were described in detail in Chapt. V [1,2]. Aluminum was doped as acceptors and nitrogen as donors. Substrates of p type 6H SiC ($p \simeq 1\times10^{18}$ cm^{-3}) were dipped in the Si melt doped with 2.5 at. % Al metal in Ar gas flow, and p layers of about 20 μm with $p \simeq 2.5\times 10^{18}$ cm^{-3} were grown. Subsequently, 0.1-0.5 vol % N_2 gas was added to the Ar gas flow and n layers of about 10 μm were grown. Two representative diodes were studied. The n layer of diode 1 (D1) was grown for 1.5 h in the ambient doped with 0.1 vol % N_2 gas, and the electron concentration was determined to be 1.1×10^{19} cm^{-3} by Hall measurement. The n layer of diode 2 (D2) was grown for 2 h in the ambient doped with 0.5 vol % N_2 gas, and the electron concentration was 2.5×10^{19} cm^{-3}. Since the electron concentrations of the n layers of both diodes were nearly equal or in excess of the density of states of the conduction band 1.7×10^{19} cm^{-3} [10] at room temperature and did not vary from ∿100 K to ∿300 K, the conduction bands of the n layers were degenerated. The p layers of both diodes were not degenerated.

6-3. Diode Characteristics

Figure 1 shows capacitance vs. voltage (C-V) characteristics of D1 and D2. Linear relations are obtained in C^{-3}-V and C^{-4}-V characteristics for D1 and D2, respectively. Most of the diodes studied indicated linear relations in C^{-3}-V characteristics, and a few diodes

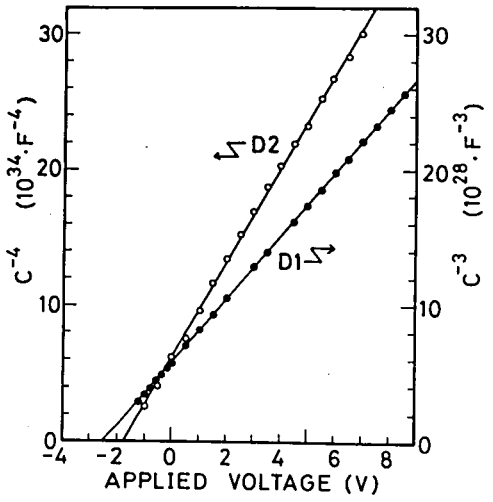

Fig. 1 Capacitance vs. voltage characteristics of D1 and D2.

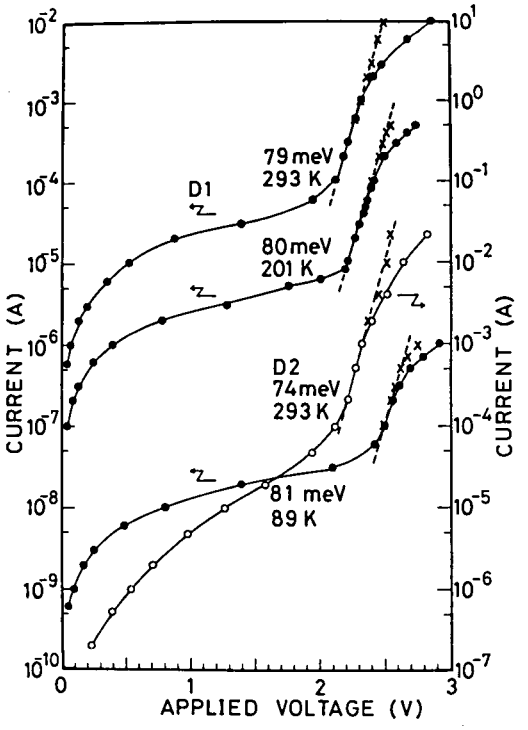

Fig. 2 Current vs. voltage characteristics of D1 and D2 at various temperatures. The crosses indicate the data after subtracting the voltage drops due to series resistances.

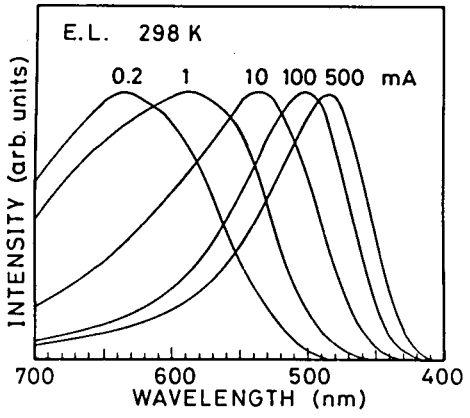

Fig. 3 Electroluminescence spectra of D2 under various driving currents at 298 K.

indicated linearity between powers less than -3 of the capacitance and bias. Figure 2 shows current vs. voltage (I-V) characteristics of D1 and D2. The slopes of the logI-V characteristics of D1 measured at 89, 201, and 293 K are almost the same. The value of E_1 in the expression of $I \propto \exp(eV/E_1)$ is 80 meV. The temperature dependence of logI-V characteristics of D2 was not measured. The value

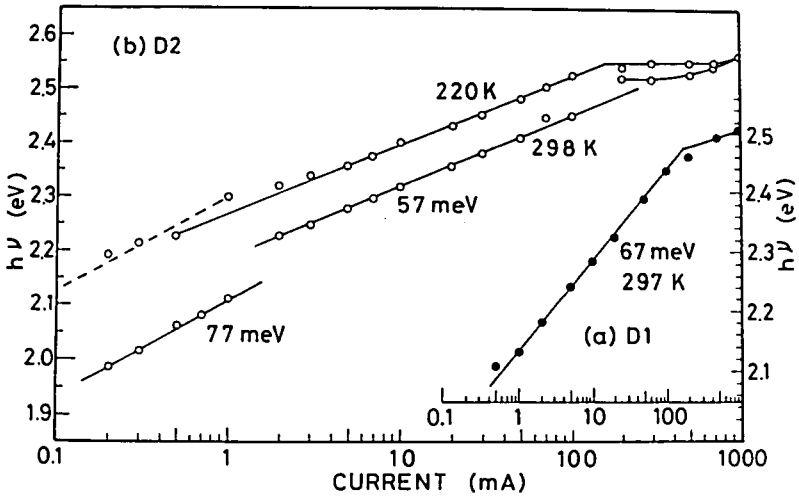

Fig. 4 Peak energy ($h\nu$) vs. current (I) characteristics of (a) D1 at 297 K and of (b) D2 at 220 and 298 K.

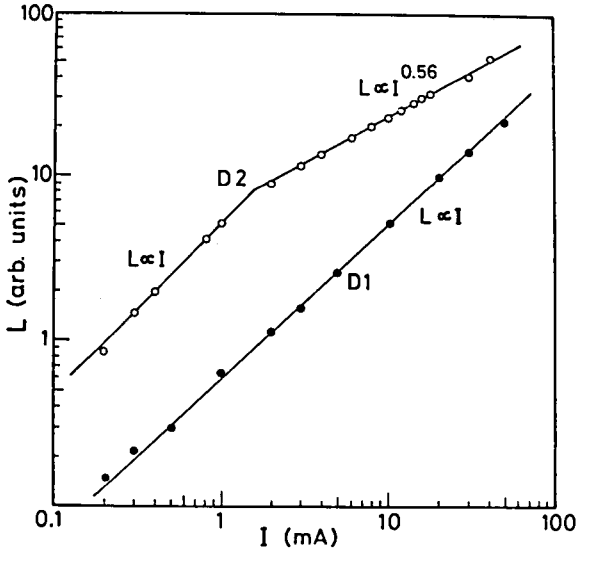

Fig. 5 Luminescence intensity (L) vs. current (I) characteristics of D1 and D2 at room temperature.

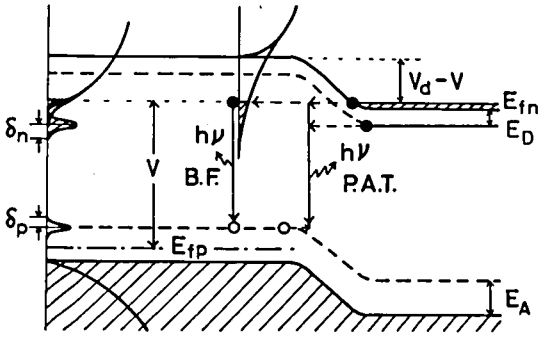

Fig. 6 Schematic diagram to illustrate the photon assisted tunneling (P.A.T.) and the band filling (B.F.).

of E_1 of D2 is 74 meV. The excess current in the low bias region may be due to tunneling current to the tail states and leakage current. Built-in potentials determined from the I-V and C-V characteristics are nearly the same and are 2.5 and 1.9 V for D1 and D2, respectively.

Electroluminescence was measured by driving diodes with pulse currents of 1 kHz and duty cycles of 0.2-0.001. Figure 3 shows that the peak of EL spectrum of D2 shifts with current at room temperature. Such peak shifts were observed at other temperatures. D1 also indicated similar peak shift. Figure 4 shows that the peak energy varies linearly with logI for both D1 and D2. The value of E_2 in the expression of $I \propto \exp(h\nu/E_2)$ of D1 is 67 meV. The slopes of the $h\nu$-logI characteristics of D2 at 220 and 298 K are nearly the same, and E_2 is 57 meV. The $h\nu$-logI characteristics of D2 at 298 K has a kink around 2 mA, and below 2 mA E_2 is 77 meV. Figure 5 shows the luminescence intensity vs. current (L-I) characteristics of D1 and D2. The L-I characteristics of D1 show a relation of $L \propto I$ in all the current range. The L-I characteristics of D2 have a kink around 2 mA and show a relation of $L \propto I$ below 2 mA and $L \propto I^{0.56}$ above 2 mA.

6-4. Discussion

In both the photon assisted tunneling and the band filling models illustrated in Fig. 6, tunneling current expressed as $I \propto \exp(eV/E_1)$ is assumed to be dominant. Both models require the following relations between the EL intensity and the EL peak energy and the bias,

$$L \propto \exp(h\nu/E_2), \tag{1}$$

$$L \propto \exp(eV/E_3). \tag{2}$$

In both models, E_2 and E_3 are the same. From Eqs. (1) and (2) a linear relation between $h\nu$ and V is expected. If all the currents participate in radiative recombinations, a relation of $L \propto I$ is obtained, and the L's in Eqs. (1) and (2) can be replaced by I's. In the case of photon assisted tunneling, E_1 should be equal to E_2 and E_3 which are determined from the electric field in the depletion layer. Whereas in the case of band filling, E_1 is usually not equal to E_2 and E_3 which are determined from the shape of the tail states. The final state of the radiative transitions of EL in D1 and D2 may be acceptor levels, because the probability of band-to-band transitions is small in SiC owing to the indirect band structure. Furthermore, the peak energies of $\sim$2.5 eV in the saturated region in Fig. 4 where diffusion current is dominant, are in good agreement with the peak energy of N-Al pair luminescence in normal LED's (Chapt. VII) [11].

When a diode has a charged impurity profile of a function of the distance (x) as $-a_1|x|^n$ for the p side and $a_2|x|^n$ for the n side in the depletion layer, the capacitance (C) and the depletion width (W) are expressed as,

$$C = [e\varepsilon_S^{n+1}/(n+2)(a_1^{-1/(n+1)} + a_2^{-1/(n+1)})^{n+1}(V_d - V)]^{1/(n+2)}, \quad (3)$$

$$W = [(n+2)\varepsilon_S(V_d - V)/e(a_1^{-1/(n+1)} + a_2^{-1/(n+1)})^{n+1}]^{1/(n+2)}, \quad (4)$$

where ε_S is the static dielectric constant, V_d the built-in potential, and V the applied voltage. Since C^{-3}-V characteristics show a linear relation in Fig. 1, D1 has a linear impurity profile. A quadratic impurity profile is expected for D2 from the linearity of the C^{-4}-V characteristics in Fig. 1. From the C-V characteristics, the depletion width at zero bias and the average coefficient of the impurity profile $\bar{a} = (a_1^{-1/(n+1)} + a_2^{-1/(n+1)})^{-(n+1)}$ are calculated using $\varepsilon_S = 9.78\varepsilon_0$[12], and the values of W = 1700 Å and $\bar{a} = 3.4\times10^{22}$ cm^{-4} for D1 and W = 300 Å and $\bar{a} = 4.7\times10^{29}$ cm^{-5} for D2 are obtained.

Since the gradient of the logI-V characteristics of D1 does not vary with temperature in Fig. 2, the injection mechanism is

tunneling and not diffusion. This result indicates that tunneling is possible for a diode with a thick depletion layer of 1700 Å at zero bias, which is supported by the observation of tunneling in GaAs diodes with depletion width more than 2500 Å at zero bias [8]. Although the temperature dependence of the I-V characteristics of D2 has not been measured, the injection mechanism may be tunneling because of the thinner depletion width of 300 Å than that of D2. The characteristic energies, E_1 in the logI-V characteristics and E_2 in the $h\nu$-logI characteristics in the current region where the relation of $L \propto I$ is satisfied in Fig. 4 are 79 and 67 meV for D1 and 74 and 77 meV for D2, respectively. The relatively good agreement between E_1 and E_2 is one evidence of photon assisted tunneling.

For a linearly graded junction, the luminescence intensity in photon assisted tunneling is expressed as [6,13],

$$L \propto \exp[-2\pi\sqrt{\mu e}\, W_1 (V_d - V)^{5/6}/3\hbar], \qquad (5)$$

where W_1 is the depletion width at zero bias, μ given by $\mu^{-1} = m_e^{-1} + m_h^{-1}$ is the reduced mass, and the barrier for electrons and holes to tunnel through is assumed to be $V_d - V$. From Eq. (5), the slope of logL vs. V is given by,

$$E_3^{-1} = (5/6)(2\pi\sqrt{\mu e}\, W_1/3\hbar)(V_d - V)^{-1/6}. \qquad (6)$$

From Eq. (6), E_3 = 57 meV is obtained for D1 at about 10 mA [$V_d - V \sim$ 0.1 (V)], which is a moderate current in Fig. 4(a), using $m_e = 0.25\, m_0$ [14] in the normal direction of the junction plane, (0001) face, and $m_h = 1.0 m_0$ [15]. In the photon assisted tunneling, the observed values of E_1 = 79 meV in logI-V characteristics and E_2 = 67 meV in $h\nu$-logI characteristics are to be compared with the calculated value of E_3 = 57 meV, and they are in moderated agreement. The factor $(V_d - V)^{-1/6}$ in Eq. (6) requires a variation of E_3 of about 25 % from $V_d - V$ = 0.3 (V) (I $\sim$ 0.3 mA) to $V_d - V$ = 0.05 (V) (I $\sim$ 100 mA) for D1. For a junction with a quadratic impurity profile like D2, a relation of $E_3^{-1} \propto (V_d - V)^{-1/4}$ is expected from its potential barrier of V =

$-Ax^4 + Bx + C$, where A,B,C are constants. This relation requires a variation of E_3 of about 35 % in the range of V_d-V from 0.05 to 0.3 (V). However, such large variations are not observed in E_1 and E_2 of D1 and D2 as shown in Figs. 2 and 4. Similar results were obtained in GaAs linearly graded junctions [6-9]. These results seem to imply that under the large bias condition where shifting peak is observed and the depletion width is thin, the impurity profile can be regarded as abrupt, since only in the case of abrupt junction characteristic energies of E_1 and E_2 are independent of bias.

From Eqs. (1) and (2), a linear relation between $h\nu$ and V is expected. Considering the photon assisted tunneling model in Fig. 6, this relation is expressed as,

$$h\nu = eV - (E_D + E_A) + E_{fp} - (\delta_n + \delta_p) = eV - \Delta. \qquad (8)$$

Here, E_D and E_A are the donor and acceptor ionization energies and 155 and 245 meV (Chapt. IV) [16], respectively, E_{fp} is the hole quasi Fermi level in the p layer, and δ_n and δ_p are the broadenings of the donor and acceptor impurity bands, respectively. For D1, good linearity between $h\nu$ and V was not obtained, but if we dared to estimate, the relation was $h\nu \sim eV - 0.2$ (V). For D2 in a wide range of bias, $h\nu \simeq eV - 0.4$ (V) was obtained. From the estimated acceptor concentration of $\sim 1\times10^{20}$ cm^{-3}[17] ($p = 2.5\times10^{18}$ cm^{-3}), $E_{fp} \simeq 95$ meV is calculated. Since the excess hole concentration of $\sim 2\times10^{18}$ cm^{-3} at 100 mA, which is roughly estimated by assuming that all the electrons recombine with holes within the tunneling length of 500 Å with a lifetime of 0.1 μsec [18], is comparable with $p = 2.5\times10^{18}$ cm^{-3}, the hole quasi Fermi level may not move until a current level of 100 mA. In the case of D2, if the extended donor band merges with the conduction band, Δ is estimated as 0.4 eV. Here, $\delta_n + \delta_p = 95$ meV is assumed, which is a reasonable value [19]. If the band filling model is applied, a reasonable value of Δ is $E_A - E_{fp} + \delta_p \sim 0.2$ (V) which is far smaller than 0.4 V of D2. For D1, if the donor level is

assumed not to merge with the conduction band because of the small donor concentration near the junction expected from the wide depletion width of 1700 Å, the value of Δ can be explained as $E_A - E_{fp} + \delta_p \sim 0.2$ (V) in the photon assisted tunneling model.

Kinks similar to those observed in the $h\nu$-logI (Fig. 4) and L-I (Fig. 5) characteristics of D2 were also observed in GaAs linearly graded junctions [6,8,9]. Archer et al. [6] and Leite et al. [8] have explained the current region above the kink by the band filling. However, in the case of D2, the large shift of about 0.3 eV is difficult to be explained by this model, since the conduction band tail more than 0.3 eV is necessary for the p layer. Casey et al. [9] have well explained the low current region with the relation of $L \propto I^{2.3}$ by the current via deep trap levels based on Morgan's analysis [20]. However, if Morgan's analysis is applied to SiC LED's, a power of 2.0 is obtained, which is far greater than the observed value of 1.0 in the low current region. Therefore, explanation of the kink is difficult. One possible explanation is saturation of luminescence caused by the larger concentration of injected electrons than that of acceptors because of the thin depletion width of D2 [21]. The parallel shift of the $h\nu$-logI characteristics of D2 in Fig. 4 may be due to the variation of the quasi Fermi level like the shift of the logI-V characteristics of D1 in Fig. 2.

6-5. Summary

Shifting EL peaks in the diodes with a linear and a quadratic impurity profiles prepared by the overcompensation method are studied. Most of the characteristics of these diodes are explained by the photon assisted tunneling model, and explanation by the band filling model is difficult. One remarkable result is that the impurity profile of the diode does not make significant effect on

photon assisted tunneling.

References

[1] A. Suzuki, M. Ikeda, N. Nagao, H. Matsunami, and T. Tanaka, J. Appl. Phys. 47, 4546 (1976).

[2] H. Matsunami, M. Ikeda, A. Suzuki, and T. Tanaka, IEEE Trans. Electron Devices ED-24, 958 (1977).

[3] W. v. Münch and W. Kürzinger, Solid-Stale Electron. 21, 1129 (1978).

[4] C. E. Barnes, J. Appl. Phys. 45, 193 (1974).

[5] See a review article by J. I. Pankov, "Optical Processes in Semiconductors" (Prentice-Hall, Inc., Englewood Cliffs, N.J., 1971), p. 177.

[6] R. J. Archer, R. C. C. Leite, A. Yariv, S. P. S. Porto, and J. M. Whelan, Phys. Rev. Lett. 10, 483 (1963).

[7] J. I. Pankov, J. Appl. Phys. 35, 1890 (1964).

[8] R. C. C. Leite, J. C. Sarace, D. H. Olson, B. G. Cohen, and J. M. Whelan, Phys. Rev. 137, A1583 (1965).

[9] H. C. Casey, Jr. and D. J. Silversmith, J. Appl. Phys. 40, 241 (1969).

[10] P. J. Colwell and M. V. Klein, Phys. Rev. 6, 498 (1972); J. A. Lely and F. A. Kröger, in "Semiconductors and Phosphors", edited by M. Schön and H. Welker (Interscience, New York, 1958), p.367.

[11] M. Ikeda, T. Hayakawa, S. Yamagiwa, H. Matsunami, and T. Tanaka, J. Appl. Phys. 50, 8215 (1979).

[12] L. Patrick and W. J. Choyke, Phys. Rev. B2, 2255 (1970).

[13] L. V. Keldysh, Sov. Phys. - JETP 6, 763 (1958).

[14] B. Ellis and T. S. Moss, Proc. Roy. Soc. A299, 383 (1967).

[15] H. J. van Daal. W. F. Knippenberg, and J. D. Wasscher, J. Phys. Chem. Solids 24, 109 (1963).

[16] M. Ikeda, H. Matsunami, and T. Tanaka, J. Lumin. 20, 111 (1979).

[17] G. A. Lomakina, Yu. A. Vodakov, E. N. Mokhov, V. G. Oding, and G. F. Kholuyanov, Sov. Phys. - Solid State 12, 2356 (1971).

[18] R. B. Campbell and H. C. Chang, in "Semiconductors and Semimetals", edited by R. K. Willardson and A. C. Beer (Academic Press, New York, 1971), Vol. 7, p. 625.

[19] When $N_D = 2\times10^{19}$ cm^{-3}, a half width of the impurity band (2δ) of about 120 meV is predicted by S. M. Sze, "Physics of Semiconductor Devices" (Wiley-Interscience, New York, 1969), p. 152.

[20] T. N. Morgan, Phys. Rev. 148, 890 (1966).

[21] Although situation is different, in the case of diffusion current and in the saturated region, a relation of $L\propto I^{0.5}$ is predicted and observed by D. F. Nelson, Phys. Rev. 149, 574 (1966); M. Gershenzon, R. A. Rogan, and D. F. Nelson, Phys. Rev. 149, 580 (1966).

VII. 6H SiC LED'S BY ROTATION DIPPING TECHNIQUE: ELECTROLUMINESCENCE MECHANISMS

7-1. Introduction

In Chapt. V, SiC blue LED's with relatively high efficiency have been realized with the overcompensation method [1,2]. However, the efficiency is not yet satisfactory. The indirect band structure of SiC makes it difficult to attain high efficiency through intrinsic recombination processes. Therefore, introduction of impurities and full use of these luminescent centers are inevitable to attain high efficiency. However, research on the mechanisms of electroluminescence (EL) of SiC LED's is limited [3-5] and the results have been primitive because of the lack of reliable knowledge on photoluminescence (PL).

In this chapter, recombination mechanisms of EL and methods to improve the efficiency are studied on the basis of the results of PL in Chapts. III and IV [6]. For the study of EL mechanisms, separate doping of p and n layers is desirable, but it is impossible by the overcompensation method. Therefore, a rotation dipping technique, which satisfies this condition and enable p-n junction formation in one process [7] is proposed by the author. The relation between the N concentration in the n layers and the efficiency of the LED's is studied. Methods to improve the efficiency are discussed on the results of recombination mechanisms, injection mechanisms, and the dependence of the PL intensity on doping levels in the n layers.

7-2. Crystal Growth and Diode Fabrication

7-2-1. Apparatus

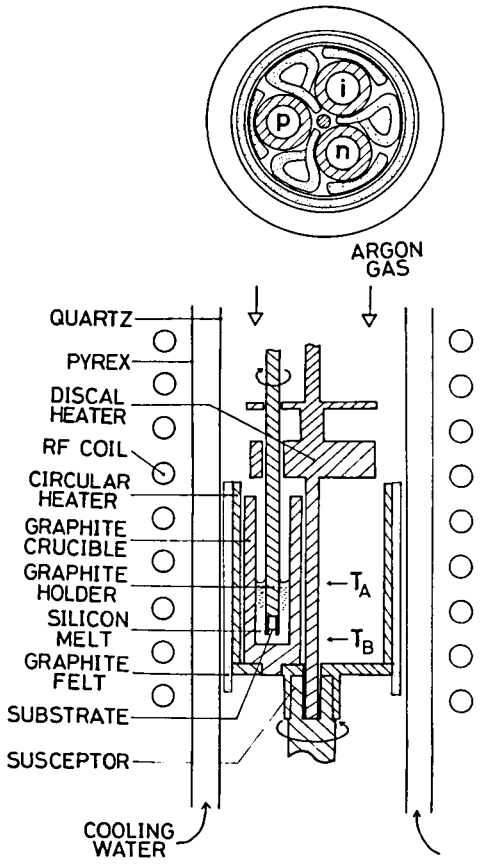

Fig. 1 Growth system for the rotation dipping technique.

Figure 1 sketches a growth system which is composed of three crucibles containing melts for the growth of p and n layers and for rinsing, and a circular heater to keep uniform temperature distribution among the crucibles. The discal heater was equipped to prevent Si melt adhered to the crystal from solidifying upon changing melts. Around the circular heater and the crucibles, graphite felt was fastened for thermal insulation. The substrate holder could be rotated at a rate of 2 rpm and be translated vertically. The crucibles could be exchanged by the rotation of the susceptor for subsequent growth of multilayers. The procedures of the crystal growth are similar to those described in Chapt. II [1,7]. The surface polarity was identified by etching in molten NaOH at 760°C [8] or thermal oxidation [9]. The growth time was 3 h.

7-2-2. Results of crystal growth

Crystal growth was carried out under various conditions in order to obtain smooth surfaces which were desirable for diode fabrication. The growth temperature was varied from 1600 to 1700°C. The temperature difference between the upper part of the melt (T_A) and the bottom part of the crucible (T_B) and the height of the substrates in the melt were varied.

Good epitaxial layers were obtained at T_A = 1650°C and T_B = 1625 °C, with the substrate 3 mm above the bottom of the crucible. Therefore, diodes were grown under these conditions. At 1700°C, good layers were obtained on Si faces, whereas hexagonal islands grew on C faces. At 1600°C, small islands grew on both faces. Substrate crystlas were etched when their position was higher than 6 mm from the bottom. Therefore, meltback before p-n junction formation was carried out at this position. Since many small holes were observed on the layers grown on Si faces, C faces were used for the fabrication of p-n junctions. The polytype of the grown layers was identified by x-ray oscillation photography around the c-axis and by PL.

7-2-3. Impurity doping and diode fabrication

The substrate crystals were epitaxial layers of 100-200 μm grown at 1600°C from Si melts doped with 2.5 at. % Al metal. Crystals grown by Lely method with $p \sim 1.5\times10^{19}$ cm^{-3}, $\mu \sim 8$ $cm^2/Vsec$, and $\rho \sim 0.06$ Ωcm were also used. The crucibles were filled with Si and 2.5 at. % Al metal for the p layer growth, with Si and donor and acceptor materials for the n layer growth, and with Si for rinsing. Impurity materials for the donor were Si_3N_4 powder (99.9 %) or Si polycrystals grown in Ar ambient gas doped with 0.1 vol % N_2 gas. Impurity materials for acceptors were Al metal (99.99 %), Ga metal (99.9999 %),

or B_4C powder (99.9 %). The graphite crucible and the holder were baked at about 1800°C until a vacuum of 1×10^{-5} Torr was obtained. The reaction tube was pumped down to a vacuum of 1×10^{-6} Torr after the growth system was assembled, and Ti-Zr purified Ar gas (∿99.9999 %) was introduced in the tube. After the meltback of the substrate in the melt for p layer growth (p melt) for 10 min, a p layer was grown for 1 h. After the meltback of the grown crystal for 10 min in the rinsing melt and for 20 min in the n melt, an n layer was grown for 2 h. On pulling up, Si melt adhered to the crystal was wiped off to avoid the stress by solidification. The thicknesses of the p and n layers were both 30±10 μm. After lapping of the backside, the grown crystal was cleaved into small dice ∿1×1 mm^2. Al-Si (89:11) [1] was used as an ohmic contact for the p layer, and for the n layer, Au-Ta (99:1) [1] or Ni-Au was used (Chapts. II and V). The die was mounted p-side down on a header by alloying with Au-Ge (88:12) in Ar gas at about 350 °C and a Au wire was bonded to the Au-Ta or Ni-Au contact.

Table I Electrical properties of epitaxial layers.

Sample	Dopant				Conduction type	Carrier concentration (cm^{-3})	Mobility (cm^2/Vsec)	Resistivity (Ωcm)
	Acceptor	(at.%)	Donor	(wt%)				
P-1	Al	2.5			p	2.4×10^{18}	18	0.18
DU-1					n	4.8×10^{17}	174	0.07
D-3	Al	0.1			n	1.0×10^{16}	138	4.2
D-14	Al	0.1	Si_3N_4	0.00025	n	8.7×10^{16}	47	1.5
D-1	Al	o.1	M.A.[a]	1.0	n	3.0×10^{17}	8.3	2.5
D-2	Al	0.1	M.A.[a]	5.0	n	4.9×10^{17}	6.0	3.4
D-9	Al	0.1	Si_3N_4	0.001	n	1.5×10^{18}	8.9	0.46
D-4	Al	0.1	Si_3N_4	0.003	n	2.8×10^{18}	16	0.15
D-5	Al	0.1	Si_3N_4	0.02	n	7.8×10^{18}	75	0.01
DG-2	Ga	5.0	Si_3N_4	0.001	n	1.2×10^{18}	227	0.02
DB-1	B_4C	0.1	Si_3N_4	0.001	n	1.0×10^{18}	63	0.06

[a] A mother alloy of Si polycrystals grown in the ambient gas of 0.1 vol.% N_2 and 99.9 vol% Ar.

Table I shows the electrical properties of the p and n epitaxial layers of the diodes. Hall measurements were carried out at room temperature by the van der Pauw method. The nominally undoped crystal (DU-1) (hereafter referred to as the undoped crystal) was n type with $n \sim 5\times10^{17}$ cm^{-3}, which may be due to nitrogen contamination of the ambient. There was a tendency for the mobilities of the Ga-doped and B-doped SiC crystals to be higher than that of the Al-doped ones [10]. Crystals doped with Al have a tendency for the mobility to reach a minimum in the range $n = 10^{17} - 10^{18}$ cm^{-3}.

7-3. Electrical Properties of Diodes

The capacitance was measured using a YHP-digital-LCR meter 4261A. Figure 2 shows the capacitance (C)-voltage (V) characteristics of a typical diode grown by a normal process, which shows a step junction. Diodes with n layers grown after a briefer meltback time of 10 min have linear graded junctions with C^{-3} varying with voltage (not shown). This is attributed to the gradual impurity profile probably due to mixing of the p melt with the n melt by a short meltback.

Figure 3 shows the forward logI-V characteristics of a relatively good diode. The n value of the current given by $I = I_0 \exp(eV/nkT)$ is 3.1. This value is greater than 2 in the case of the generation-recombination current, which might be due to the leakage current caused by the stress at the time of cleaving, because n = 2 is obtained by mesa etch with Cl_2-O_2-Ar gas system which will be presented in Chapt. VIII. A typical breakdown voltage in the reverse bias is more than 10 V. The series resistance of a typical diode is 10 Ω, whereas diodes grown by a process with short meltback before the n layer growth show larger series resistances of 50-500 Ω. This indicates the importance of the meltback before the n layer growth.

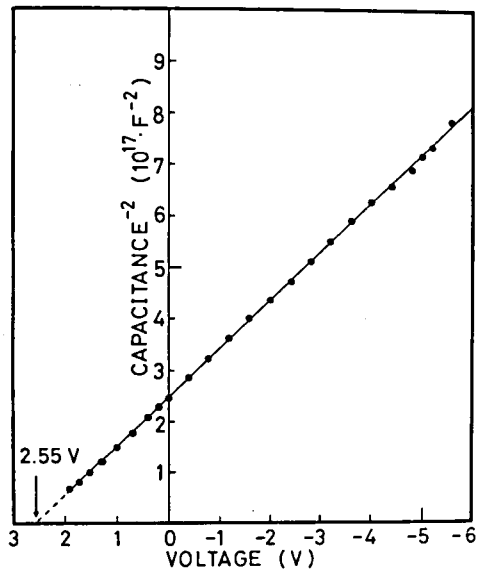

Fig. 2 Capacitance-voltage characteristics of a typical diode.

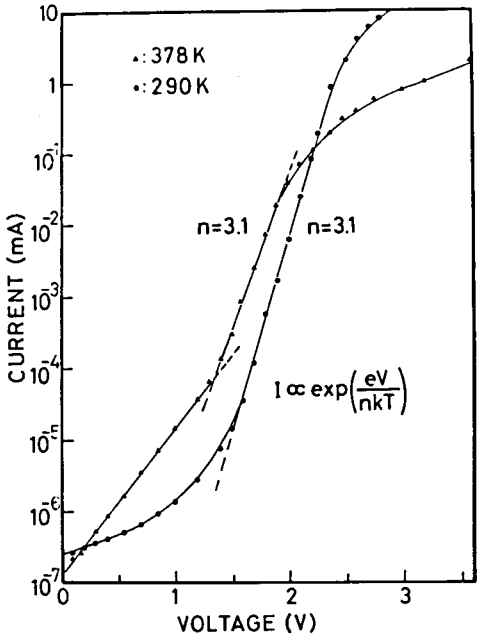

Fig. 3 Forward current-voltage characteristics of a relatively good diode at 290 and 378 K.

7-4. Radiative Recombination Mechanisms

7-4-1. Optical measurements

The diodes for EL measurements were mounted on copper blocks. The diodes were driven with pulse currents of 1 kHz and a duty cycle of 0.1-0.4. For the measurements of time-resolved spectra of EL, the diodes were driven with pulse currents of 3 μsec and 2 kHz, and the current intensity was varied from 500 to 1000 mA. Signals from the photomultiplier were analyzed with an NFC BX530A boxcar integrator. In the PL measurements, samples were excited with 365 nm light from a suitably filtered 250 W Hg lamp or 325 nm light of about 10 mW from a KEC He-Cd laser. Samples were immersed in liquid helium or liquid nitrogen for the PL measurements at 4.2 and 77 K, respectively. For the measurements of PL and EL at ∿100-400 K, a cryostat with a heater was used, and the temperature was monitored by a chromel-alumel

thermocouple.

7-4-2. Temperature dependence of EL

Figures 4(a)-4(d) show the temperature dependences of the EL spectra at various temperatures of an undoped diode (UD), an Al-doped diode (AlD), a Ga-doped diode (GaD), and a B-doped diode (BD). The p layers of all the diodes are doped with Al and $p \sim 2\times10^{18}$ cm^{-3}, Main broad bands (M) vary according to the kind of acceptors doped in the n layers. Since the main broad bands are dominant at room temperature, EL appears green for UD, blue for AlD and GaD, and yellow for BD. Peaks F at about 425 nm are observed in all the spectra and become dominant with increasing temperature. Peaks E at about 455 nm are intense in the spectra of UD and AlD and are significant in the temperature range ∿150-250 K. Peaks D, a series of sharp peaks beginning at about 470 nm, are remarkable in the spectra of UD and AlD, and more intense at low temperatures.

Figure 5 show PL spectra of the n and p layers and EL spectrum of AlD around 100 K. The PL spectrum of the n layer is composed of the A_0 peak due to recombinations of electrons in the conduction band with holes at acceptors, B series peaks due to donor-acceptor (D-A) pair transitions between the donors in the hexagonallike sites and acceptors, and C series peaks due to D-A pair transitions between the donors in the cubiclike sites and acceptors (Chapt. IV). The PL spectrum of the p layer has only C series. The EL spectrum also has only C series like the PL of the p layer. Figure 4 shows that all the EL below about 150 K show similar spectra as the PL of the p layer. The EL of GaD below about 150 K is different from the PL of the n layer which is due to the N-Ga pair luminescence, and above about 180 K the EL spectrum becomes similar to PL. Similar results were obtained for BD. Therefore, we conclude that below about 150 K

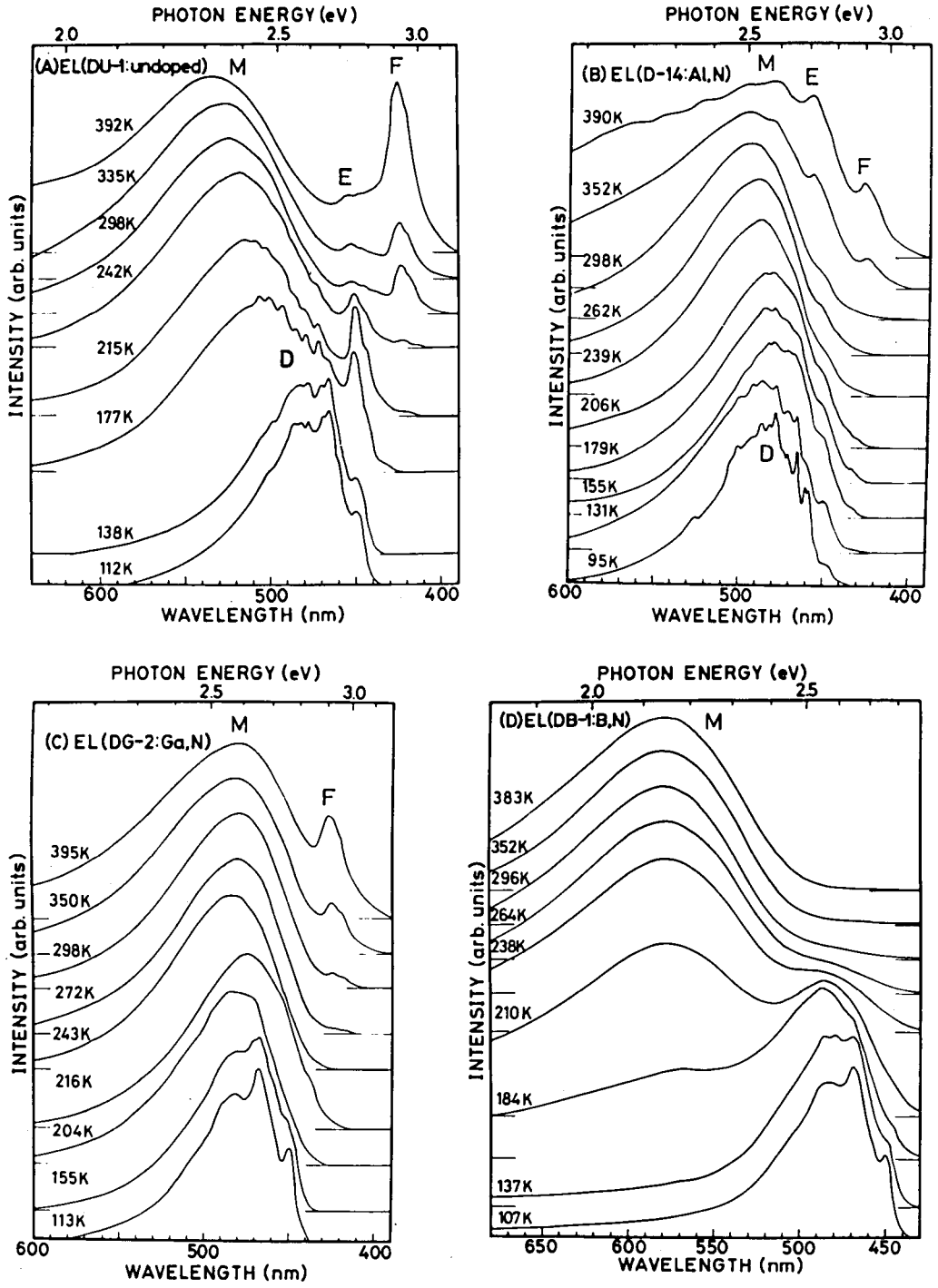

Fig. 4 Temperature dependence of the EL spectra for (a) an undoped diode, (b) an Al-doped diode, (c) a Ga-doped diode, and (d) a B-doped diode.

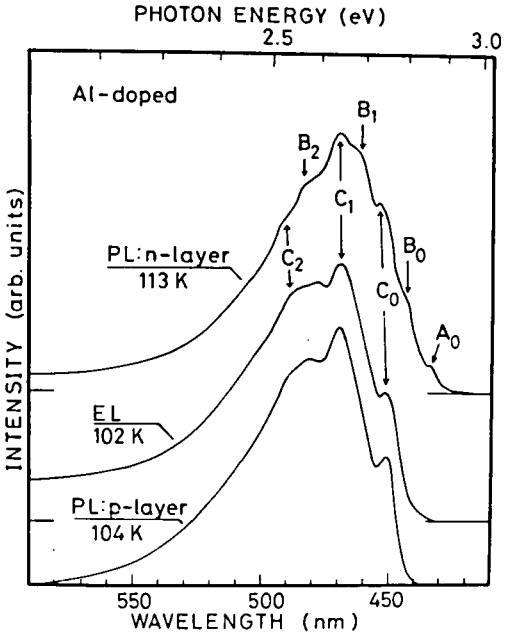

Fig. 5 Comparison between the EL spectrum and the PL spectra of the n and p layers.

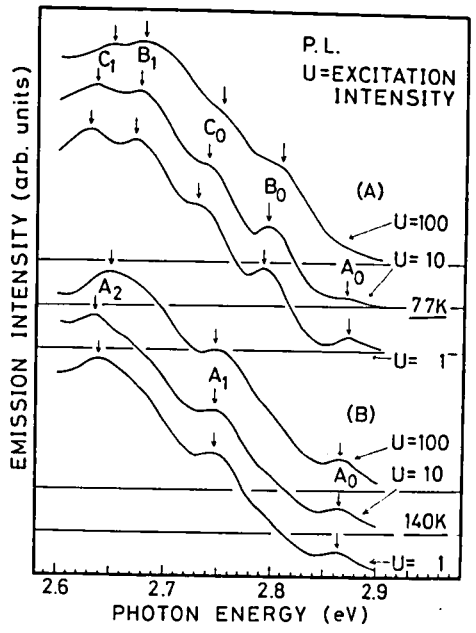

Fig. 6 Photoluminescence spectra of 6H SiC:Al,N under various excitaion intensities at (a) 77 K and (b) at 140 K.

EL originates mainly in the p layers, while above about 180 K it originates in the n layers.

7-4-3. Main broad band

Since the peak energies of the main broad bands at room temperature shift according with the ionization energies of acceptors (see Table II in Chapt. IV), acceptors undoubtedly participate in these bands. The acceptor levels play the role of the final states of the following two recombination mechanisms. Figure 6 shows the dependence of PL of 6H SiC:Al,N on the excitation intensity at 77 K and 140 K. At 77 K, B and C series due to D-A pair transitions are dominant, whereas at 140 K A series due to free-to-acceptor transitions

are dominant. Ionization of N donors with the temperature increase may cause the change of the luminescence mechanism from D-A pair to free-to-acceptor luminescence.

Figures 7(a)-7(d) show the dependence of the EL spectra of UD, AlD, GaD, and BD on the current intensity at room temperature. The spectra of AlD, GaD, and BD show slight peak shift toward the higher energy side. Although each of the phonon replicas cannot be separated in EL due to thermal broadening, the peak shifts of the whole

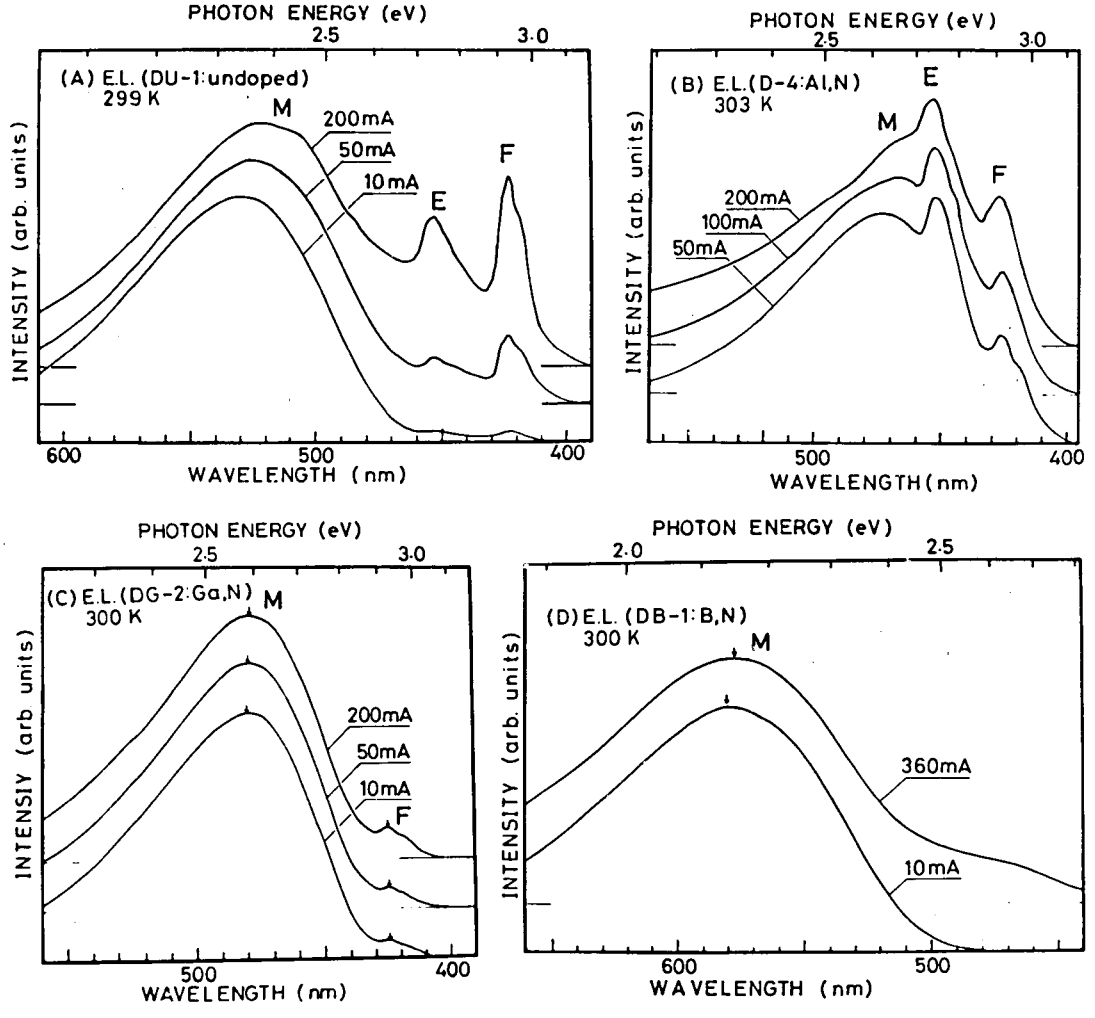

Fig. 7 Electroluminescence spectra under various driving currents for (a) an undoped diode, (b) an Al-doped diode, (c) a Ga-doped diode, and (d) a B-doped diode.

broad bands may indicate the contribution of D-A pair transitions. At room temperature EL exhibits a smaller energy shift than at low temperatures (not shown). This may be due to the large participation of free-to-acceptor transitions at room temperature. The quite large peak shift of the EL of UD in Fig. 7(a) may be due to overlapping of many peaks and the relative change in their intensities with excitation. The main broad band of UD is due to divacancies (Sec. 7-4-5).

Figure 8 shows the time-resolved spectra of AlD at 209 K and 293 K. The spectra at 209 K clearly show a peak energy shift. The peak shift of the spectra in Fig. 8(b) indicates a large participation of D-A pair transitions even at room temperature. Owing to the short decay time at room temperature, spectra at long delay time could not be measured. The decay time of the main broad band luminescence at room temperature is less than a few microseconds, which is the time

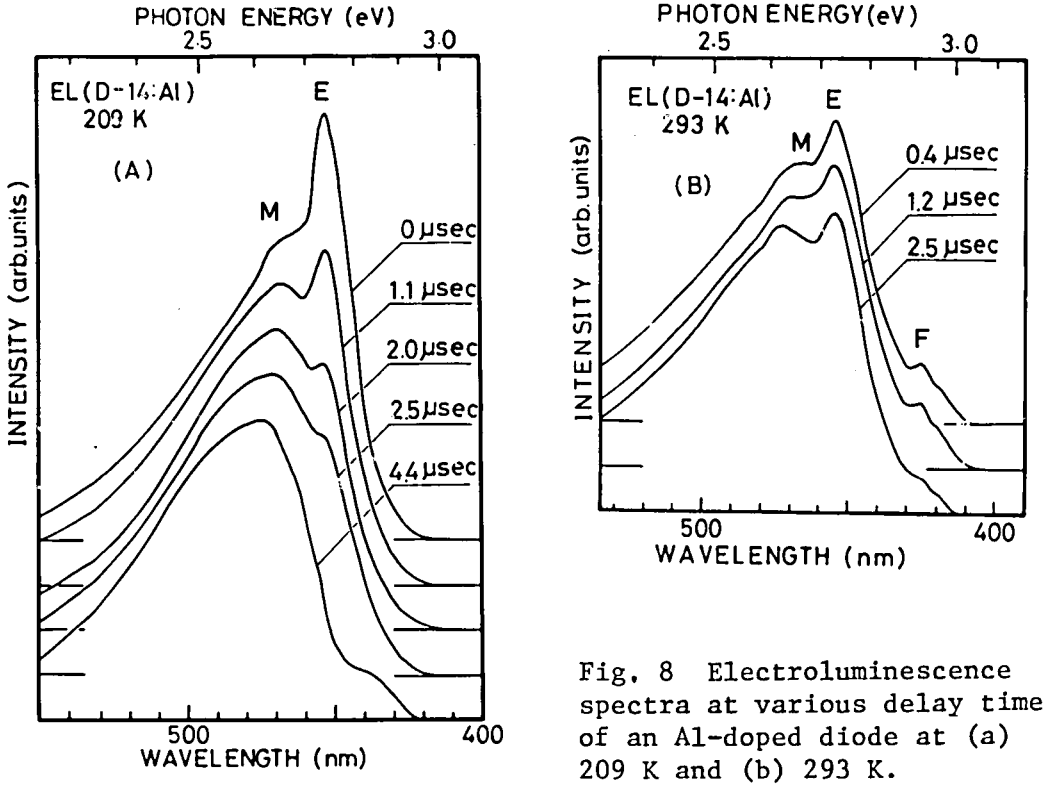

Fig. 8 Electroluminescence spectra at various delay times of an Al-doped diode at (a) 209 K and (b) 293 K.

constant of the measuring system, and several microsecond at 209 K. More distinct peak shifts were observed for GaD and BD. Other evidence of the dominance of the D-A pair transitions at room temperature is a large contribution of N donors to the main broad band. The intensity of the main broad band of AlD with n $\sim 10^{16}$ cm^{-3} in Fig. 9 is far smaller than that with n $\sim 10^{18}$ cm^{-3} in Fig. 7(b).

On the basis of all the above discussion, the dominant luminescence mechanism for the main broad bands at room temperature is D-A pair transitions, and the contribution of free-to-acceptor transitions is rather small. This conclusion contradicts the result that free-to-acceptor transitions are dominant in PL. This may be explained by the difference of the excitation intensity between EL, $\sim 10^{23}$/ cm^3sec at 10 mA (which will be shown in Sec. 7-5), and PL, $\sim 10^{20}/cm^3$ sec. Because of the high excitation in EL, a large portion of the recombinations takes place through D-A pair transitions in small pair distance with a high recombination rate [11] rather than through free-to-acceptor transitions with a low recombination rate.

7-4-4. F peaks

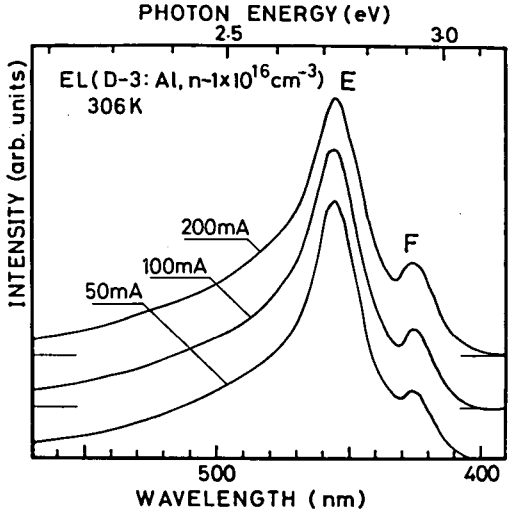

Fig. 9 Electroluminescence spectra of an Al-doped diode slightly doped with N donors under various driving currents.

The F peaks with the peak energy at about 425 nm are observed in all the EL spectra of UD, AlD, GaD, and BD. (For BD, F peaks were observed at a high current density of about 1 A.) The F peaks become more significant with increasing temperature (Fig. 4), and at a fixed temperature the intensity of the F peaks increases with increasing excitation intensity (Fig. 7). In the time-resolved spectra of all the diodes the F peaks exhibit no shift and indicate fast decay [e. g., Fig. 8(b)]. Since the F peaks are observed in EL of all the diodes, the F peaks are due to an intrinsic process or due to N donors which are unintentionally doped from the air.

The energy relations of all the recombination processes with the peak wavelength around 425 nm are as follows:
interband transitions

$$h\nu = E_{GX} + E_X + 2kT - n\hbar\omega \quad (n \geq 1), \tag{1}$$

free exciton recombination

$$h\nu = E_{GX} + \frac{1}{2}kT - n\hbar\omega \quad (n \geq 1), \tag{2}$$

donor-to-valence band

$$h\nu = E_{GX} + E_X - E_D + \frac{1}{2}kT - n\hbar\omega \quad (n \geq 0), \tag{3}$$

bound exciton recombination

$$h\nu = E_{GX} - E_{BX} - n\hbar\omega \quad (n \geq 0). \tag{4}$$

Here, E_{GX}, E_X, E_D, and E_{BX} are the exciton band gap, the free exciton binding energy, the ionization energy of N donors, and the bound exciton binding energy, respectively. $\hbar\omega$ is the phonon energy, and n is the number of emitted phonons. Since SiC is an indirect band gap material, only the recombinations associated with phonon emission are permitted in the interband transitions and the free exciton recombinations.

Figure 10 shows detailed EL spectra of UD at various temperatures and the PL spectrum at 77 K for the F peaks. Figure 10 reveals that the F peaks of EL are composed of three unresolved

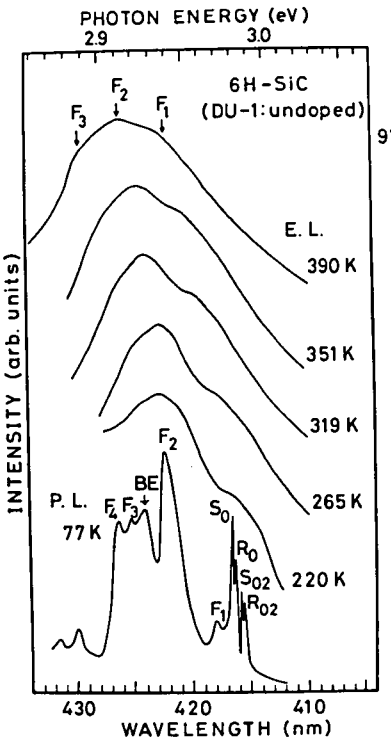

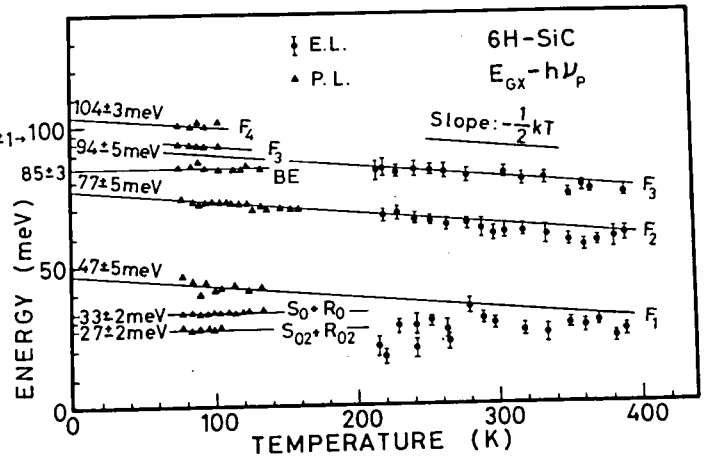

Fig. 11 Temperature dependence of $E_{GX} - h\nu_p$ for F peaks of 6H SiC.

Fig. 10 Detailed spectra of F peaks of 6H SiC. Electroluminescence spectra at various temperatures and PL spectra at 77 K are shown.

peaks. The PL spectrum shows three peaks BE, F_3, and F_4 in addition to the F_1 and F_2 peaks which seems to correspond to the F_1 and F_2 peaks of EL. Figure 11 shows the temperature dependence of the difference between E_{GX} [12,13] and the peak energies ($h\nu_p$) of the F peaks of EL and PL. Figure 11 shows that $E_{GX} - h\nu_p$ decreases with increasing temperature with a slope of -k/2. Up to now the F peaks have been believed to be due to interband transitions as proposed by Brander [3]. If this is the case, the F peaks should indicate a 2k dependence as in Eq. (1). The lowest energy peak due to interband transitions with the emission of a LO phonon (104 meV) is located at 3.02 eV from Eq. (1) using E_{GX} = 2.997 eV at 300 K [13] and E_X = 78 meV [14]. This energy is larger than the ∿2.96 eV (∿419 nm) energy of the highest energy F peak (F_1). Therefore,the F peaks are not due to interband transitions. Also, F peaks are not due to bound excitons

because the values of $E_{GX} - h\nu_p$ exhibit a temperature dependence of k/2.

If the F peaks are due to electron transitions from N donors to the valence band, the energy differences between the band gap and the F peaks will vary from polytype to polytype because of the strong dependence of the N ionization energies on polytypes (Chapt. IV) [15].

Fig. 13 Detailed spectra of F peaks of 3C SiC. Electroluminescence spectrum at 389 K and PL spectrum at 77 K are shown.

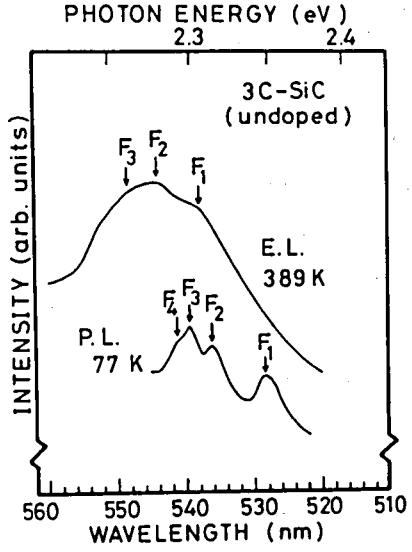

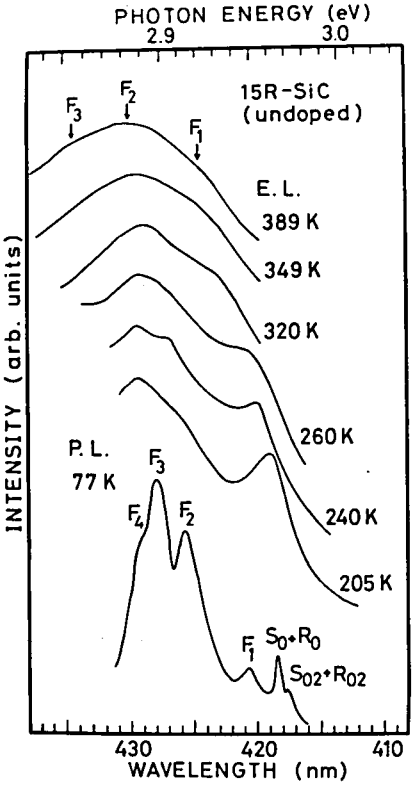

Fig. 12 Detailed spectra of F peaks of 15R SiC. Electroluminescence spectra at various temperature and PL spectra at 77 K are shown.

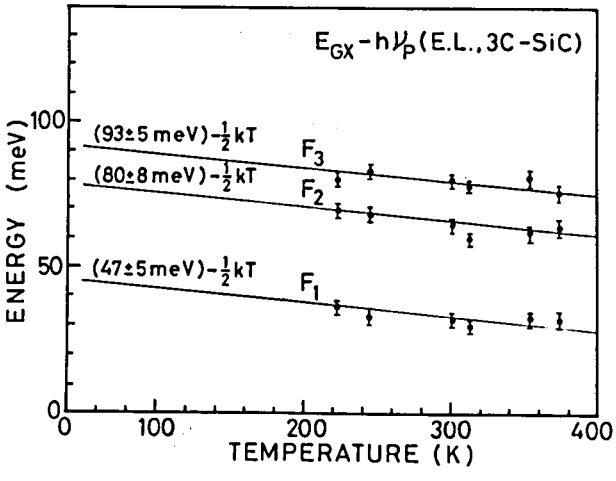

Fig. 14 Temperature dependence of $E_{GX} - h\nu_p$ for F peaks of 3C SiC.

Especially in the case of 3C SiC, the number of the F peaks should be one because the N level is only one (Chapt. IV). Figure 12 shows EL spectra of the F peaks of 15R SiC at various temperatures and PL spectrum at 77 K. Figure 13 shows PL at 77 K and EL at 389 K of the F peaks of 3C SiC. Figure 14 shows $E_{GX} - h\nu_p$ vs. temperature for 3C SiC using the estimated values of E_{GX} by Choyke [13]. The R_0, S_0, and R_{02}, S_{02} peaks in PL of 6H and 15R SiC are exciton lines bound to neutral N donors as studied by Choyke et al. [12,16] around 4.2 K.

As shown in Figs. 11 and 14 (not shown for 15R SiC), all of the F_1, F_2, and F_3 peaks of 6H, 15R, and 3C SiC indicate the k/2 dependence, and the difference of E_{GX} and F_1, F_2, and F_3 peaks are $\sim$46, $\sim$77, and $\sim$95 meV, respectively. These values are in fair agreement with the phonon energies, 46(TA), 78(LA), and 95(TO) meV which are almost independent of polytypes [13] (Chapt. III). F_4 peaks in the PL spectra of 3C and 15R SiC are due to LO phonons because the energy differences between E_{GX} and the F_4 peaks of about 104 meV agree with the LO phonon energy of 104 meV [13]. Compared with PL of 3C and 15R SiC, the F_3 and F_4 peaks in PL of 6H SiC are due to LA and LO phonons. The peak denoted by BE is due to bound excitons from the analysis in Chapt. III. As shown above, the independence of $E_{GX} - h\nu_p$ of polytypes indicates that the F peaks are not due to N donor-to-valence band transitions.

From all the above discussion, we conclude that the F peaks are due to the free exciton recombinations with phonon emission. Free exciton recombinations were also proposed in the cathodoluminescence of 3C SiC [17]. Also, for GaP fairly large participation of the free exciton recombinations around room temperature has been reported [18].

7-4-5. E peaks and D peaks

As shown in Fig. 4, the E peaks with the peak energy at about

455 nm are observed only in EL of UD and AlD and are very weak for GaD and BD. The E peaks emerge at about 150 K and begin to be quenched above room temperature. In the time-resolved spectra in Fig. 8, the E peaks exhibit rather fast decay and indicate no peak shift with the increase of the delay time. Figure 15 shows minute EL spectra at various temperatures and PL spectrum of an undoped crystal at 77 K for the E peaks. The E peaks are composed of many sharp peaks. Figure 16 shows the temperature dependence of $E_{GX} - h\nu_p$ for the E peaks. Since the E peaks follow the temperature dependence of E_{GX}, free carriers do not contribute to these recombinations. The PL intensity of E peaks in undoped crystals varies with the growth conditions such as the growth rate and the growth temperature, though systematic study has not been carried out. From the above discussion, the E peaks are considered to be due to the recombinations of excitons bound to some unknown intrinsic defects.

The D peaks which are a series of sharp peaks beginning about 470 nm are intense in the EL of UD and AlD. Figure 17 shows EL spectra of a typical AlD ($n = 5.8\times10^{16}$ cm^{-3}) under driving currents of around 1 mA at various temperatures and PL spectrum of an undoped crystal at 77 K. The EL spectrum at 128 K is a sum of the D-A pair luminescence (Fig. 5) and the series of sharp peaks (D peaks) as those of PL at 77 K in Fig. 17. With increasing temperature, the peak height of each sharp peak becomes weak compared with the main broad band composed of their phonon replicas. The main broad band at 293 K coincides with that of UD in Fig. 7(a). The D peaks in PL at 77 K in Fig. 17 are assigned by Dean, Choyke, and Patrick [19,20] to be due to recombinations of excitons bound to some neutral intrinsic defect complexes with a symmetry axis parallel to the c-axis. They proposed the divacancy for the defect. The differences between the PL peak energies and the exciton band gap at 77 K [12] are 387, 432, 470 meV, and so on. The arrows in EL spectra in Fig. 17 indicate the peak energies obtained by subtracting these binding energies

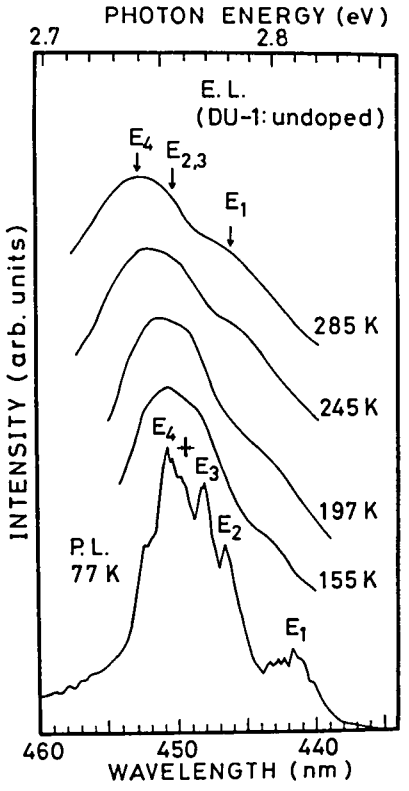

Fig. 15 Detailed spectra of E peaks for EL at various temperatures and PL at 77 K.

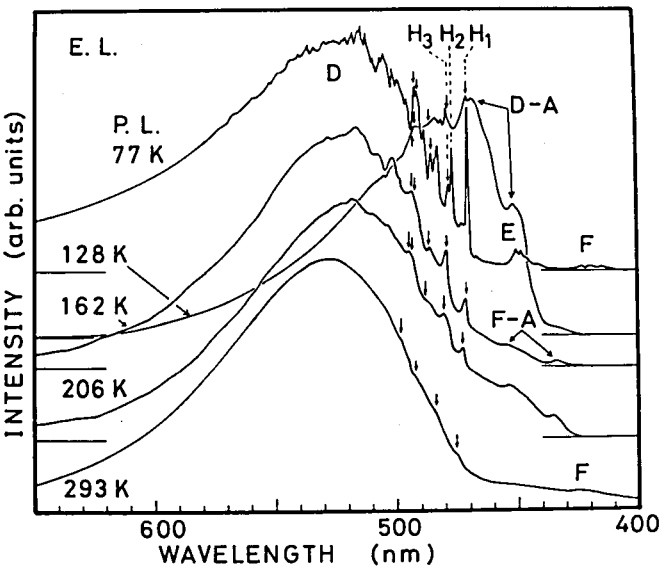

Fig. 17 Electroluminescence spectra at various temperatures and PL spectrum at 77 K of D peaks.

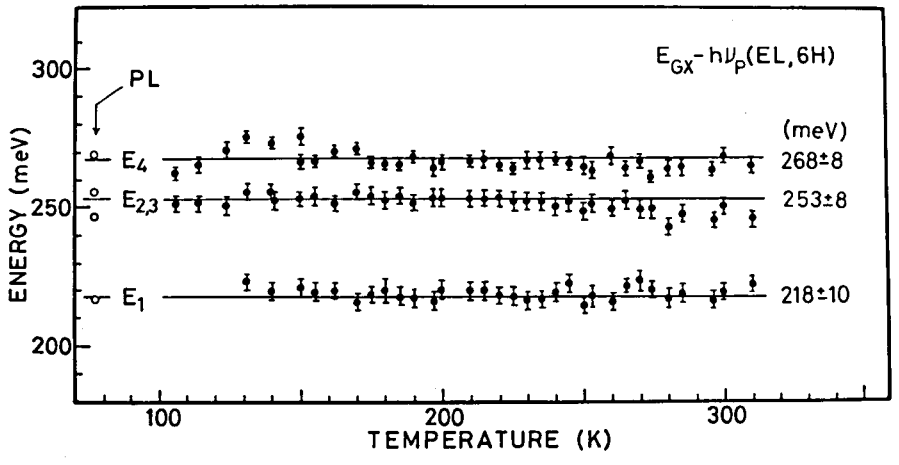

Fig. 16 Temperature dependence of $E_{GX} - h\nu_p$ for E peaks.

from the exciton band gap at each temperature [12,13]. The EL peaks at different temperatures well coincide with the calculated energies. This result indicates that the green peak at about 530 nm in EL at room temperature is due to the recombinations of excitons bound to divacancies. The spectrum due to divacancies is composed of three series of peaks H_1, H_2, and H_3 [19] because of three crystallographically inequivalent sites in 6H SiC. The shallower two series H_1 and H_2, especially H_2, quench more rapidly than the deepest H_3 series, and the H_2 series disappear at about 130 K. The F-A peak in Fig. 17 may be due to free-to-acceptor transitions, because the peak wavelength 434 nm (2.86 eV) and 453 nm (2.74 eV) are in good agreement with those of free-to-acceptor luminescence in Fig. 6(b).

Since the green color of the D peaks spoils the blue color of the N-Al pair luminescence in EL, suppression of these peaks is desirable. Peaks similar to D peaks were reported by many researchers [3,4,21,22]. The D peaks were observed in all the 3C, 4H, 6H, and 15R SiC [23] crystals grown from Si melts. However, Geitsi et al. [24] reported that D peaks were very weak compared with the free exciton peak (1:100) in 3C SiC crystals grown by thermal decomposition of trimethyl-chlorosilane in the temperature range of 1500-2000°C which includes the growth temperature of the present crystals. Also, in the crystals grown by Lely method at about 2500°C, D peaks were not observed [19]. Therefore, the D peaks due to divacancies in the present crystals may be generated by large deviation of the melt from stoichiometry; the solubility of C in Si melt at 1650°C is about 0.03 at. % [25]. This deduction implies that increase of C solubility in the growth melt is necessary in order to suppress this green peak.

7-5. Radiative Efficiency

7-5-1. Experimental results

Measurements of the external quantum efficiency were carried out by driving diodes with pulse currents of 1 kHz and duty cycle of 0.1 using the integration sphere method. Figure 18 shows EL intensity (L) vs. current (I) characteristics of UD, AlD, GaD, and BD at room temperature. In the case of AlD above about 10 mA, the EL intensity is proportional to the current intensity, and so the efficiency is nearly constant. In the cases of UD, GaD, and BD, the L-I characteristics are superlinear below about 10 mA and are sublinear above about 10 mA, and so the efficiencies of these diodes show maxima around 10 mA. The maximum external quantum efficiencies obtained at room temperature are 1.2×10^{-5} for AlD, 9×10^{-6} for GaD, 2.5×10^{-5} for BD, and 1.8×10^{-6} for UD. When the diodes are coated with epoxy resin, the efficiencies are improved by a factor of 2 as shown for BD in Fig. 18 as an example.

Figure 19 shows the external quantum efficiency, the PL intensity of the n layers at 77 K, and the injection efficiency of holes into the n layers vs. the electron concentration at room temperature. The p layers of all diodes are doped with Al acceptors and $p \sim 2\times10^{18}$ cm^{-3}, and the n layers are grown from the melts doped with 0.1 at. % Al acceptors and various amount of N donors. The efficiency increases with increasing electron concentration and shows a maximum around $n \sim 3\times10^{17}$ cm^{-3}. Above $n \sim 3\times10^{17}$ cm^{-3}, the efficiency decreases with increasing electron concentration, whereas the efficiency at 77 K is around 6×10^{-5} independent of doping level of N in the n layer. The PL intensity is nearly constant below $n \sim 3\times10^{18}$ cm^{-3}, and decreases above $n \sim 3\times10^{18}$ cm^{-3} with the increase of the electron concentration. The injection efficiency is roughly estimated using a diffusion current model. The diffusion length and the mobility of holes are assumed to be independent of doping, and typical values of the mobilites of electrons and holes were used (L_n = 1.6 μm, L_p = 0.85 μm, μ_n = 50 cm^2/Vsec, and μ_p = 20 cm^2/Vsec) [26].

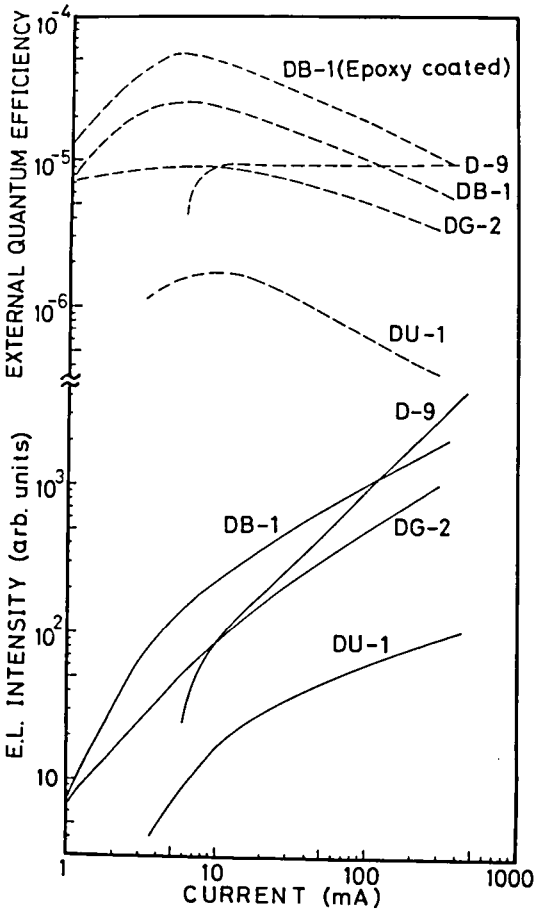

Fig. 18 Electroluminescence intensity and external quantum efficiency vs. current intensity for an undoped diode(DU-1), an Al-doped diode(D-9), a Ga-doped diode(DG-2), and a B-doped diode(DB-1). For DB-1 the characteristics after epoxy coating are also shown.

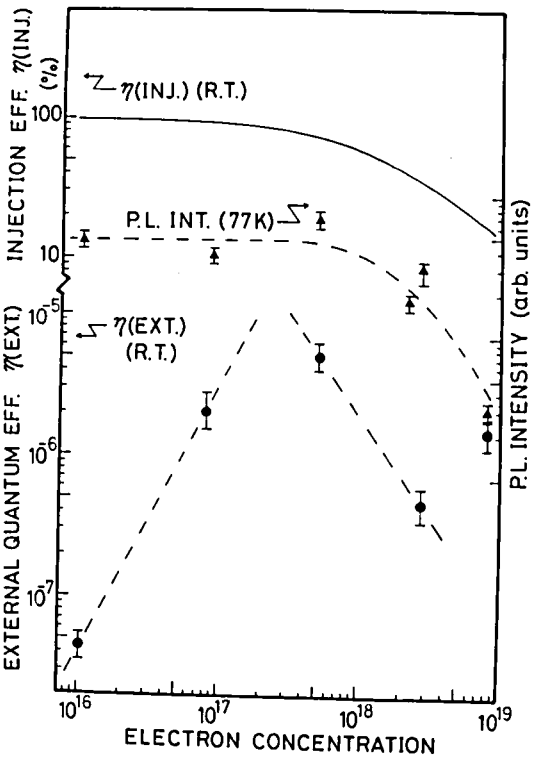

Fig. 19 Dependence of the external quantum efficiency of Al-doped diodes, the PL intensity of the n layers at 77 K, and the injection efficiency on the electron concentration of the n layers at room temperature.

7-5-2. Discussion

The saturation of the L-I characteristics of GaD and BD in contrast to the nonsaturation of AlD is explained by the low concentrations of Ga and B acceptors compared with Al acceptors as follows.

The Al concentration in SiC grown from a melt doped with 0.1 at. % Al is estimated to be $\sim 10^{20}$ cm^{-3}. Whereas, the Ga concentration in SiC grown from a melt doped with 5 at. % Ga is estimated to be $\lesssim 10^{18}$ cm^{-3} from the solubility limit of Ga in the C face at 1650°C of $\sim 2\times 10^{18}$ cm^{-3} by Vodakov et al. [27]. Also, the solubility of B at 1650°C seems to be small because the PL intensity is weak and does not vary in the doping range of B from 0.0001 to 1 at. % in Si melt.

When a current of 10 mA flows through a junction with an area (A) of 1 mm^2, the injected hole rate is

$$g = I/eL_pA \sim 7\times 10^{22}/cm^3sec, \qquad (5)$$

on the assumption that the hole current is dominant and all the holes recombine within the diffusion length (L_p = 0.85 μm). Since the decay time of the recombination is estimated to be ∿3 μsec, the minority carrier concentration is $\sim 3\times 10^{17}$ cm^{-3}. For GaD with the Ga concentration of $\lesssim 10^{18}$ cm^{-3}, the saturation of the L-I characteristics is expected to occur at a current ∿30 mA. Although this value is greater than ∿10 mA of the peak efficiency current, this may explain the saturation of the EL intensity of GaD. By this model for AlD, the saturation may not occur until ∿10 A, and this explains the nonsaturation of the L-I characteristics up to ∿1 A.

By comparing the EL efficiency, the PL intensity, and the injection efficiency in Fig. 19, the decrease of the EL efficiency above $n \sim 10^{18}$ cm^{-3} is explained by the decrease of the injection efficiency and the decrease of the PL intensity probably due to the increase of the Auger nonradiative recombinations. The efficiency of EL decreases with decreasing electron concentration below $\sim 10^{17}$ cm^{-3}, but the PL intensity remains constant. This may be due to the difference of the excitation rate between EL ($\sim 10^{23}/cm^3sec$) and PL ($\sim 10^{20}/cm^3sec$). In the case of low N concentration, saturation of D-A pair transitions occurs for EL because of high excitation, but not for PL. Furthermore, at room temperature, D-A pair transitions compete with thermal ionization of N donors. In this competition, thermal

ionization becomes more dominant with decreasing N concentration because D-A pair transition probability decreases with increasing average pair distance [11]. In Fig. 19, a diode with a high electron concentration, $n \sim 10^{19}$ cm^{-3}, indicates rather high efficiency. This may be due to the recombination mechanism of this diode, which is photon assisted tunneling (Chapt. VI). The independence of the EL efficiency of the doping level at 77 K may be due to the fact that the radiation in the p layer is dominant.

By the above discussion, the following methods to improve the efficiency may be deduced. It is necessary to increase donor and acceptor concentrations to decrease the average D-A pair distance and to decrease the electron concentration by compensation in order to increase the injection efficiency and decrease the Auger recombinations. The Ga-doped diodes exhibit a comparable efficiency to that of the Al-doped diodes in spite of the low concentration of Ga. This may be due to the small ionization rate of Ga acceptors as a result of deeper level compared with Al acceptors (Chapt. IV). Therefore, high efficiency Ga-doped blue LED's may be realized by increasing the growth temperature to increase the solubility of Ga acceptors [27]. Furthermore, an increase in the growth temperature causes an increase of the carbon solubility in Si melt [25], which may improve the crystal perfection.

7-6. Summary

Good epitaxial layers of 6H SiC are reproducibly obtained by the rotaion dipping method which is proposed by the author. This method is convenient in the case that the melt reacts with the crucible and so a sliding boat method cannot be used. Furthermore, this method permits the reuse of melts and crucibles. By the study of the luminescence mechanisms in this chapter the following conclusions are obtained. At low temperatures EL originates mainly in the p layers

and around room temperature mainly in the n layers. The main broad bands are mainly due to D-A pair transitions. The F peaks which have been explained by the interband transitions are shown to be due to the free exciton recombinations associated with phonon emission. The E peaks are due to transitions of excitons bound to some unknown intrinsic defects. The D peaks are due to the transitions of excitons bound to divacancies. The dependences of EL and PL efficiencies on the doping of N donors in the n layers are studied and the maximum efficiency of EL is obtained at $n \sim 10^{17} - 10^{18}$ cm^{-3}. Methods to improve the efficiency are discussed using the results. The maximum external quantum efficiencies obtained for the uncoated diodes are 1.2×10^{-5} for Al-doped, 9×10^{-6} for Ga-doped, and 2.5×10^{-5} for B-doped diodes. By a preliminary experiment, an efficiency of 0.3 % at 77 K is obtained for an Al-doped diode. By the encapsulation with epoxy resin these efficiencies are improved by a factor of 2.

References

[1] A. Suzuki, M. Ikeda, N. Nagao, H. Matsunami, and T. Tanaka, J. Appl. Phys. 47, 4546 (1976).

[2] H. Matsunami, M. Ikeda, A. Suzuki, and T. Tanaka, IEEE Trans. Electron Devices ED-24, 958 (1977).

[3] R. W. Brander, General Electric Company J. Science Tech. 32, 15 (1965).

[4] R. W. Brander and R. P. Sutton, J. Phys. D2, 24 (1969).

[5] Yu. S. Krasnov, T. G. Kmita, I. V. Ryzikov, V. I. Pavlichenko, O. T. Sergeev, and Yu. M. Suleimanov, Sov. Phys. - Solid State 10, 905 (1968).

[6] M. Ikeda, H. Matsunami, and T. Tanaka, J. Lumin. 20, 111 (1979).

[7] M. Ikeda, T. Hayakawa, S. Yamagiwa, H. Matsunami, and T. Tanaka, J. Appl. Phys. 50, 8215 (1979).

[8] J. W. Faust, Jr., in "Silicon Carbide", edited by J. R. O'Connor and J. Smiltens (Pergamon Press Ltd, Oxford, 1960), p. 403.

[9] W. von Münch and I. Pfaffender, J. Electrochem. Soc. 122, 642 (1977).

[10] This may be explained by the smaller concentrations of Ga and B compared with Al, or by the impurity effect that Ga and B impurities prevent defects such as dislocations as reported by Y. Seki, H. Watanabe, and J. Matsui, J. Appl. Phys. 49, 822 (1978).

[11] D. G. Thomas, J. J. Hopfield, and W. M. Augustyniak, Phys. Rev. 140, A202 (1965).

[12] W. J. Choyke and L. Patrick, Phys. Rev. 127, 1868 (1962).

[13] W. J. Choyke, Mater. Res. Bull. 4, S141 (1969).

[14] V. I. Sankin, Sov. Phys. - Solid State 17, 1191 (1975).

[15] G. A. Lomakina, Yu. A. Vodakov, E. N. Mokhov, V. G. Oding, and G. F. Kholuyanov, Sov. Phys. - Solid State 12, 2356 (1971).

[16] L. Patrick, D. R. Hamilton, and W. J. Choyke, Phys. Rev. 132, 2023 (1963).

[17] I. I. Geiczy and A. A. Nesterov, in "Silicon Carbide - 1973", edited by R. C. Marshall, J. W. Faust, Jr., and C. E. Ryan (University of South Carolina Press, Columbia, 1974), p. 313.

[18] R. Z. Bachrach and O. G. Lominor, Phys. Rev. B7, 700 (1973).

[19] L. Patrick and W. J. Choyke, Phys. Rev. B5, 3253 (1972).

[20] P. J. Dean, D. Bimberg, and W. J. Choyke, in "Defects and Radiation Effects in Semiconductors 1978", edited by J. H. Albany (The Institute of Physics, Bristol and London, 1979), p. 447.

[21] W. von Münch, W. Kürzinger, and I. Pfaffender, Solid-State Electron. 19, 871 (1976).

[22] V. M. Gusev, K. D. Demakov, M. G. Kosaganova, M. B. Reifman, and V. G. Stolyarova, Sov. Phys. - Semicond. 9, 820 (1976).

[23] V. V. Makarov, Sov. Phys. - Solid State 9, 457 (1967).

[24] I. I. Geitsi, A. A. Nesterov, and L. S. Smirnov, Sov. Phys. - Semicond. 2, 224 (1968); I, I, Geitsi, A. A. Nesterov, and L. S. Smirnov, ibid. 4, 744 (1970); S. N. Gorin and A. A. Pletyushkin, Izv. Akad, Nauk SSSR Ser. Phys. 28, 1310 (1964) (in Russian).

[25] R. I. Scace and G. A. Slack, J. Chem. Phys. 30, 1551 (1959).

[26] The diffusion lengths of electrons and holes were measured by electron beam induced currents.

[27] Yu. A. Vodakov, G. A. Lomakina, E. N. Mokhov, E. I. Radovanova, V. I. Sokolov, M. M. Usmanova, G. F. Yuldashev, and

B. S. Machmudov, Phys. Status Solidi A35, 37 (1979).

VIII. ETCHING OF SiC WITH Cl_2-O_2-Ar GAS SYSTEM

8-1. Introduction

Silicon carbide is a promising material [1] for light-emitting diodes [2], for devices operating at high temperatures, and for high power devices because of its large band gap and chemical stability. These advantageous properties, on the contrary, make fabrication process difficult. The etching process with Cl_2, O_2, and Ar mixed gas [3] together with a native oxide, SiO_2 - a good etch mask, is an excellent fabrication process, which enables even planar technique. Etch rate can be easily varied by changing gas composition. Actually, this technique has been successfully applied to the fabrication of junction-gate unipolar transistors [4], bipolar transistors [5], and light-emitting diodes [6]. Another etching gas H_2 is reported by some researchers [7,8], which is commonly used to etch substrate crystals before gas phase epitaxial growth. Kumagawa et al. [9] reported thermodynamical analysis of H_2 gas system. This system needs higher temperatures of 1600-1700°C than those of Cl_2-O_2-Ar gas system of 1000-1100°C, while etch rates are comparable. Therefore, the Cl_2-O_2-Ar gas system is more suitable for a device fabrication process. However, no detailed studies and thermodynamical analyses of this system have been reported.

In this chapter, etching of SiC with Cl_2, O_2, and Ar gas mixture is studied in various temperature range, gas composition range, and gas flow rate range. These conditions involve the condition commonly used in device fabrication [1,6]. Thermodynamical analysis of this system is tried and good agreement is obtained between experiment and a simple theory using one parameter. The reason for the large difference of the etch rates between the Si face and the C face [1,6] is discussed based on the result of the thermodynamical analysis. The effect of mesa etch with this gas system on diode characteristics

is examined.

8-2. Experimental Procedure

Crystals grown by Acheson method [10] were used for the experiment. These crystals were 6H SiC of $n \simeq 1\times10^{18}$ cm^{-3}. The (0001) faces were lapped with SiC abrasive powders and polished with diamond paste. These crystals were thermally oxidized in wet oxygen gas. The thicknesses of the oxide layers were about 2000 Å for $(000\bar{1})$C faces and several hundred angstroms for (0001)Si faces. These crystals were cut into a dimension of about $1\times5\times0.3$ mm^3 and some parts of the oxide layers were etched off with HF solution. The oxide layer acted as an etch mask.

A schematic diagram of the etching system was described in Fig. 1. The inner diameter of the quartz reaction tube was 30 mm. Samples were loaded on a quartz sample holder. An electric furnace was made to be easily moved in order to enable rapid increase and decrease of the temperature of the reaction tube. Ar gas flew until the furnace was heated up to a given temperature, and Cl_2 and O_2

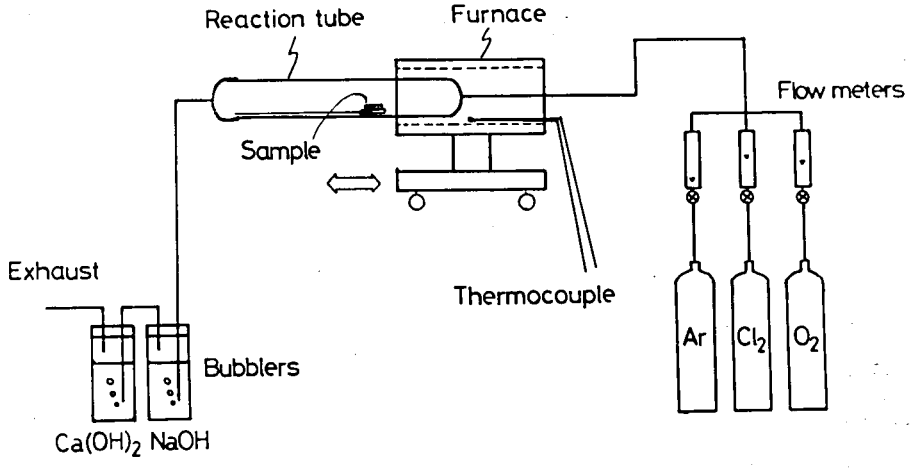

Fig. 1 Cl_2-O_2-Ar gas etching system.

gases were supplied. As soon as the etching time was over, the supply of Cl_2 and O_2 gases were stopped, the furnace was moved away, and the reaction tube was cooled down rapidly. The standard etching time was 10 min. The flow rates of Cl_2, O_2, and Ar gases were monitored by flowmeters. The temperature of the outside of the reaction tube was measured by a chromel-alumel thermocouple and was converted to the inside temperature. Etch rate was determined by measuring the difference of the thicknesses between the etched layer and the unetched layer covered with SiO_2 film with an interference microscope.

8-3. Results

Figure 2 shows SEM photographs of typical etched layers of a C face and a Si face. Unetched layers are covered with SiO_2. The etched C face shows a rather smooth surface and small etch pits. The etched Si face shows many lines of scratches at the time of polishing which are emphasized by the etching. Some parts of the SiO_2 film are removed owing to small thickness of SiO_2 layer on the Si face. These photographs show that the step height on the Si face is far smaller than that on the C face.

Figure 3 shows etch rate on C faces vs. square root of the total gas flow. The ratio of the partial pressures of the mixed gases is constant, $P_{Cl_2}:P_{O_2}:P_{Ar} = 45:10:120$. The etching reaction in this figure on the C face is divided into two regions [11,12]. One is the slow flow rate region where the etch rate increases linearly with square root of the total gas flow. This region corresponds to mass transfer controlled condition. The other is the fast flow rate region where the etch rate is almost constant. This region corresponds to surface reaction controlled condition. For the Si face in the same range of the flow rate, etch rate was nearly constant of 0.01-0.02 μm/min, although the data points scattered because of the large experimental uncertainty due to thin etched layers. These results

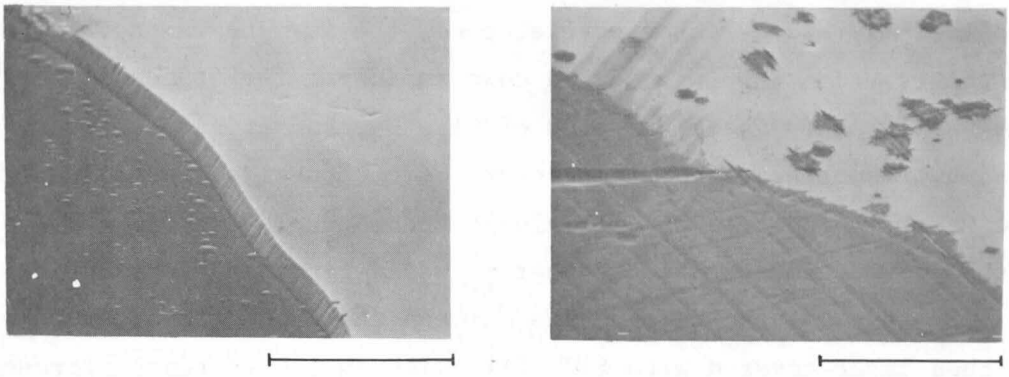

(a) C face (b) Si face

Fig. 2 Typical etched surfaces of a C face and a Si face. The etching conditions are 1000°C, Cl_2:45 cc/min, O_2:10 cc/min, Ar:120 cc/min, and etching times are 20 min for the C face and 10 min for the Si face.

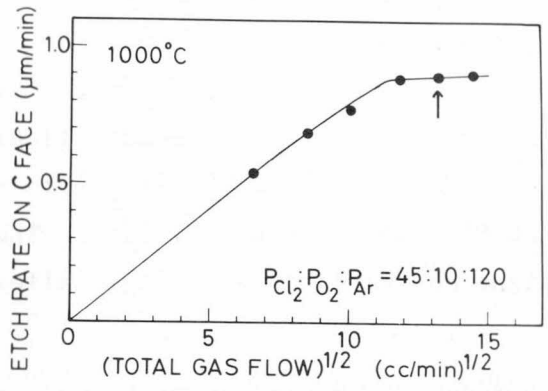

Fig. 3 Etch rate vs. square root of total flow at 1000°C for C faces.

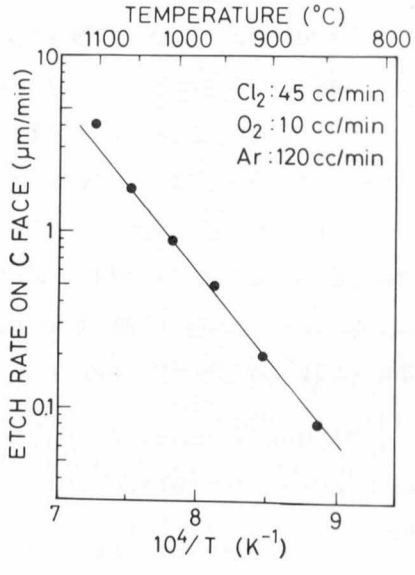

Fig. 4 Temperature dependence of the etch rate on C faces.

indicate that the etching on the Si face is also under surface reaction controlled condition. Etching experiments hereafter are carried out under the condition indicated by an arrow in Fig. 3 which belongs to surface reaction controlled condition. Good linearity between the thickness of the etched layer and etching time is obtained under this condition. This etching condition is commonly used in device

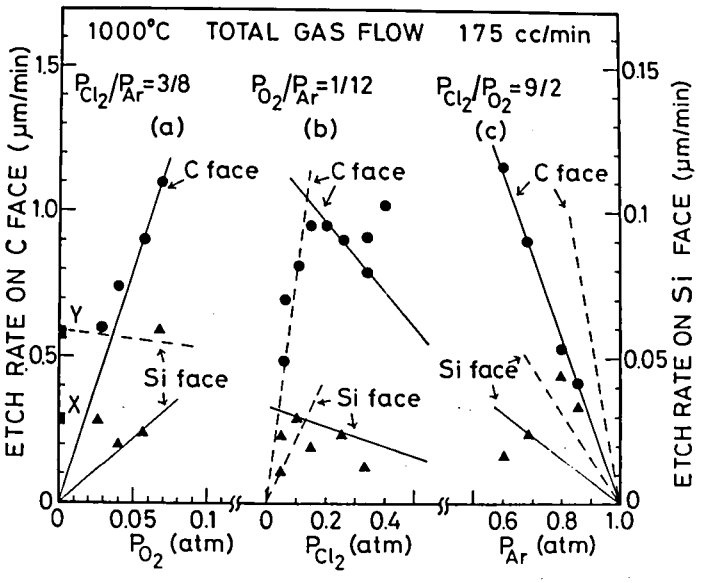

Fig. 5 Etch rate under various gas compositions at 1000 °C. The circles are for C faces and triangles for Si faces. The square denoted by X indicates the etch rate with a carbon film and that denoted by Y indicates that after removing the carbon film. Solid lines denote the calculated lines of L_{O_2} and broken lines of L_{Cl_2} from Eq. (13). The L_{O_2} line in the case of constant P_{Cl_2}/P_{Ar} is out of range of Fig. 5(a).

fabrication peocesses [1,6]. Figure 4 shows etch rate on C faces vs. reciprocal temperature with a total gas flow of 175 cc/min (P_{Cl_2}:P_{O_2} :P_{Ar} = 45:10:120). The etch rate on the C face is expressed as $\exp(-E_a/RT)$ with E_a=42.6 kcal/mol. The etch rate on the Si face is also expressed as $\sim\exp(-E_a/RT)$ with $E_a\sim$48 kcal/mol, though the data points scatter.

Figures 5(a)-5(c) show the etch rate under various gas composition with a constant total gas flow of 175 cc/min at 1000°C. The ratio of two kinds of gases out of three is kept constant, and the flow rate of the other is varied. The gas mixing ratio of this experiment was limited by the range of the flowmeters, and out of this range experiment could not be carried out. Under the conditions in this figure, etched surfaces are relatively smooth, and remarkable change of the surface smoothness is not observed.

Firstly, results on C faces denoted with circles are explained. Figure 5(a) shows linear dependence between the etch rate and the

partial pressure of O_2 gas, P_{O_2}. However, near the lowest limit of P_{O_2}, the etch rate deviates from the linear line, and the etched surface is covered with a black material, probably carbon. A point denoted by X indicates the etch rate for the film including the carbon film, and Y indicates that for the film after removing the carbon film. Figure 5(a) shows that with increasing P_{Cl_2} the etch rate first increases and then decreases and finally indicates a tendency to increase. In the limit of the smallest Cl_2 gas flow, SiO_2 film was formed, and further etching was not observed. Figure 5(c) shows that the etch rate decreases in proportion to the increase of P_{Ar}. Etch rates on Si faces indicated with triangles in Fig. 5 are 0.1-0.01 times of those on C faces. The results on Si faces under constant P_{Cl_2}/P_{Ar} and constant P_{O_2}/P_{Ar} show generally similar tendency to those on C faces. However, the results under constant P_{Cl_2}/P_{O_2} on Si faces show opposite tendency to those on C faces. The results on both Si and C faces at other temperatures indicated similar tendencies as those in Fig. 5 with different etch rates which varied with temperature according to Fig. 3.

8-4. Discussion

In this gas etching system, many kinds of processes take place, reactions of SiC with Cl_2 and O_2 gases, and decomposition and evaporation of SiC. Argon gas acts as only a buffer for the reaction by diluting Cl_2 and O_2 gases. Among many processes, those with small standard free energies (ΔG's) are expected to become dominant. These processes and their standard free energies at 1300 K are given in Table I [13]. Decomposition and evaporation of SiC are difficult to take place at the temperature range studied because of their large free energies. The reaction of O_2 with SiC which forms SiO_2 and C [reaction (3)] has smaller free energy than that of Cl_2 [reaction (1)]. However, since SiO_2 acts as an etch mask and prevents further

Table I Various reactions with their standard free energies (ΔG's) at 1300 K.

	Reaction	ΔG (kcal/mol)
(1)	$SiC(s) + 2Cl_2(g) = SiCl_4(g) + C(s)$	-98.130
(2)	$C(s) + O_2(g) = CO_2(g)$	-94.701
(3)	$SiC(s) + O_2(g) = SiO_2(s) + C(s)$	-143.749
(4)	$C(s) + 2Cl_2(g) = CCl_4(g)$	16.229
(5)	$Si(s) = Si(g)$	60.112
(6)	$C(s) = C(g)$	122.249

progress of the reaction, the reaction (3) can not be dominant. The reaction of O_2 with C [reaction (2)] has smaller free energy than that of Cl_2 [reaction (4)]. Therefore, the plausible dominant processes in this etching reaction are,

$$SiC(s) + 2Cl_2(g) = SiCl_4(g) + C(s), \quad (1)$$

$$C(s) + O_2(g) = CO_2(g). \quad (2)$$

The molar number of SiC etched away per unit area and unit time, J_{SiC}, is given by,

$$J_{SiC} = Ld/M, \quad (3)$$

where L, d, and M are etch rate, the density of SiC, and the molar weight of SiC, respectively. The flux of $SiCl_4$ (J_{SiCl_4}) and that of CO_2 (J_{CO_2}) carried away from the SiC surface of unit area into the gas state are given by,

$$J_{SiCl_4} = P_{SiCl_4}u/RT, \quad (4)$$

$$J_{CO_2} = P_{CO_2}u/RT. \quad (5)$$

Here, P_{SiCl_4} and P_{CO_2} are the partial pressures of $SiCl_4$ and CO_2, respectively, u the velocity of the gas flow, R the gas constant, and T the absolute temperature. If the rate of formation of $SiCl_4$ is much larger than that of CO_2, the surface of a sample may be covered

with carbon. On the contrary, if the rate of formation of CO_2 is much larger than that of $SiCl_4$, the surface of the sample may be covered with silicon. In the gas composition range studied, such results are not observed except for the case of the samllest limit of P_{O_2}. Therefore, we can expect that Si atoms and C atoms are equally etched away:

$$P_{SiCl_4} = P_{CO_2}. \tag{6}$$

Considering that $J_{SiC} = J_{SiCl_4} = J_{CO_2}$, the etch rate is given by,

$$L = MuP_{SiCl_4}/RTd = MuP_{CO_2}/RTd. \tag{7}$$

If the system is near the thermal equilibrium, the following equations are given by the reactions (1) and (2).

$$P^*_{SiCl_4} = K_1 P^{*2}_{Cl_2}, \tag{8}$$

$$P^*_{CO_2} = K_2 P^*_{O_2}, \tag{9}$$

where $P^*_{SiCl_4}$, $P^*_{Cl_2}$, $P^*_{CO_2}$, $P^*_{O_2}$ are the pressures of the gases under thermal equilibrium, and K_1 and K_2 are the equilibrium constants of the reactions (1) and (2), respectively. Since K is given by $K \simeq \exp(-\Delta G/RT)$ in this system and K_1 and $K_2 >> 1$ from Table I, all the Cl_2 and O_2 gases supplied to the SiC surface may react into $SiCl_4$ and CO_2, respectively. This condition gives the relations,

$$P_{SiCl_4} = \frac{1}{2} P_{Cl_2}, \tag{10}$$

$$P_{CO_2} = P_{O_2}. \tag{11}$$

In this case, the etch rate of Eq. (7) is written in the relation of P_{Cl_2} and P_{O_2}.

$$L = MuP/RTd, \tag{12}$$

where P is the smaller one between $P_{Cl_2}/2$ and P_{O_2}. However, when the etch rate calculated from Eq. (12) is compared with the experimental results, good agreement is not obtained. This result indicates that under the etching condition studied, thermal equilibrium is not attained. Therefore, we assume that only some parts of supplied Cl_2

and O_2 gases (αP: $\alpha \leq 1$) react with SiC and transform into CO_2 and $SiCl_4$ under nonequilibrium condition. Furthermore, considering that etch rate does not depend on the gas velocity under the surface reaction controlled condition (Fig. 3), a parameter $k = \alpha u$ is introduced. In this case, the etch rate is expressed as,

$$L = kMP/RTd. \tag{13}$$

This parameter k is determined from the experimental result. The value of k = 13.2 cm/min is obtained from the etch rate of 0.904 μm/min at 1237 K, under the partial gas pressures P_{Cl_2} = 0.257 atm and P_{O_2} = 0.057 atm, and using the molar weight M = 40.10 g/mol and the density d = 3.211 g/cm^3 of SiC. In Fig. 5, the values of $L_{Cl_2} = kMP_{Cl_2}/2RTd$ and $L_{O_2} = kMP_{O_2}/RTd$ are shown by solid lines and broken lines, respectively, which are calculated from Eq. (13) using k = 13.2 cm/min for the C face. L_{Cl_2} and L_{O_2} denote the etch rates expected from the partial pressures of the supplied Cl_2 and O_2 gases. The results of C faces in Figs. 5(a)-5(c) show fairly good agreement between theory and experiment, if we take into account of the simpleness of the theory and that only one value of k is used. These figures show that the actual etch rate is limited by the smaller one between L_{Cl_2} and L_{O_2}, which indicates that the stoichiometry of the etched C atoms and Si atoms is preserved [Eq. (6)]. Results at other temperatures also indicated good agreement between theory and experiment. These results show that the etch rate under various gas compositions at a given temperature is expressed with only one value of k. The temperature dependence of $k = 2.89\times10^8\exp(-E_a/RT)$ cm/min with E_a = 42.6 kcal/mol is determined using the etch rate in Fig. 3.

At the highest temperature of 1100°C, an etch rate larger than that predicted from the theory is observed. This deviation may be due to the fact that the reactions (1) and (2) in Table I saturate and other reactions such as (4) simultaneously take place. In Fig. 5(a) in the low oxygen gas flow region, deviation from the theory arises due to the formation of carbon film. This deviation indicates

that in this region stoichiometry of C atoms and Si atoms is not preserved and the reaction (1) selectively takes place. In Fig. 5(b) in the high Cl_2 gas region ($P_{Cl_2} \geq 0.35$ atm), the observed etch rates are larger than the calculated line. This deviation may be due to the additional etching caused by the combined reaction of (1) and (4) which does not need O_2 gas.

For Si faces, the experimental data points scatter due to the large experimental uncertainty because of thin etched layers. However, Fig. 5(b) shows that the etch rate on Si faces varies similarly to that on C faces with P_{Cl_2}. The experimental results are relatively well explained by the theoretical curves calculated with the value of $k = 0.36$ cm/min at 1000°C. The temperature dependence of $k \simeq 6.7\times10^7 \exp(-E_a/RT)$ cm/min with $E_a \simeq 48$ kcal/mol is obtained from the etch rates on the Si face at various temperatures. The accuracy of k is not good because of the scatter of the data points on Si faces. Figures 5(a) and 5(c) show that the deviation from the calculated curves are large in the cases of constant P_{O_2}/P_{Ar} and P_{Cl_2}/P_{O_2}, respectively. Especially in the case of constant P_{Cl_2}/P_{O_2}, the signs of the slopes of the experimental result and theoretical one are opposite. If the experimental data points are correct, this etching process may be caused by the reaction between SiC and Ar gas. However, such a reaction is difficult to occur, because Ar is an inert gas. Therefore, this opposite dependence can not be explained. The deviation in the case of constant P_{Cl_2}/P_{Ar} may be due to the fact that selective etching of silicon by the reaction (1) takes place because of the reduction of the reaction (2) due to small P_{O_2} similarly to the case of the C face, although the experimental data points scatter.

Now we consider the physical meaning of the parameter k. By a simple theory [12], in the mass transfer controlled region, etch rate is proportional to the diffusion constant of the etching gas which is expressed as $D \propto T^m$. Both theory [14] and experiment

[15,16] give values of $1.5 \leq m \leq 2$. In the surface reaction controlled region, the etch rate is proportional to the surface reaction rate constant k_S which varies as $\exp(-E_a/RT)$. Since the present parameter k is expressed as $\exp(-E_a/RT)$ and the etching is under surface reaction controlled condition, the parameter k seems to relate with the surface reaction rate constant k_S. Moreover, Eq. (12) is transformed as follows.

$$L = \frac{P\ Mk}{RT\ d} = \frac{n\ Mk}{V\ d} = \frac{nA\ k}{V\ \frac{dA}{M}} = C_G \frac{k}{N_1}. \qquad (14)$$

Here, n is the molar number, V the volume of the gas at one atm, A Avogadro's number, C_G the molecular density of the gas, and N_1 the molecular density of SiC. The last expression of Eq. (14) coincides with the formula of $L = C_G k_S / N_1$ in Ref. 12. Therefore, k and k_S are the identical physical constants.

Since k is the surface reaction rate constant, the large difference of the etch rates between the C face and the Si face, about 50 times, is due to the difference of the reaction velocities on different faces. This conclusion is assisted by the fact that the Si face and the C face have different stacking sequences of Si atoms and C atoms and that terminative planes of Si and C faces are composed of Si and C atoms, respectively.

8-5. Improvement of Diode Characteristics by Mesa Etch

In Chapts. V-VII, cleaving was employed in the diode fabrication process to cut crystals into dies. The current - voltage (I-V) characteristics of the diodes fabricated by the process indicated large leakage currents. The n values of these diodes were far greater than 1-2, sometimes more than 10, when the expression of $I \propto \exp(eV/nkT)$ was assumed. However, when mesa etch was carried out by Cl_2-O_2-Ar gas system, the n values of all the diodes were decreased

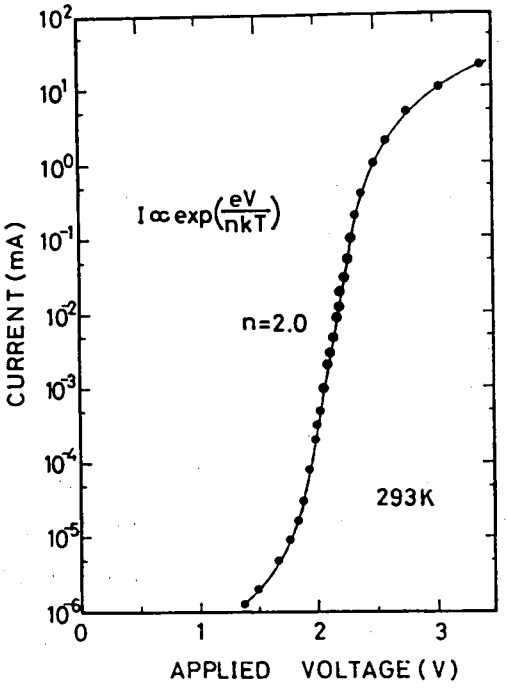

Fig. 6 Forward current - voltage characteristics of a diode after mesa etch.

to $2 \leq n \leq 3$. Figure 6 shows the I-V characteristics of a diode after mesa etch. In this characteristics, exponential relation is obtained more than 4 orders and the n value is 2.0, which is well explained by the generation-recombination current. Moreover, the breakdown voltage of this diode is more than 140 V at a current level of 1 mA. These results indicate that the mesa etch with Cl_2-O_2-Ar gas system greatly decreases the leakage current and improves the diode characteristics.

8-6. Summary

The etching of SiC with Cl_2, O_2, and Ar gas mixture has been studied in the temperature range of 850-1100°C. The gas composition is varied, which includes the composition commonly used in the device fabrication processes, and the dependence of the etch rate on gas

flow rate is measured. Good agreement is obtained between the experimental results and a simple theory using one parameter k which is the surface reaction rate constant. The etch rate in all the gas composition range studied is expressed using a single value of k at a given temperature. The only variable affecting k is the temperature. The temperature dependences of the parameters k on the Si face and the C face are determined. The etch rate on the C face is about 50 times larger than that on the Si face, which is concluded to be due to the smaller surface reaction rate constant on the Si face. The difference of the surface reaction rate constant may be caused by the difference of the stacking sequence of Si and C atomic planes between the Si face and C face. The etch rate at a given temperature in a wide range of gas composition can be easily predicted using the determined value of k. The improvement of diode characteristics by the mesa etch with the present gas system is verified.

References

[1] R. B. Campbell and H. C. Chang, in "Semiconductors and Semimetals", edited by R. K. Willardson and A. C. Beer (Academic Press, New York, 1971), Vol. 7, p. 625.

[2] A. Suzuki, M. Ikeda, N. Nagao, H. Matsunami, and T. Tanaka, J. Appl. Phys. 47, 4546 (1976); H. Matsunami, M. Ikeda, A. Suzuki, and T. Tanaka, IEEE Trans. Electron Devices, ED-24, 958 (1977); M. Ikeda, T. Hayakawa, S. Yamagiwa, H. Matsunami, and T. Tanaka, J. Appl. Phys. 50, 8215 (1979).

[3] R. W. Bartlett and M. Barlow, J. Electrochem. Soc. 117, 1436 (1970).

[4] Cambell and Chang, op. cit., p. 666.

[5] W. v. Münch and P. Hoeck, Solid-State Electron. 21, 479 (1978).

[6] W. Kürzinger, Doctoral Thesis, Hannover Technical University (1977); W. v. Münch and W. Kürzinger, Solid-State Electron. 21, 1129 (1978).

[7] T. I. Chu and R. B. Campbell, J. Electrochem. Soc. 112, 955

(1965).

[8] E. Modrak, I. Swiderski, and T. Niemski, J. Cryst. Growth 22, 181 (1974).

[9] M. Kumagawa, H. Kuwabara, and S. Yamada, Jpn. J. Appl. Phys. 8, 421 (1969).

[10] See, for example, W. F. Knippenberg, Philips Res. Rep. 18, 161 (1963).

[11] See a review article by A. S. Grove, " Physics and Technology of Semiconductor Devices" (John Wiley and Sons, Inc., New York, 1967), p. 7.

[12] A. S. Grove, Ind. Eng. Chem. 58, 48 (1966).

[13] JANAF Thermochemical Tables, Dow Chemical Co., Midland, Mich.

[14] S. Chapman and T. G. Cowling, "The Mathematical Theory of Nonuniform Gases" (Cambridge University Press, London, 1939), p. 248.

[15] W. H. Shepherd, J. Electrochem. Soc. 112, 988 (1965).

[16] International Critical Tables 5, 62 (1929).

IX. CONCLUSIONS

In this thesis, studies have been carried out on the subjects related with the fabrication processes and the physical properties which are necessary for the analysis and the design of SiC LED's with a purpose to develope efficient SiC blue LED's. With the aid of the results of liquid phase epitaxial growth and photoluminescence study, relatively high efficiency blue and yellow LED's have been realized, and the luminescent and electrical properties of the diodes have been studied. Based on the electroluminescence mechanisms determined using the results of the photoluminescence study, methods to improve the efficiency have been discussed.

In Chapt. II, process of the epitaxial growth of SiC by the dipping technique has been described, and the conditions to obtain good layers have been determined. A method to decrease the carrier concentration of the undoped crystal has been devised, and the electrical properties of the layers doped with Al acceptors or N donors have been studied.

In Chapt. III, photoluminescence due to free excitons and excitons bound to N donors in undoped 3C, 4H, 6H, and 15R SiC crystals has been studied in the temperature range of 4.2 and about 100 K. The energies of a large number of phonons associated with free excitons have been determined and compared with the energies of phonons associated with bound excitons. The exciton band gaps of 4H, 6H, and 15R SiC have been determined from the free exciton peaks. The free exciton binding energies of 3C, 4H, 6H, and 15R SiC have been estimated from thermal quenching of the free exciton luminescence.

In Chapt. IV, systematic study has been carried out on the intense visible photoluminescence in 3C, 4H, 6H, and 15R SiC crystals doped with Al, Ga, or B acceptors and N donors. The luminescence mechanisms have been assigned to be D-A pair luminescence and

free-to-acceptor luminescence. Verification and the first determination of site dependent acceptor levels have been carried out by analyzing free-to-acceptor luminescence. The site dependent donor levels have been confirmed from the dependence of the D-A pair luminescence on doping and excitation, and by the analysis of the configuration coordinate phonons. The ionization energies of donors and acceptors in cubiclike sites are always larger than those in hexagonallike sites. The ratios of the ionization energies are approximately constant independent of the polytype and the kind of impurity in spite of the wide range of the ionization energies. The origin of the site effect on the impurity level is explained by a model which assumes the local dielectric constants and the local effective masses. The possibility of the existence of the site effect in other materials has been pointed out. Haynes rule relatively well applies to N donors in different sites in various polytypes, which enables to predict the donor level from the binding energy of the bound exciton.

In Chapt. V, blue light-emitting diodes of 6H SiC have been fabricated by doping Al acceptors and N donors using the overcompensation method which has been proposed in this thesis. A quantum efficiency of 1.0×10^{-5} was obtained which had been one of the highest values. The electrical and luminescent properties of the diodes have been studied and a method to improve the efficiency has been discussed.

In Chapt. VI, the mechanism has been studied on the shifting peaks from red to blue in diodes prepared by the overcompensation method. From the analysis of the electrical properties, the injection mechanisms, and the luminescent properties of the diodes, the shifting peaks have been determined to be due to photon assisted tunneling.

In Chapt. VII, various LED's doped in the n layers with Al, Ga, or B acceptors and N donors have been fabricated using the rotation

dipping technique proposed in this thesis. This technique has advantages that multilayers can be grown in one growth run and that melts and crucibles can be reused. Detailed study of recombination mechanisms in the diodes from about 100 to 400 K has been carried out using photoluminescence, electroluminescence, and time-resolved spectra. At low temperatures the radiation originates mainly in the p layer, and around room temperature in the n layer. The luminescence mechanisms are free exciton recombinations for the peak at about 425 nm which had been considered to be due to interband transitions, D-A pair recombinations for the main broad band, transitions of excitons bound to some unknown intrinsic defects for the peak at about 455 nm, and recombinations of excitons bound to divacancies for the peak at about 530 nm. The dependence of the EL efficiency on the N concentration in the n layer has been studied and the maximum efficiency was obtained around $n \sim 10^{17}$-10^{18} cm^{-3}. Based on these results, methods to improve the efficiency have been discussed. The maximum quantum efficiency and peak energies were 1.2×10^{-5} and 460 nm for Al-doped, 9×10^{-6} and 485 nm for Ga-doped, and 2.5×10^{-5} and 580 nm for B-doped LED's, and the efficiency was improved by a factor of 2 by using the epoxy coating.

In Chapt. VIII, etching of SiC with Cl_2-O_2-Ar gas system has been studied. The dependences of the etch rate on the temperature, gas flow rate, and gas composition have been measured. Good agreement is obtained between the experiment and a simple theory using a parameter k which relates to surface reaction velocity. The temperature dependences of the values of k on the C and Si faces have been determined to be $k = 2.89\times10^{8}\exp(-E_a/RT)$ cm/min with E_a = 42.6 kcal/mol and $k \simeq 6.7\times10^{7}\exp(-E_a/RT)$ cm/min with $E_a \simeq 48$ kcal/mol, respectively. Etch rate at a given temperature and gas composition can be easily predicted by using the value of k. The large difference of the etch rates between the Si face and C face is explained by the difference of the value of k.

Among many problems remained for further investigation, growth of ingot crystals for substrates and improvement of efficiency are the most essential in order to realize practical use of SiC blue LED's. Both problems need excellent and continuous investigations, because they are caused by the refractory properties of SiC. One possible principle for the former is the sublimation growth in low pressure ambient which was reported by Tairov et al. who made large and pure ingot crystals at low temperatures with relatively high growth rates. One possible suggestion for the latter is increase of the carbon solubility in the growth melt, and precise controle of doping of luminescent centers.

APPENDIX

A. Dielectric Constants of 2H, 4H, and 15R SiC.

There have been no reports on the dielectric constants of 2H, 4H, and 15R SiC. Therefore, values of them are estimated from the Lyddane-Sachs-Teller [1] (LST) relation following the procedure in the report by Patrick and Choyke [2] and using refractive indices and phonon energies in the literatures.

The static dielectric constant can be written

$$\varepsilon_S = \varepsilon_{el} + \varepsilon_{lat}, \qquad \text{(A1)}$$

where ε_{el} is the electronic contribution, and the lattice contribution ε_{lat} is related to the ratio of phonon energies that enter into the LST formula. The value of ε_∞, which is considered to be equal

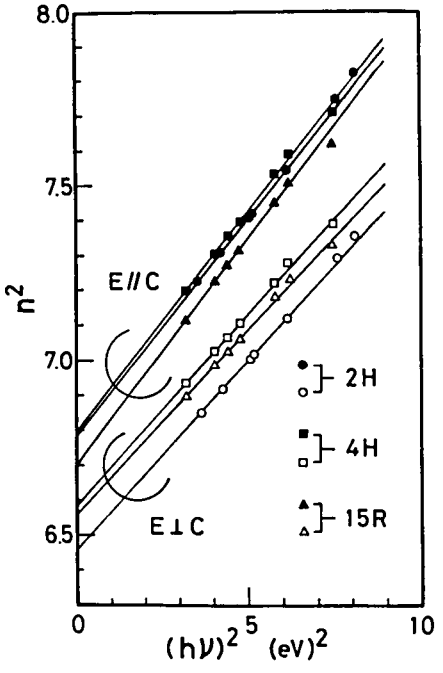

Fig. 1 n^2 vs. $(h\nu)^2$ for 2H, 4H, and 15R SiC.

Table I The values of ε_∞, ε_S, $\hbar\omega_L$, and $\hbar\omega_T$ for 2H, 4H, and 15R SiC.

Polytype	ε_∞	$\hbar\omega_L$ (cm^{-1})	$\hbar\omega_T$(cm^{-1})	ε_S
2H($\perp$)	6.46	970	797	9.57
2H(//)	6.79	964	767	10.73
4H($\perp$)	6.59	970	797	9.76
4H(//)	6.79	964	782	10.32
15R($\perp$)	6.56	970	979	9.72
15R(//)	6.70	964	785	10.10

to ε_{el}, should denote the value of $n^2 = \varepsilon_\infty$ extrapolated to zero photon energy (see Fig. 1). This expression is reasonable, because in the one-oscillator model the value of n^2 is expressed as

$$n^2 = 1 + \frac{\varepsilon_g}{1 - (h\nu/E_g)^2} \sim \varepsilon_\infty + \varepsilon_g(h\nu/E_g)^2. \qquad \text{(A2)}$$

Here, $h\nu$ is the photon energy, E_g is a parameter which represents the average band gap, and ε_g is a parameter which is proportional to the oscillator strength. The second form in Eq. (A2) with $\varepsilon_\infty = 1 + \varepsilon_g$, is a good approximation if $h\nu >> E_g$, where E_g is close to 8 eV in SiC [3].

Figure 1 shows n^2 vs. $(h\nu)^2$ of 2H, 4H, and 15R SiC which are plotted by using the refractive indices reported by Powell [4] for 2H and by Shaffer [5] for 4H and 15R SiC. Open symbols denote the ordinary indices (E $\perp$ c) and closed symbols the extraordinary indices (E // c). The value of the static dielectric constant can be determined by using the LST formula:

$$\varepsilon_S = \varepsilon_\infty(\hbar\omega_L/\hbar\omega_T)^2, \qquad \text{(A3)}$$

using the longitudinal and transverse phonon energies, $\hbar\omega_L$ and $\hbar\omega_T$. Table I shows the values of ε_∞ and ε_S in the direction parallel and

perpendicular to c-axis for 2H, 4H, and 15R SiC. The values of $\hbar\omega_L$ and $\hbar\omega_T$ for all the polytypes are taken from the Raman measurements by Feldman et al. [6]. The value of $\hbar\omega_T(//)$ for 2H SiC is estimated by the extrapolation of the plots in Fig. 9 in Ref. 6 assuming the "percent h low" [6]. For all the polytypes, the values of $\hbar\omega_L(\perp)$, $\hbar\omega_L(//)$, and $\hbar\omega_T(\perp)$ of 6H SiC are used, because these values are independent of the polytype [6].

B. Modified Bohr Radii

Table II Values of modified Bohr radii ($a^*\nu$) of electrons and holes bound to N donors and Al, Ga, or B acceptors in hexagonallike sites (H) and cubiclike sites (C), and values of m_e^*, m_h^*, and ε_S in 3C, 4H, 6H, and 15R SiC.

	$a^*\nu$ (Å) 3C	4H	6H	15R
N(H)		12.5	7.7	13.9
N(C)	15.0	9.1	6.1	10.5
Al(H)		4.5	4.0	4.2
Al(C)	3.9		3.9	4.1
Ga(H)		3.8	3.5	3.6
Ga(C)	3.3		3.4	3.5
B(H)		2.4	2.3	2.4
B(C)	2.3		2.3	2.3
$m_e^{*a)}$	∿0.30	∿0.37	∿0.65	∿0.31
$m_h^{*b)}$	∿1.0	∿1.0	∿1.0	∿1.0
ε_S	9.72[c)]	∿9.95	9.78[c)]	∿9.85

a) Ref. 8.
b) Refs. 9 and 10.
c) Ref. 2.

The modified Bohr radius $a^*\nu$ is given as follows.

$$\nu = \sqrt{R^*/E(obs)}, \tag{B1}$$

$$R^* = m^* e^4 / 2\hbar^2 \varepsilon_S^2, \tag{B2}$$

$$a^* = e^2 / 2\varepsilon_S R^*. \tag{B3}$$

For the notations, refer to Sec. 4-4 [7]. In the calculation, the values of m_e^* [8] and m_h^* [9,10] of 3C, 4H, 6H, and 15R SiC and ε_S of 3C and 6H SiC [2] are taken from literatures and ε_S of 4H and 15R SiC are taken from APPENDIX A. For the ionization energies of donors and acceptors, refer to Table II in Chapt. IV. Table II shows the values of $a^*\nu$, m_e^*, m_h^*, and the averaged value of ε_S for the impurities in 3C, 4H, 6H, and 15R SiC.

References

[1] R. H. Lyddane, R. G. Sachs, and E. Teller, Phys. Rev. 59, 673.

[2] L. Patrick and W. J. Choyke, Phys. Rev. B2, 2255 (1970).

[3] W. J. Choyke and L. Patrick, J. Opt. Soc. Am. 58, 377 (1968).

[4] J. A. Powell, J. Opt. Soc. Am. 62, 341 (1972).

[5] R. T. B. Shaffer, Appl. Opt. 10, 1034 (1971).

[6] D. W. Feldman, J. H. Parker, Jr., W. J. Choyke, and L. Patrick, Phys. Rev. 173, 787 (1968).

[7] H. B. Bebb and R. A. Chapman, J. Phys. Chem. Solids 28, 2087 (1967); H. B. Bebb, Phys. Rev. 185, 1116 (1969).

[8] Y. M. Tairov and Y. A. Vodakov, in "Electroluminescence", edited by J. I. Pankov (Spinger-Verlag, Berlin, 1977), p. 31.

[9] H. J. van Daal, W. F. Knippenberg, and J. D. Wasscher, J. Phys. Chem. Solids 24, 109 (1963).

[10] G. A. Lomakina, Yu. A. Vodakov, E. N. Mokhov, V. G. Oding, and G. F. Kholuyanov, Sov. Phys. - Solid State 12, 2356 (1971).

LIST OF PUBLICATION

I. Full Papers

5) "Free Exciton Luminescence in 3C, 4H, 6H, and 15R SiC",
M. Ikeda and H. Matsunami,
Phys. Status Solidi A58 (1980) pp. 657-663.

6) "Site Effect on the Impurity Levels in 4H, 6H, and 15R SiC",
M. Ikeda, H. Matsunami, and T. Tanaka,
Phys. Rev. B (to be published).

8) "Photon Assisted Tunneling in SiC LED's Prepared by Overcompensation Method",
M. Ikeda, H. Matsunami, and T. Tanaka,
Jpn. J. Appl. Phys. 19 (1980) pp. 1323-1328.

II. Short Notes

2) "Defect Luminescence in SiC Light-Emitting Diodes",
M. Ikeda, H. Matsunami, and T. Tanaka,
Jpn. J. Appl. Phys. 19 (1980) pp. 1201-1202.

LIST OF PUBLICATION

I. Full Papers

1) "Liquid-Phase Epitaxial Growth of 6H-SiC by the Dipping Technique for Preparation of Blue-Light-Emitting Diodes", A. Suzuki, M. Ikeda, N. Nagao, H. Matsunami, and T. Tanaka, J. Appl. Phys. 47 (1976) pp. 4546-4550.

2) "SiC Blue LED's by Liquid Phase Epitaxy", H. Matsunami, M. Ikeda, A. Suzuki, and T. Tanaka, IEEE Trans. Electron Devices ED-24 (1977) pp. 958-961.

3) "Site-Dependent Donor and Acceptor Levels in 6H-SiC", M. Ikeda, H. Matsunami, and T. Tanaka, J. Lumin. 20 (1979) pp. 111-129.

4) "Fabrication of 6H-SiC Light-Emitting-Diodes by a Rotation Dipping Technique: Electroluminescence Mechanisms", M. Ikeda, T. Hayakawa, S. Yamagiwa, H. Matsunami, and T. Tanaka, J. Appl. Phys. 50 (1979) pp. 8215-8225.

5) "Free Exciton Luminescence in 3C, 4H, 6H, and 15R SiC", M. Ikeda and H. Matsunami, Phys. Status Solidi A (to be published).

6) "Site Effect on the Impurity Levels in 4H, 6H, and 15R SiC", M. Ikeda, H. Matsunami, and T. Tanaka, (submitted to Phys. Rev.).

7) "Etching of SiC with Cl_2-O_2-Ar Gas System", M. Ikeda, M. Kobayashi, H. Matsunami, and T. Tanaka, (submitted to J. Electrochem. Soc.).

8) "Photon Assisted Tunneling in SiC LED's Prepared by the Overcompensation Method",

M. Ikeda, H. Matsunami, and T. Tanaka,
(submitted to Jpn. J. Appl. Phys.).

II. Short Notes

1) "Liquid-Phase Epitaxial Growth of 6H-SiC by Vertical Dipping Technique",
A. Suzuki, M. Ikeda, H. Matsunami, and T. Tanaka,
J. Electrochem. Soc. 122 (1975) pp. 1471-1472.

2) "Defect Luminescence in SiC Light-Emitting Diodes",
M. Ikeda, H. Matsunai, and T. Tanaka,
(submitted to Jpn. J. Appl. Phys.).

III. International Conference

1) "SiC Blue LED's by Liquid Phase Epitaxy",
H. Matsunami, M, Ikeda, A. Suzuki, and T. Tanaka,
2nd IEEE Specialist Conference on the Technology of Electroluminescent Diodes, Nemu-no-Sato, MIE, Japan, September, 1976, E-V-3. [This has been published as I-2).]